COPERNICUS
MARINE ENVIRONMENT MONITORING SERVICE

QUALITY INFORMATION DOCUMENT

Mediterranean Sea Production Centre
MEDSEA_ANALYSISFORECAST_BGC_006_014

Issue: 2.1

Contributors: L. Feudale, A. Teruzzi, S. Salon, G. Bolzon, P. Lazzari, G. Coidessa, V. Di Biagio, G. Cossarini

Approval date by the CMEMS product quality coordination team: 02/12/2021

CHANGE RECORD

When the quality of the products changes, the QuID is updated and a row is added to this table. The third column specifies which sections or sub-sections have been updated. The fourth column should mention the version of the product to which the change applies.

Issue	Date	§	Description of Change	Author	Validated By
1.0	31/08/2017	All	Release of V3.2 version of the Med-biogeochemistry at 1/24° resolution	G.Cossarini, S. Salon, G. Bolzon, A. Teruzzi, P. Lazzari, L. Feudale	
1.1	30/04/2018	All	Release of V4.1 version of the Med-biogeochemistry at 1/24° resolution	G.Cossarini, S. Salon, G. Bolzon, A. Teruzzi, P. Lazzari, L. Feudale	
1.2	27/01/2019	All	Release of version at Q2/2019 of the Med-biogeochemistry at 1/24° resolution with BFM version 5 and open boundary at Dardanelles	A. Teruzzi, G.Cossarini, S. Salon, G. Bolzon, P. Lazzari, L. Feudale	Mercator Ocean
1.3	06/12/2019	All	Release of version Q1/2020 of the Med-biogeochemistry at 1/24° resolution with BGC-Argo float assimilation	A. Teruzzi, G. Cossarini, L. Feudale, G. Bolzon, S. Salon	Mercator Ocean
2.0	15/01/2021	All	Release of version Q2/2021 of the Med-biogeochemistry with new products (silicate, ammonium and biomass of zooplankton) and new boundary condition in Atlantic	L. Feudale, A. Teruzzi, S. Salon, G. Bolzon, P. Lazzari, G. Coidessa, Di Biagio V., G. Cossarini	Emanuela Clementi
2.1	03/09/2021	All	Release of version Q4/2021 of the Med-biogeochemistry with the addition of the daily discharges of nutrients and carbonate system variables for the Po River (Adriatic Sea)	L. Feudale, A. Teruzzi, S. Salon, G. Bolzon, P. Lazzari, G. Coidessa, Di Biagio V., G. Cossarini	Emanuela Clementi

TABLE OF CONTENTS

I EXECUTIVE SUMMARY

I.1 Products covered by this document

This document describes the quality of the product MEDSEA_ANALYSISFORECAST_BGC_006_014, the nominal product for the analysis and forecast of the biogeochemical state of the Mediterranean Sea. The MED Biogeochemistry product includes 2D and 3D daily and monthly fields at 1/24° horizontal resolution (which for the Mediterranean basin is about 4 km) of 14 variables grouped in 5 datasets:

PFTC: chlorophyll, phytoplankton carbon biomass and zooplankton carbon biomass;

NUTR: phosphate, nitrate, ammonium and silicate;

BIOL: oxygen and primary production;

CARB: pH (reported on Total Scale), dissolved inorganic carbon and alkalinity;

CO2F: surface partial pressure of CO2 and surface CO2 flux.

This CMEMS product can be acknowledged using the following citations:

Feudale, L., Bolzon, G., Lazzari, P., Salon, S., Teruzzi, A., Di Biagio, V., Coidessa, G., & Cossarini, G. (2021). Mediterranean Sea Biogeochemical Analysis and Forecast (CMEMS MED-Biogeochemistry, MedBFM3 system) (Version 1) [Data set]. Copernicus Monitoring Environment Marine Service (CMEMS). https://doi.org/10.25423/CMCC/MEDSEA_ANALYSISFORECAST_BGC_006_014_MEDBFM3

Salon, S., Cossarini, G., Bolzon, G., Feudale, L., Lazzari, P., Teruzzi, A., Solidoro, C., Crise, A., 2019. Marine Ecosystem forecasts: skill performance of the CMEMS Mediterranean Sea model system. Ocean Sci. Discuss. 1–35. https://doi.org/10.5194/os-2018-145

I.2 Summary of the results

The quality of the product MEDSEA_ANALYSISFORECAST_BGC_006_014 for Mediterranean Sea biogeochemistry analysis and forecasts has been assessed over the period 1/1/2019-31/12/2019 by means of comparison with observational in-situ datasets, semi-independent data (satellite and BGC-Argo float datasets used in the assimilation) and literature estimates. A detailed and scientific description of the MedBFM model system and of the validation framework is in Salon et al. (2019). The main results of the present quality product assessment are summarized in the following points:

Chlorophyll: it is the mass concentration of chlorophyll a in sea water. In the CMEMS catalogue, the unit of chlorophyll is [mg m^{-3}]. Results give evidence of the model capability of reproducing spatial patterns, seasonal cycle with surface winter bloom period, and the related vertical properties at mesoscale and weekly temporal scale. At surface, the western open sea sub-basins are generally characterized by higher uncertainty and variability (estimated by the RMSD) than eastern ones, with a basin-averaged RMSD of 0.05 (0.01) mg m^{-3} in winter (summer). In the coastal areas the basin-averaged uncertainty rises up to 0.21 (0.18) mg m^{-3} in winter (summer), with higher values in areas more affected by river inputs and shelf dynamics, and a general model underestimation of the high values of observed chlorophyll. The use of the available BGC-Argo floats data shows model consistency in reproducing the key mechanisms coupling physics and biogeochemistry at mesoscale and along the vertical dynamics. The mean RMSD of chlorophyll vertical profiles computed between model and BGC-Argo floats observations

is 0.04 mg m^{-3}. Further, to quantify the model skill to reproduce the chlorophyll dynamics key properties we used some novel metrics: averaged content of chlorophyll in the photic layer (0-20 0 m), depth of the Deep Chlorophyll Maximum (DCM) and thickness of the winter bloom layer (WBL). Considering areas with a sufficient number of float profiles per month, the modelled averaged content of chlorophyll in the photic layer (0-20 0 m) has a mean RMSD of 0.03 mg m^{-3}, the DCM is reproduced with an uncertainty of around 13 m, while WBL has an uncertainty of 24 m.

Primary production: it is the net primary production of carbon per unit of volume in sea water and it is reported in [mg m^{-3} day^{-1}]. Comparison has been made with available peer-reviewed publications, showing that the simulation consistently reproduces basin-scale and sub-basin-scale patterns and estimations.

Phytoplankton carbon biomass: it is the carbon mole concentration of phytoplankton in sea water. In the CMEMS catalogue the unit of phytoplankton carbon biomass is [mmol m^{-3}]. It represents the sum of the carbon content of the four phytoplankton groups of BFM model (i.e., diatoms, picophytoplankton, nanoflagellates and dinoflagellates). In this document, the phytoplankton carbon biomass is expressed as (mgC/m^3) since it is the most common unit used in observations. Model reproduces satisfactorily the vertical profiles shape and values of particulate backscattering coefficient at 700nm (bbp700) converted to carbon biomass provided by BGC-Argo optical data. The mean uncertainty computed with the BGC-Argo data is of 0.85 mg m^{-3} considering the average phytoplankton carbon biomass in the 0-20 0 m layer.

Zooplankton carbon biomass: it is the carbon mole concentration of zooplankton in sea water. In the CMEMS catalogue the unit of zooplankton carbon biomass is [mmol m^{-3}]. It represents the sum of the carbon content of the four zooplankton groups of BFM model (i.e., heterotrophic nano flagellates, microzooplankton and 2 groups of mesozooplankton). In this document, the zooplankton carbon biomass is expressed as carbon mass per square meter for the layer 0-20 0 m (gC/m^2) since it is the most common unit used for zooplankton data. Most of the observations, which are pretty scarce and sparse, are reported in terms of integrated values in the layer 0-20 0 m. The model is able to reproduce the order of magnitude of this variable and the main spatial patterns inferred from estimations.

Phosphate: it is the mole concentration of phosphate expressed in [mmol m^{-3}]. Uncertainties at basin scale (measured in terms of RMSD) are 0.03 mmol m^{-3} in the upper 60 m and 0.04 mmol m^{-3} in the deeper layers. General basin-wide gradients and vertical profile shapes are simulated consistently with respect to observations (correlation higher than 0.90, except in the Adriatic Sea), with model vertical profiles within the observed climatological variability.

Nitrate: it is the mole concentration of nitrate expressed in [mmol m^{-3}]. Major horizontal spatial gradients (sub-basin wide patterns) and vertical patterns are consistent with observations except in the eastern basin where the model overestimates in the surface levels and underestimates in the deeper layers (correlation higher than 0.96). Mean monthly vertical profiles are within the observed climatological variability, and uncertainty (i.e. RMSD) at basin scale is 0.48 mmol m^{-3} in the upper 60 m and around 0.85 mmol m^{-3} in the deeper layers. The use of the BGC-Argo floats data corroborates the model consistency in reproducing the key mechanisms coupling physics and biogeochemistry at mesoscale and along the vertical dimension. The mean RMSD of model and vertical nitrate observations from BGC-Argo floats is 0.40 mmol m^{-3}. Further, to quantify the model skill to reproduce key vertical characteristics we use 2 novel metrics: the averaged content of nitrate in the photic layer (0-20 0 m) and the depth of the nitracline. Considering areas with a sufficient number of float profiles per month, the modelled averaged nitrate in the 0-20 0 m layer has a mean RMSD of 0.35 mmol m^{-3}, the nitracline depth is reproduced with a mean uncertainty (RMSD) of 20 m.

Oxygen: it is the mole concentration of dissolved molecular oxygen expressed in [mmol m^{-3}]. Considering the comparison of model results with climatological vertical profiles, the basin-scale uncertainties do not exceed 7 mmol m^{-3} in the first 10 0 m. Model profiles are in agreement with climatology (correlation higher than 0.95) and generally within the observed variability. Model outputs consistently reproduce the oxygen dynamics at the mesoscale and its vertical properties as shown by the model-BGC-Argo comparison. The overall RMSD equals to 7 mmol m^{-3}.

Ammonium: it is the mole concentration of ammonium expressed in [mmol m^{-3}]. Considering the comparison of model results with climatological vertical profiles, the order of magnitude is captured, but the surface horizontal patterns are not always well reproduced; that is also for the vertical profiles (the vertical mean RMSD is 0.33 mmol m^{-3}). Limited data availability affected the validation of this variable.

Silicate: it is the mole concentration of silicate expressed in [mmol m-3]. Basin vertical profiles are well simulated within the range of variability of the climatology except in the western sub-basins where the model overestimates concentration at the surface.

pH: pH is reported in total scale and at in-situ conditions (i.e., at the temperature, salinity and pressure conditions of the water parcel). Uncertainty of modelled pH is 0.017 according to the comparison with reconstructed climatological vertical profiles among the different Mediterranean sub-basins.

Dissolved Inorganic Carbon: in the CMEMS catalogue, dissolved inorganic carbon (DIC) is expressed in [mol m^{-3}], however the present document reports the DIC results in [µmol kg^{-1}] which is the common unit used for in-situ observations. The sea water density is needed for the conversion. Considering the comparison of model results with climatological vertical profile, the basin-scale overall uncertainty of DIC is around 22 µmol kg^{-1}.

Alkalinity: alkalinity, the other master variable of the carbonate system together with DIC, is reported in [µmol kg^{-1}] in this document, which is the common unit used for in-situ observations. In the CMEMS catalogue, alkalinity is expressed in [mol m^{-3}]. Overall uncertainty of modelled alkalinity is 22.9 µmol kg^{-1} according to the comparison with reconstructed climatological vertical profiles among the different Mediterranean sub-basins.

Surface partial pressure of CO2: the CMEMS catalogue provides the 2D surface partial pressure of carbon dioxide expressed in Pascal [Pa]. Validation results report pCO2 in [µatm]: the conversion is 1 µatm equals to 101.325 kPa. Uncertainty of modelled pCO2 is 40 µatm according to the comparison with climatological vertical profiles among the different Mediterranean sub-basins. Uncertainty of the surface pCO2, estimated using the SOCAT dataset, is about 50 µatm; the comparison shows the good agreement of the model to simulate the seasonal cycle and spatial heterogeneity among sub-basins.

Surface flux of CO2: it is the surface downward (i.e., positive values indicate sink of atmospheric CO2 in to the sea) mass flux of carbon dioxide expressed in carbon and reported in [kg m^{-2} s^{-1}] in the CMEMS catalogue. Validation of the surface flux of CO2, which uses the unit of [mmol m^{-2} d^{-1}], is based on the comparison with the climatology published in the Chapter 1.7 Air-to-sea carbon flux of the Ocean State Report #2 (Von Schuckmann et al., 2018) and other literature. Present CO2 flux estimates are consistent with the multi-decadal climatology in term of spatial patterns.

I.3 Estimated Accuracy Numbers

Chlorophyll [mg/m^3]				
	RMSD		BIAS	
	win	sum	win	sum
OPEN SEA				
Mod-Sat	0.05	0.01	0.02	<0.005
log_{10}(Mod)-log_{10}(Sat)	0.13	0.06	0.06	<0.005
COASTAL AREAS				
Mod-Sat	0.21	0.18	-0.05	-0.05
log_{10}(Mod)-log_{10}(Sat)	0.18	0.16	<0.005	-0.05

Table I.1. Mean RMSD and BIAS (model minus satellite) of surface chlorophyll [mg m^{-3}] over the open sea and coastal areas of the Mediterranean Sea. Winter corresponds to January to April, summer corresponds to June to September.

	RMSD									
LAYERS (m)	**0-10**	**10-30**	**30-60**	**60-100**	**100-150**	**150-300**	**300-600**	**600-1000**	**Whole column (0-1000)**	**CORR**
PHOSPHATE [mmol/m^3]	0.03	0.03	0.03	0.02	0.05	0.03	0.05	0.04	0.03	0.94
NITRATE [mmol/m^3]	0.42	0.44	0.58	0.77	0.80	0.72	1.11	0.84	0.69	0.98
OXYGEN [mmol/m^3]	4.84	4.70	6.79	5.45	7.13	6.71	12.71	8.51	7.36	0.96
AMMONIUM [mmol/m^3]	0.40	0.21	0.15	0.24	0.31	0.32	0.44	0.55	0.24	0.15
SILICATE [mmol/m^3]	0.93	0.96	0.78	0.55	0.70	'.73	0.73	0.85	0.69	0.90
DIC [µmol/kg]	43.83	39.73	30.83	19.41	16.52	9.37	12.93	5-54	18.45	0.87
Alkalinity [µmol/kg]	44.34	38.69	30.63	21.35	14.76	13.22	10.79	9.54	18.14	0.55
pH [-]	0.033	0.027	0.033	0.026	0.018	0.017	0.017	0.009	0.017	0.78

Table I.2. Basin-scale mean RMSD and correlation of phosphate, nitrate, oxygen, ammonium, silicate, DIC, alkalinity and pH (i.e., pH in total scale and in-situ condition) estimated by comparing the present qualification run and a reference vertical profile climatology based on in-situ observations.

Variables	RMSD
Nitrate [mmol/m^3]	0.41
Oxygen [mmol/m^3]	10.53
Chlorophyll [mg/m^3]	0.04
Phytoplankton carbon Biomass [mg/m3] for integral 0-200 m	0.85

Table I.3. Basin-scale mean RMSD of nitrate, oxygen chlorophyll and phytoplankton carbon biomass estimated by comparing the present qualification run and vertical profiles from BGC-Argo floats.

Variables	RMSD
EMODnet2018; pCO2 at 0-10 m	40..15
SOCAT v2; surface pCO2	49.95

Table I.4. Basin-scale mean RMSD of partial pressure of carbon dioxide in seawater (pCO2) based on the comparison with a reference vertical profile climatology and surface basin-scale mean RMSD of pCO2 based on the comparison with SOCAT dataset.

II PRODUCTION SYSTEM DESCRIPTION

II.1 Production centre details

Production centre name: Med-MFC
Production system name: Mediterranean Sea Biogeochemistry Analysis and Forecast (CMEMS name: MEDSEA_ANALYSISFORECAST_BGC_006_014)
Production Unit: Med-BIO; Istituto Nazionale di Oceanografia e di Geofisica Sperimentale - OGS (Italy)

Description
The biogeochemical analysis and forecasts for the Mediterranean Sea at 1/24° of horizontal resolution (ca. 4 km) are produced by means of the MedBFM3.2 model system. MedBFM3.2, which is run by OGS (IT), includes the transport model OGSTMv4.3 coupled with the biogeochemical flux model BFMv5.1 and the variational data assimilation module 3DVAR-BIOv3.3. The biogeochemical MedBFM system, which is off-line coupled with the NEMO-OceanVar model (MEDSEA_ANALYSISFORECAST_PHY_006_013 product run by CMCC), produces seven days of analysis (weekly on Tuesday) with the assimilation of surface chlorophyll (CMEMS-OCTAC NRT product) and of vertical profiles of chlorophyll and nitrate (BGC-Argo floats provided by CORIOLIS DAC). One day of hindcast and ten days of forecast are produced daily.
The analysis and forecast products are released after completion of the Med-PHY workflow (Fig II.1). On Tuesday, the workflow consists of 7 days of analysis (-8 to -2), one day of hindcast (-1) and 10 days of forecast (0 to 9). From Wednesday to Monday, the workflow consists of one day of hindcast and 10 days of forecast. The data assimilation cycle (Tuesday run) uses the satellite chlorophyll (i.e., a composite average in the range of ±3 days) at 12:00 UTC of the Monday of the previous week (day -8) and the in situ vertical profiles of chlorophyll and nitrate at 12:00 UTC from day -8 to day -2. On day -8, satellite and float assimilation is performed disjointedly.

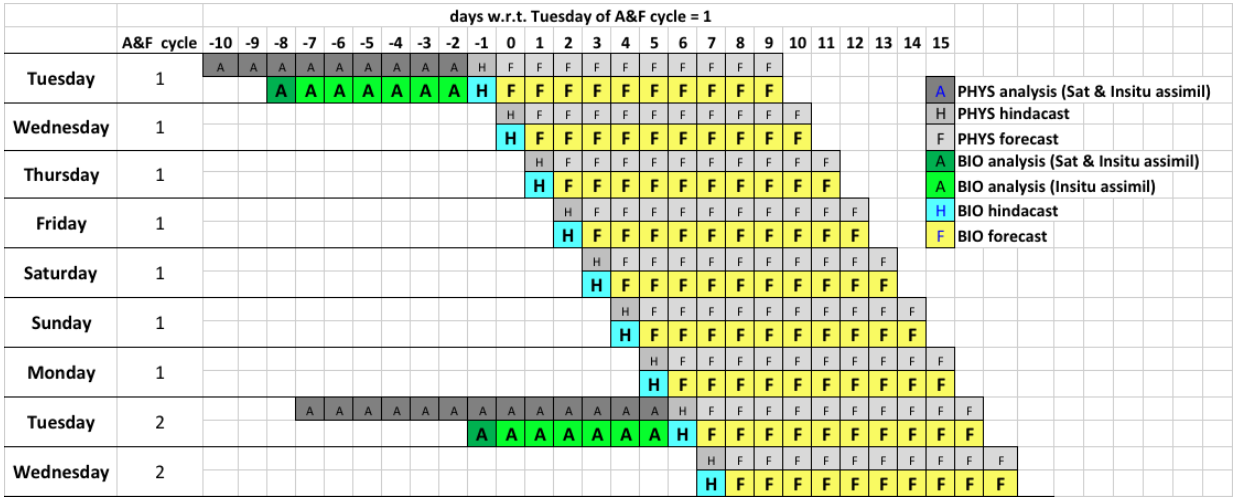

Figure II.1. Scheme of the functioning of the Med-MFC-biogeochemistry system (Med-BIO) for analysis and forecast. Dark, regular and light grey boxes represent the days of analysis, hindcast and forecast of the Med-PHY. Green, blue and yellow boxes represent the days of analysis, hindcast and forecast of the Med-BIO workflow. The production week days when the workflow is executed are reported on the left column.

II.2 Description of the MedBFM3.2 model system

The Med-biogeochemistry products are provided by the MedBFM version 3.2 model system. MedBFM3.2 consists of the coupled physical-biogeochemical OGSTM-BFM model and the 3DVarBio assimilation scheme (Salon et al., 2019; Lazzari et al., 2010, 2012, 2016; Cossarini et al., 2015; Teruzzi et al., 2014, 2018, 2019; Cossarini et al., 2019). The OGSTM-BFM is designed with a transport model based on the OPA system and a biogeochemical reactor featuring the Biogeochemical Flux Model (BFM), while 3DVarBio is the data assimilation scheme for the correction of phytoplankton functional type and nutrient (i.e., nitrate and phosphate) variables using surface chlorophyll from satellite observations and vertical profiles of chlorophyll and nitrate from BGC-Argo floats (Fig.II.2).

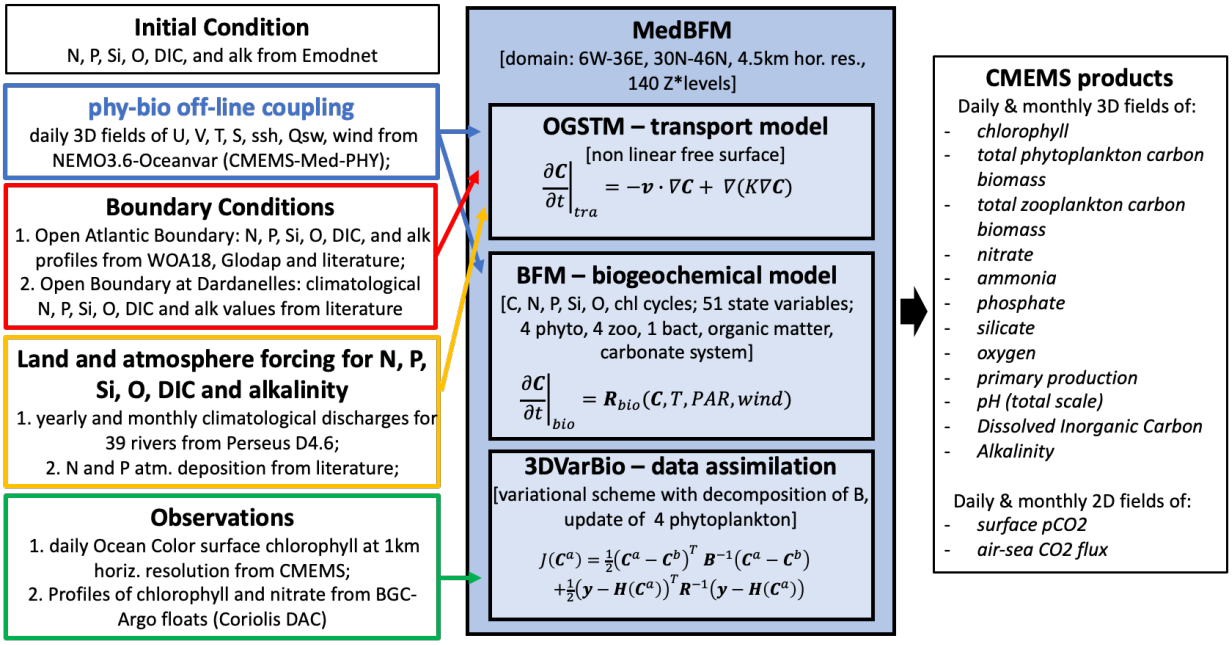

Figure II.2. The Med-BIO model system and interfaces with other components of CMEMS system.

The OGSTMv4.3 transport model is a modified version of the OPA 8.1 transport model (Foujols et al., 2000), which resolves the advection, the vertical diffusion and the sinking terms of the tracers (biogeochemical variables). The OGSTM resolves the free surface and variable volume layer effects on the transport of tracers being fully consistent with NEMO3.6 vvl output provided by Med-PHY. The horizontal meshgrid is based on 1/24° longitudinal scale factor and on 1/24°cos(ϕ) latitudinal scale factor. The vertical discretization accounts for 141 vertical z-levels, with 125 active in the Mediterranean domain: 35 in the first 200 m depth, 60 between 200 and 2000 m, 30 below 2000 m. The temporal scheme of OGSTM is an explicit forward time scheme for the advection and horizontal diffusion terms, whereas an implicit time step is adopted for the vertical diffusion.

The sinking term is a vertical flux, which acts on a sub-set of the biogeochemical variables (particulate matter and phytoplankton groups). Sinking velocity is fixed for particulate matter and dependent on nutrients for two phytoplankton groups (diatoms and dinoflagellates).

The daily mean physical dynamics (i.e. the forcing fields) are off-line coupled with the transport-biogeochemical processes, and are pre-computed by the Med-PHY model system, which supplies the temporal evolution of the fields of horizontal and vertical current velocities, vertical eddy diffusivity, potential temperature, salinity, sea surface height in addition to surface data for solar shortwave irradiance and wind stress (see section on upstream data and boundary conditions for further details).

The features of the biogeochemical reactor BFM (Biogeochemical Flux Model) have been chosen to target the energy and material fluxes through both “classical food chain” and “microbial food web” pathways (Thingstad and Rassoulzadegan, 1995), and to take into account co-occurring effects of multi-nutrient interactions. Both of these factors are very important in the Mediterranean Sea, wherein microbial activity fuels the trophodynamics of a large part of the system for much of the year and both phosphorus and nitrogen can play limiting roles (Krom et al., 1991; Bethoux et al., 1998).
BFMv5 model (i.e., the official version released by www.bfm-community.eu) describes the biogeochemical cycles of 4 chemical compounds: carbon, nitrogen, phosphorus and silicon through the dissolved inorganic, living organic and non-living organic compartments (Figure II.3). The model includes nine plankton functional types (PFTs). Phytoplankton PFTs are diatoms, flagellates, picophytoplankton and dinoflagellates. Heterotrophic PFTs consist of carnivorous and omnivorous mesozooplankton, bacteria, heterotrophic nanoflagellates and microzooplankton. Nitrate and ammonia are considered for the dissolved inorganic nitrogen. The non-living compartment consists of 3 groups: labile, semilabile and refractory organic matter. The first two are described in terms of carbon, nitrogen, phosphorus and silicon contents. The model is fully described in Lazzari et al. (2012, 2016), where it was corroborated for chlorophyll, primary production and nutrients in the Mediterranean Sea for a 1998-2004 simulation. The BFM model is also coupled to a carbonate system model (Cossarini et al., 2015, Melaku Canu et al., 2015), which consists of three prognostic state variables: alkalinity (ALK) and dissolved inorganic carbon (DIC) and particulate inorganic carbon (PIC) which are driven by biological processes (i.e. photosynthesis, respiration, precipitation and dissolution of CaCO3, nitrification, denitrification, and uptake and release of nitrate, ammonia and phosphate by plankton cells) and physical processes (exchanges at air-sea interface and dilution-concentration due to evaporation minus precipitation process). In particular, PIC precipitation occurs in correspondence of phytoplankton mortality and grazing by zooplankton (Orr et al., 2017). Dissolution of PIC occurs for oversaturated calcite conditions according to Berner and Morse (1972). pCO2 and pH (expressed in total scale) are calculated at the in-situ temperature and pressure conditions using Mehrbach et al. (1973) refit by Lueker et al. (2000). Formulations for the kinetic constants of thermodynamic equilibrium of carbon acid dissociation as prescribed in Orr and Epitaloni (2015). CO2 air-sea gas exchange formulation is computed according to updates provided by Wanninkhof (2014).

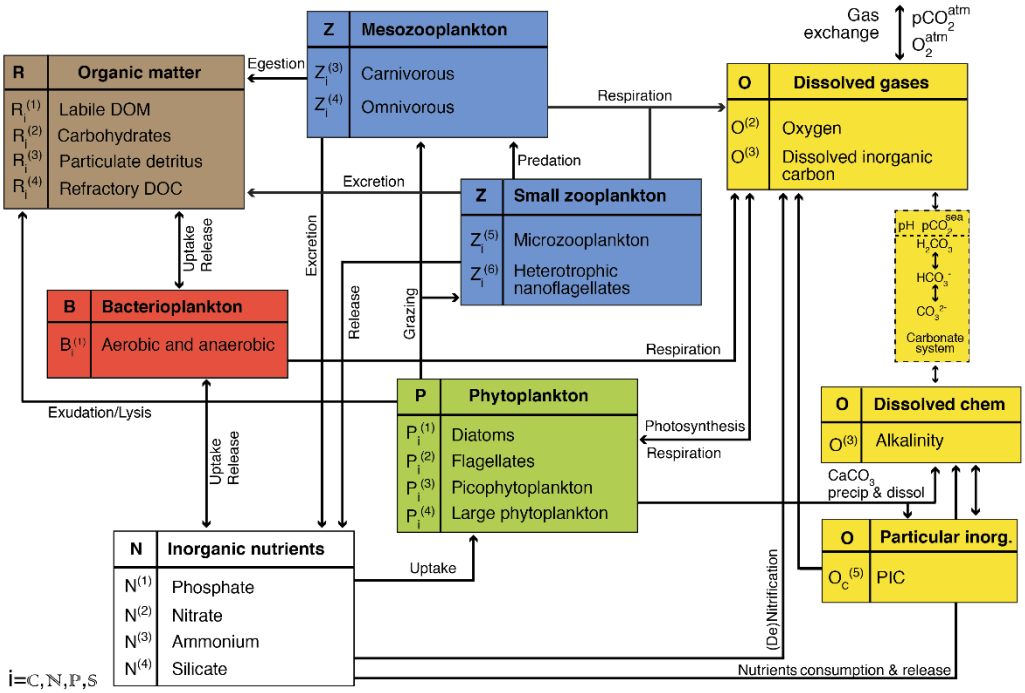

Figure II.3. Scheme of the state variables and significant processes of the upgraded Biogeochemical Flux Model (BFM) version 5.

II.3 Description of the Data Assimilation scheme

1. The data assimilation of the surface chlorophyll concentration and of the vertical in situ profiles of chlorophyll and nitrate is performed through a variational scheme (3DVAR-BIOv3.3) during the 7 days of analysis of the Tuesday run of Fig. II.1 (see details on 3DVarBio in Teruzzi et al., 2014, 2018, 2019 and Cossarini et al., 2019). The surface chlorophyll concentration is provided by satellite observations produced by the OCTAC; the in situ vertical profiles of chlorophyll and nitrate are provided by BGC-Argo floats data made available by CORIOLIS DAC.
2. The data assimilation corrects the four phytoplankton functional groups (17 state variables including carbon, chlorophyll, nitrogen phosphorus and silicon internal quotas) and two nutrients (i.e., phosphate and nitrate) of the BFM. The 3DVarBio scheme decomposes the background error covariance matrix using a sequence of different operators that account separately for the vertical covariance (Vv), the horizontal covariance (Vh) and the covariance among biogeochemical variables (Vb). Vv is defined by a set of synthetic profiles that are evaluated by means of an Empirical Orthogonal Function (EOF) decomposition applied to a validated multi-annual 1998-2015 run (Teruzzi et al., 2018). EOFs are computed for 12 months and 30 coastal and open sea sub-regions in order to account for the variability of 3D chlorophyll and nitrate anomaly fields. The assimilation is performed from 0 to 600 meters for chlorophyll and nitrate profiles, and from 0 to 200 meters for satellite chlorophyll. Vh is built using a Gaussian filter whose correlation radius modulates the smoothing intensity. A non-uniform and direction-dependent correlation radius has been implemented (Teruzzi et al., 2018, Cossarini et al., 2019). Vb operator consists of monthly and sub-region varying covariances among the biogeochemical variables. Further, Vb operator maintains the ratio among the phytoplankton groups and preserves the physiological status of the phytoplankton cells (i.e. preserve optimal values for the internal chlorophyll and carbon nutrients quota).

3. The operational workflow of the analysis run (the Tuesday row in Fig. II.1) consists of a sequence of seven days of assimilation: the satellite surface chlorophyll map (i.e., a composite average in the range of ±3 days) is assimilated at 12:00 UTC of the previous Monday (i.e., day -8) and the insitu vertical profiles of chlorophyll and nitrate are assimilated at 12:00 UTC from day -8 to day -2. A pre-processing quality control is applied prior of the assimilation:
    - Ocean Color chlorophyll daily data (±3 days maps of L3 CMEMS product) are checked for spikes (i.e., values whose anomalies is higher than 3 times the daily climatology standard deviation), temporally averaged (i.e., geometric means) and spatially interpolated (i.e., linear operator) on the model grid. Surface chlorophyll values with misfit higher than 10 mg/m^3 are rejected.
    - BGC-Argo float chlorophyll profiles (daily data from Coriolis data repository) are checked for negative values (rejection); the quenching correction (based on Xing et al., 2012) is performed by imposing a constant Chl value in the MLD (as done in LOV PQ repository; Schmechtig et al., 2018). Additionally during assimilation, if the misfit model minus observation is higher than 5 mg/m^3 the profile is rejected.
    - BGC-Argo float nitrate profiles (daily data from Coriolis data repository) are QC corrected with the CANYON neural network (Bittig et al., 2018) and profiles are rejected if surface value is higher than 3 mmol/m^3. Additionally, during assimilation, a profile is rejected if the misfit at surface is higher than 1 mmol/m^3 (i.e., condition requested for at least 5 points in the 0-50 m layer); observations in the layer 250-60 0 m are rejected if their misfits are higher than 2 mmol/m^3.

II.4 Upstream data and boundary conditions

The CMEMS–Med-MFC-Biogeochemistry system uses the following upstream data:

1. Initial conditions of biogeochemical variables are set as sub-basin (Fig. III.1) climatological profiles from a dataset (EMODnet2018_int) that integrates the in-situ aggregated EMODnet data collections (Buga et al., 2018) and the datasets listed in Lazzari et al. (2016) and Cossarini et al. (2015). A spin-up period (2 years) is carried out to reach the start date of the simulation (01/01/2019).
2. The physical ocean (current, temperature, salinity, vertical eddy diffusivity, SSH) and atmospheric (short wave radiation and wind stress) forcing daily fields are obtained from MEDSEA_ANALYSISFORECAST_PHY_006_013 produced by Med-PHY.
3. The surface chlorophyll and K_d are obtained from the satellite multi-sensor product OCEANCOLOUR_MED_CHL_L3_NRT_OBSERVATIONS_009_040 (i.e., a merged product of MODIS-AQUA, NOAA20-VIIRS, NPP-VIIRS and Sentinel3A-OLCI sensors).
4. The in situ vertical profiles of chlorophyll (Schmechtig et al., 2015) and nitrate (Johnson et al., 2018) are obtained from Coriolis Data Assembly Center (as described in Bittig et al., 2019) after QC procedures using Canyon B Neural Network (Bittig et al., 2018).
5. The biogeochemical open boundary conditions in the Atlantic Ocean at the longitude of 9°W are provided through a Dirichlet-type scheme. Climatological profiles of phosphate, nitrate, silicate, dissolved oxygen are computed averaging the World Ocean Atlas 2018 data (Garcia et al., 2018; data from https://www.nodc.noaa.gov/OC5/woa18) for the area: Lon=8°W-9°W and Lat=34°N-37°N. Nitrate and phosphate profiles are revised to preserve the N:P ratio values of 5 and 17 in the surface and subsurface layers, respectively. The oxygen profile unit was converted in mmol m^{-3} by using the seawater density profile computed from temperature and salinity data provided by the World Ocean Atlas 2018. Climatological profiles of DIC and Alkalinity are derived from the GLODAP v2 dataset (Olsen et al., 2016, 2019; data from

https://www.nodc.noaa.gov/ocads/oceans/GLODAPv2_2019/) by averaging the available insitu observations in the area: Lon=8°W-10°W, Lat=34°N-37°N. A nudging scheme is applied in the 9°W-7°W area using the same profiles to avoid numerical instability

6. The biogeochemical open boundary conditions at the Dardanelles Strait are provided through a Dirichlet-type scheme. The values of nitrate, phosphate, silicate, DIC, alkalinity at the open boundary are set to constant values using literature information (Yalcin et al., 2017; Tugrul et al., 2002; Souvermezoglou et al., 2014; Copin, 1993; Schneider et al., 2007) after a tuning based on the consistency of modelled fluxes with published flux estimates (Perseus D4.6; Yalcin et al., 2017; Tugrul et al. 2002; Copin, 1993) and modelled tracer concentrations in the northern Aegean Sea with published observations (Souvermezoglou et al., 2014; Krasakopoulou et al., 2017). A radiative condition at the open boundary is set for the other BFM tracers.
7. Atmospheric deposition rates of inorganic nitrogen and phosphorus were set according to the synthesis proposed by Ribera d'Alcalà et al. (2003) and based on measurements of field data (Loye-Pilot et al., 1990; Guerzoni et al., 1999; Herut and Krom, 1996; Cornell et al., 1995; Bergametti et al., 1992). Atmospheric deposition rates of nitrate and phosphate were assumed to be constant in time during the simulation year, but with different values for the western (580 Kt N yr^{-1} and 16 Kt P yr^{-1}) and eastern (558 Kt N yr^{-1} and 21 Kt P yr^{-1}) sub-basins. The rates were calculated by averaging the "low" and "high" estimates reported by Ribera d'Alcalà et al. (2003).
8. Terrestrial inputs of nutrient (N and P) and carbonate system variables (ALK and DIC) from 39 rivers, which are aligned with the Med-PHY configuration. The 39 rivers, as shown in Fig. III.1, are Nile, Vjosë, Seman, Buna/Bojana, Piave, Tagliamento, Soca/Isonzo, Livenza, Brenta-Bacchiglione, Adige, Lika, Reno, Krka, Arno, Nerveta, Aude, Trebisjnica, Tevere/Tiber, Mati, Volturno, Shkumbini, Struma/Strymonas, Meric/Evros/Maritsa, Axios/Vadar, Arachtos, Pinios, Acheloos, Gediz, Buyuk Menderes, Kopru, Manavgat, Seyhan, Ceyhan, Gosku, Medjerda, Asi/Orontes. For 38 rivers (except the Po River in Adriatic Sea), nitrogen and phosphorus climatological discharges (average of the 2000-2015 period) with a monthly modulation based on the monthly run-off are from the PERSEUS FP7-287600 project dataset (deliverable D4.6). For 38 rivers (except the Po River in Adriatic Sea), climatological monthly discharges of alkalinity and DIC are derived considering their typical concentrations per fresh water mass in macro coastal areas of the Mediterranean Sea (Copin, 1993; Meybeck and Ragu, 1995; Kempe et al., 1991) and the climatological monthly river water discharges from the PERSEUS dataset (Deliverable D4.6). For the Po River (Adriatic Sea), daily discharges of nutrient (N and P) and carbonate system variables (ALK and DIC) are derived from daily run-off observations (data from ARPAE regional environmental protection agency; the same data is used by Med-PHY) multiplied by the typical concentrations of the biogeochemical tracers. Typical concentrations are derived from PERSEUS dataset and aforementioned references.
9. Atmospheric pCO2 concentration is set equal to the yearly average measured at the Lampedusa station (Artuso et al., 2009) between 1992 and 2018 (http://cdiac.ess-dive.lbl.gov/ftp/trends/co2/lampedus.co2) with the present-day values extrapolated by linear regression.
10. Surface evaporation-precipitation effects on dilution and concentration of tracers at surface are directly computed by OGSTM through the non-linear free-surface z*-coordinate configuration and using directly the sea surface anomaly evolution provided by the NEMO3.6 output.

III VALIDATION FRAMEWORK

The CMEMS Med-MFC analysis and forecast system is validated through a qualification run spanning from 1-Jan-2019 to 31-Dec-2019. The products assessed are chlorophyll, phytoplankton carbon biomass, zooplankton carbon biomass, net primary production, phosphate, nitrate, ammonium, silicate, oxygen, pH, pCO2, DIC, alkalinity and surface flux of CO2.
Data availability represents an important constrain in biogeochemical model validation (Salon et al., 2019): depending on the variables, different uncertainty levels can be provided on the basis of the availability of reference data. Thus, the validation analysis provides a "degree of confirmation" (Oreskes et al., 1994) with respect to the different scales of variability derived from the available observations.
Three different levels of validation are presented for the model variables:

(1) model capability to reproduce basin wide spatial gradients, mean annual values in sub-basin and average vertical profiles based on GODAE Class1 metrics (level-1);
(2) model capability to reproduce the variability due to mesoscale and daily dynamics based on GODAE Class4 metrics (level-2; Hernandez et al., 2018);
(3) model capability to reproduce key biogeochemical processes based on specific metrics (level-3; Salon et al., 2019).

Almost all of the variables are validated with GODAE class1 metrics using a reference climatology computed using the available in situ data (i.e., reference mean annual vertical profiles for the 16 sub-basins, Appendix A) or literature reviews (level-1). Only chlorophyll, nitrate and oxygen can be validated with NRT observations (satellite and BGC-Argo floats) available for the year 2019 (levels 2 and 3). Validation of phytoplankton carbon biomass, that uses BGC-Argo data, should be considered cautiously since the uncertainty of the bbp700 – phytoplankton biomass relationship and the relatively low availability of BGC-Argo optical sensors.

Model chlorophyll data are compared with multi-sensor satellite chlorophyll from CMEMS OCTAC OCEANCOLOUR_MED_CHL_L3_NRT_OBSERVATIONS_009_040 using metrics that refer to the "misfits" computed as the differences between satellite chlorophyll (7-days composite map) and the model output before the data assimilation execution (every 7 days). Thus, the metrics (BIAS and Root Mean Square of the differences between model output and satellite observations, RMSD) estimate the skill performance of the forecast (i.e. uncertainty after seven days of free simulation) and are reported as time series for the sub-basins of Fig. III.1. Chlorophyll model outputs are also compared with in-situ observations of chlorophyll concentration from the BGC-Argo floats dataset (Fig. III.4) before the data assimilation execution. BIAS, RMSD, correlation along with novel metrics (e.g., deep chlorophyll maximum depth, integral values and thickness of the layer of the winter bloom) between BGC-Argo profiles and the matching model output profiles (i.e. the model output at the time and location of the in-situ profile) are reported as time series for selected layers (Table III.1) and sub-basins (Fig. III.1) and as average statistics computed from all the matching pairs of model and observation profiles for each sub-basin.

Model net primary production data are compared with literature data based on multi-annual simulations (Lazzari et al., 2012), satellite model (Bosc et al., 2004; Colella, 2006), in-situ estimates (Siokou-Frangou et al., 2010).

Model phosphate, nitrate, ammonium, silicate, dissolved oxygen, DIC, alkalinity, pH in total scale and pCO2 data are compared with a EMODnet_int climatology, i.e., aggregated EMODnet dataset (Buga et al., 2018) integrated with datasets listed in Lazzari et al. (2016) and Cossarini et al. (2015), and resumed in Tables III.2 and 3, based on the sub-basins of Fig. III.1. The validation of model variables considers

consistency both with the vertical profiles for each sub-basin and with reference values at the layers listed in Table III.1. The product quality metric is the RMSD between the model and climatology. An additional qualitative comparison for nitrate and phosphate is performed using the World Ocean Atlas (WOA2013) climatological dataset. Regarding the carbonate system variables, the most observed variables are DIC and alkalinity (about 5300 observations), while pH was collected only in less than 30% of the samplings. Thus, pH and pCO2 have been reconstructed using CO2sys software (Lewis and Wallace, 1998) with available DIC, ALK and other regulatory information (i.e., temperature, salinity and concentration of phosphate and silicate).

Nitrate and dissolved oxygen model outputs are also compared with BGC-Argo floats data (Fig. III.4) to compute the BIAS, RMSD, correlation and novel metrics (integrated vertical values and depth of nutricline) between BGC-Argo profiles and the model output profiles before the data assimilation execution. The metrics are reported as time series for selected layers (Table III.1); and for sub-basins (Fig. III.1); and as average statistics computed from all the matching pairs of model and observation profiles for each sub-basin.

Phytoplankton biomass expressed as carbon represents the sum of the carbon content of the four phytoplankton functional groups of BFM model (i.e, diatoms, picoplankton, nanoflagellates, dinoflagellates). Phytoplankton carbon biomass is compared with BGC-Argo floats dataset of bbp700 from Coriolis DAC (Schmechtig et al., 2018). Data of bbp700 is converted to carbon biomass using the relationship proposed by Bellacicco et al. (2019). Given the scarce and sparse availability of such optical measurements and the uncertainty of optical-biomass relationship only an indicative value can be provided by this level-2 validation framework.

Zooplankton biomass expressed as carbon represents the sum of the carbon content of the four zooplankton groups of BFM model (i.e., heterotrophic nano flagellates, microzooplankton and 2 groups of mesozooplankton). Zooplankton biomass is compared with very few and sparse estimations retrieved from literature. This validation represents only a rough verification of zooplankton biomass consistency with respect to carbon cycle within the ecosystem. Most of the observations is reported in terms of integrated values 0-20 0 m.

Moreover, pCO2 has been validated considering the SOCAT v6 Data Collection (Bakker et al., 2016). The dataset consists of surface ocean fugacity (fCO2) measurements (up to 6500 observations) in the Mediterranean Sea covering the period 1998-2016 (Fig. III.5). Fugacity measurements are converted to partial pressure measurements using standard formula. The spatial distribution does not cover uniformly the Mediterranean sub-basins and temporal coverage is limited to 2016. Therefore, the comparison is organized by calculating a monthly climatology for the Mediterranean sub-basins (i.e., only 10 out of 16 sub-basins have reliable data). The product quality metric is the RMSD between the model and climatology.

Surface flux of CO2 has been validated by evaluating the consistency of the model results with previously published maps of mean annual values (e.g., the Ocean State Report; von Schuckmann et al., 2018).

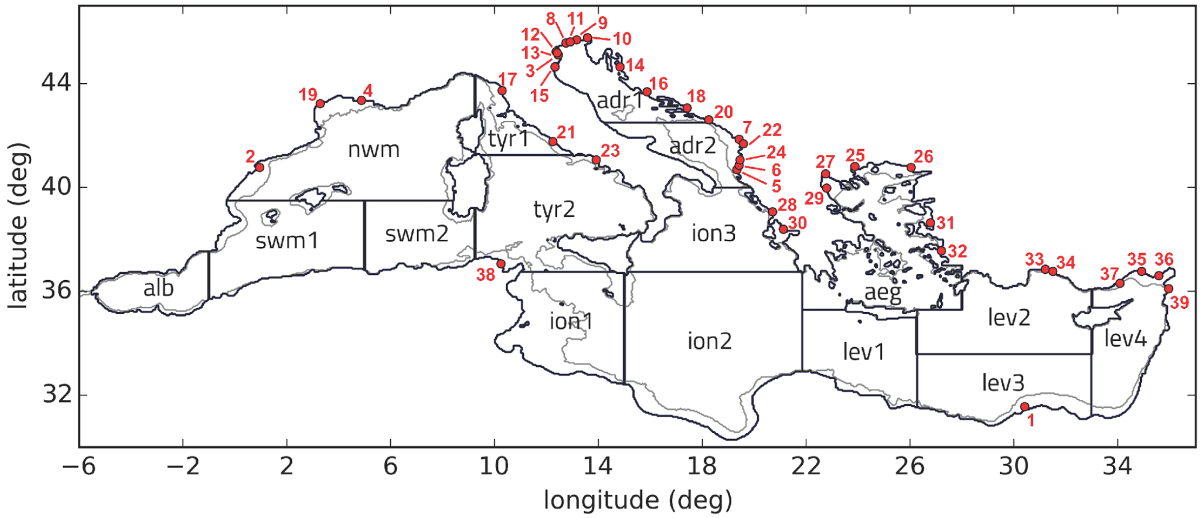

Figure III.1. Subdivision of the model domain in sub-basins used for the validation of the qualification run. According to data availability and to ensure consistency and robustness of the metrics, different subsets of the sub-basins or some combinations among them can be used for the different metrics: lev = lev1+lev2+lev3+lev4; ion = ion1+ion2+ion3; tyr = tyr1+tyr2; adr = adr1+adr2; swm = swm1+swm2. The grey line defines the bathymetric contour at 200 m. Red dots with numbers correspond to main river mouth positions: Nile (1), Ebro (2), Po (3), Rhone (4), Vjosë (5), Seman (6), Buna/Bojana (7), Piave (8), Tagliamento (9), Soca/Isonzo (10), Livenza (11), Brenta-Bacchiglione (12), Adige (13), Lika (14), Reno (15), Krka (16), Arno (17), Nerveta (18), Aude (19), Trebisjnica (20), Tevere (21), Mati (22), Volturno (23), Shkumbini (24), Struma/Strymonas (25), Meric/Evros/Maritsa (26), Axios/Vadar (27), Arachtos (28), Pinios (29), Acheloos (30), Gediz (31), Buyuk Menderes (32), Kopru (33), Manavgat (34), Seyhan (35), Ceyhan (36), Gosku (37), Medjerda (38), Asi/Orontes (39).

Layer 1	Layer 2	Layer 3	Layer 4	Layer 5	Layer 6	Layer 7	Layer 8
0-10	10-30	30-60	60-100	100-150	150-300	300-600	600-1000

Table III.1. Vertical layers (in m) considered for the validation of the qualification run products.

Dataset name	Period	Area
EMODnet (2018)	**1997-2016**	**Mediterranean**
SINAPSI 3,4	2002-2003	Eastern Med.
JGOFS-FRANCE	1999	Western Med.
BIOPT 6	2006	Eastern Med.
DYFAMED	1998-2007	North-Western Med.
RHOFI 3,2,1	2001-2003	Ligurian Sea
NORBAL 1, 2, 3, 4	2000-2003	Algerian Sea
CIESM SP1,SP2,SP3	1998-2006	Mediterranean
MELISSA	2004, 2007	Western Med.
MEDGOOS 2, 3, 4, 5	2001-2002	Mediterranean
METEOR 51	2001	Western Med.
REGINA MARIS, GARCIA DEL CID	Apr, Sep 2008	Alboran Sea
SESAME ADRIATIC SEA	Apr, Sep 2008	Adriatic Sea
CARBOGIB 01,02,03,04,05,06	2005-2006	Alboran Sea, Gibraltar Strait
METEOR 84/3	2011	Mediterranean

Table III.2. Nutrient and Oxygen dataset EMODnet2018_int: integration of the aggregated EMODnet data collections (Buga et al., 2018) and the datasets listed in Lazzari et al. (2016).

Name	Variables	Period	Location	# data	Reference
METEOR51	DIC, ALK, anc. vars	Oct-Nov 2001	TransMed	253	Schneider et al., 2007
BUOM2008	DIC, ALK, anc. vars	June-July 2008	TransMed	567	Touratier et al., 2011
PROSOPE	DIC, pH@25, anc. vars	Sep-Oct 1999	West Med	188	Begovic and Copin, 2013
METEOR 84/3	DIC, ALK, pH@25, anc. vars	Apr 2011	TransMed	845	Tanhua, et al., 2012.
SESAME-EGEO	DIC, ALK, T,S	Apr and Sep 2008	Aegean Sea	265	http://isramar.ocean.org.il/PERSEUS_Data/
SESAME regina_maris	ALK, pH@25, anc. vars	Apr 2008	Alboran Sea	254	http://isramar.ocean.org.il/PERSEUS_Data/
SESAME Garcia del Cid	ALK, pH@25, anc. vars	Sep 2008	Alboran Sea	331	http://isramar.ocean.org.il/PERSEUS_Data/
SESAME Adriatic	ALK, pH@25, anc. vars	Apr and Sep 2008	Adriatic Sea	333	http://isramar.ocean.org.il/PERSEUS_Data/
CARBOGIB	ALK, DIC, pH@25, anc. vars	May, Sept, Dec 2005; Mar, May, Dec 2006	Alboran Sea	229	Huertas, 2007a
GIFT	ALK, DIC, pH@25, anc. vars	Jun, Nov 2005	Alboran Sea	30	Huertas, 2007b
DYFAMED Station	ALK, DIC	Almost monthly from 1999 to 2004	North West Med	707	Copin-Montegut and Begovic, 2002
MEDSEA 2013	DIC, ALK, T,S	May 2013	TransMed	462	Goyet et al., 2015
MOOSE dyfamed MOOSE-GE 2013-2016	DIC, ALK, T,S	2013-2016	North West Med	700	EMODnet, 2018

Table III.3. Dissolved Inorganic Carbon, alkalinity, pH and pCO2 dataset EMODnet2018_int: integration of the aggregated EMODnet data collections (Buga et al., 2018) and the datasets listed in Cossarini et al. (2015). “TransMed” refers to the scientific cruise that covered the Mediterranean Sea from the Western sub-basin to the Eastern sub-basin; “anc. vars” refers to ancillary variables (T, S); “pH@25” refers to pH reported at 25°C.

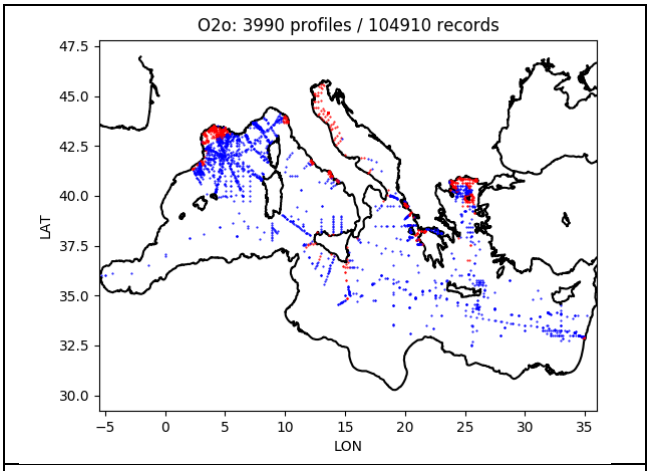

Figure III.2. Map of gathered data of oxygen through in EMODnet2018_int dataset. Nutrients (with the exception of ammonium) have similar maps. Blue dots represent the open sea data used to build climatology.

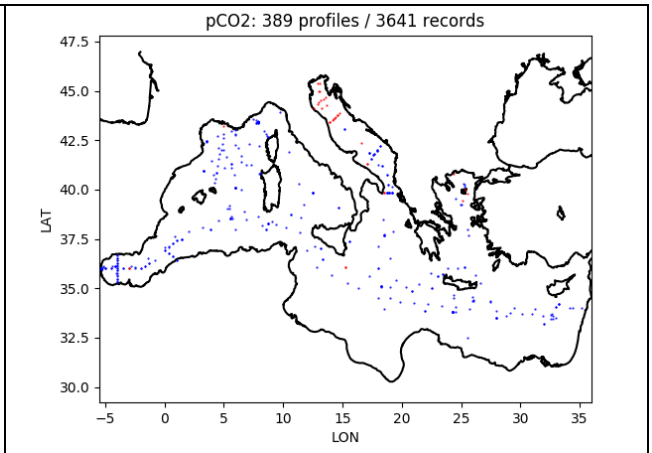

Figure III.3. Map of gathered data of alkalinity through in EMODnet2018_int dataset. DIC, pH and pCO2 have similar maps. Blue dots represent the open sea data used to build climatology.

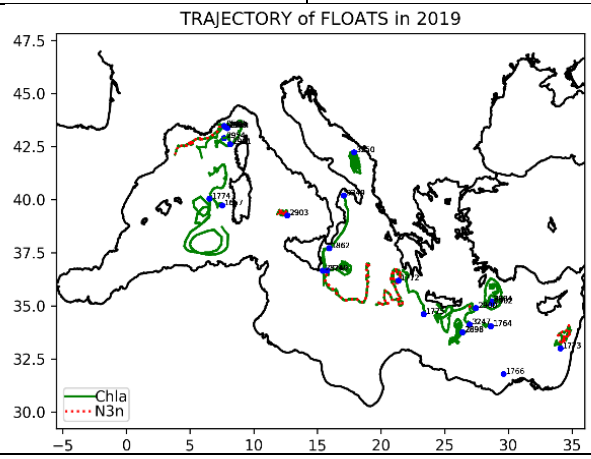

Figure III.4. Trajectories of 30 BGC-Argo floats in 2019 (i.e., 24 oxygen, 17 chlorophyll and 10 nitrate sensors). Data quality described in Bittig et al. (2019).

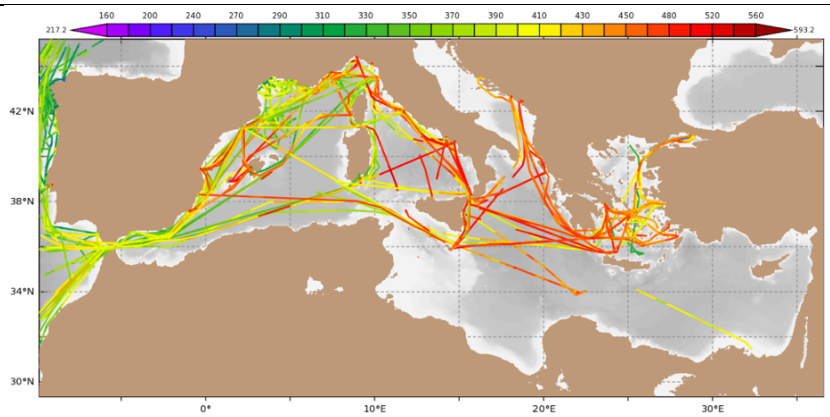

Figure III.5. Map of surface fCO2 observations from the SOCAT dataset for the period 1998-2016.

IV VALIDATION RESULTS

IV.1 Chlorophyll

Modelled chlorophyll is compared with satellite data in Fig. IV.1.1 (averaged annual maps of surface chlorophyll and of RMSD between model and satellite) and Fig. IV.1.2 (time series of weekly mean surface chlorophyll concentration for selected sub-basins). Time series of BIAS and RMS of the differences are plotted in Fig. IV.1.3 for selected sub-basins. Their seasonal averages, which are computed for both logarithm and natural values, are reported in Tab. IV.1.1 and IV.1.2 for open sea and coastal areas, respectively. The coastal areas limit is defined by the model grid isobath at 200 m. It is well known that the Mediterranean Sea is quite heterogeneous, with sub-basins characterized by different biogeochemical dynamics. The general features, widely described in literature and shown in the maps of Fig. IV.1 and in the time series of Fig. IV.2, are the higher concentrations and larger seasonal cycles that characterize the western sub-basins with respect to the eastern ones. The results of the qualification run are thus consistent with satellite observations (Tab. IV.1 and IV.2).
In the open sea areas, western sub-basins have higher uncertainty (i.e. higher RMSD, Fig. IV.3) than the eastern sub-basins, however these values never exceed 0.10 mg/m^3 (Tab. IV.1). The highest value of RMSD is in the ALB where the variability is high. In general, uncertainties are slightly higher during winter (Fig. IV.3 and Table IV.1) because the variability of the chlorophyll is also higher in winter than during the summer period. The value of the RMSD over the Mediterranean Sea, considering the 2019 average, is 0.04 and 0.001 mg/m^3 for winter and summer, respectively, while BIAS is 0.02 mg/m^3 in winter and 0.01 mg/m^3 in summer (see Tab. IV.1).
Since CMEMS version at Q2/2018, the MedBFM system assimilates chlorophyll data on both coastal and open-sea areas. Thus, MedBFM provides a good model performance also in the coastal areas (see Tab. IV.2). In these areas, the model underestimates the satellite product of about 0.05 mg/m^3 and 0.07 in winter and summer, respectively, and the mean RMSD is about 0.29 mg/m^3 and 0.33 mg/m^3, with higher values (between 0.4 and 0.6 mg/m^3) in the Adriatic sub-basins and in the areas close to the Gabes Gulf (ION1, summer) and the Nile River mouth (LEV3). In particular, the peak of RMSD in LEV3 is due to an underestimation of the very local fertilization effect of the Nile input that might be indicating an underestimation of the nutrient input from the PERSEUS project dataset.
Consistently with Fig. IV.3 and Tables IV.1 and IV.3, Fig. IV.1 (bottom) shows that the highest uncertainty values (i.e., RMSD computed for each grid cell) are located in coastal and transitional areas (i.e., Alboran Sea, western Sicily channel) and areas characterized by surface winter bloom (e.g., Gulf of Leon, Rhodes gyre).

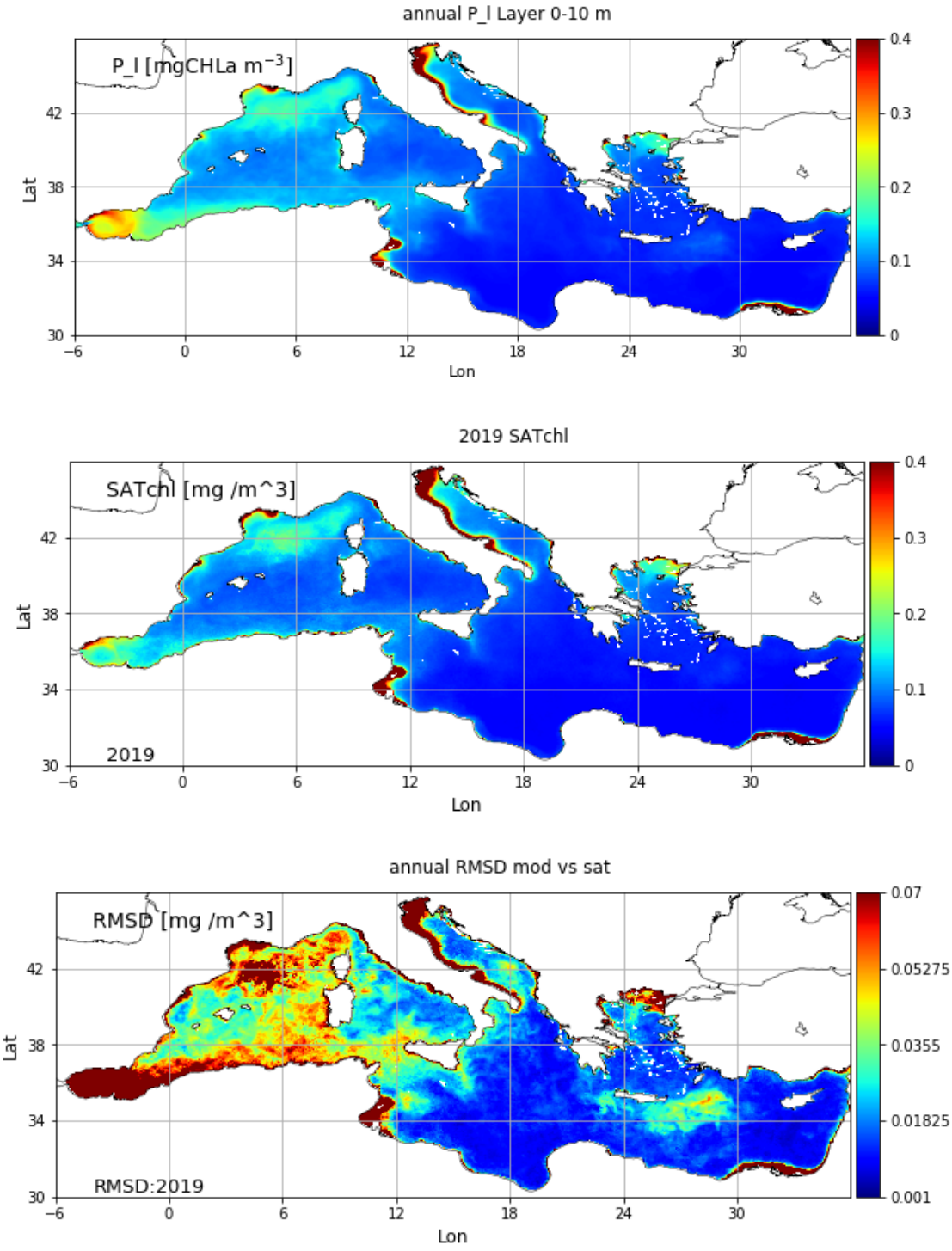

Figure IV.1.1 2019 averaged annual maps of surface chlorophyll from qualification run (top) and from NRT multi-sensor satellite (middle); 2019 map of RMSD between the qualification run and satellite data (bottom). The average is computed considering the year 2019, and the layer 0-10 m for the model results.

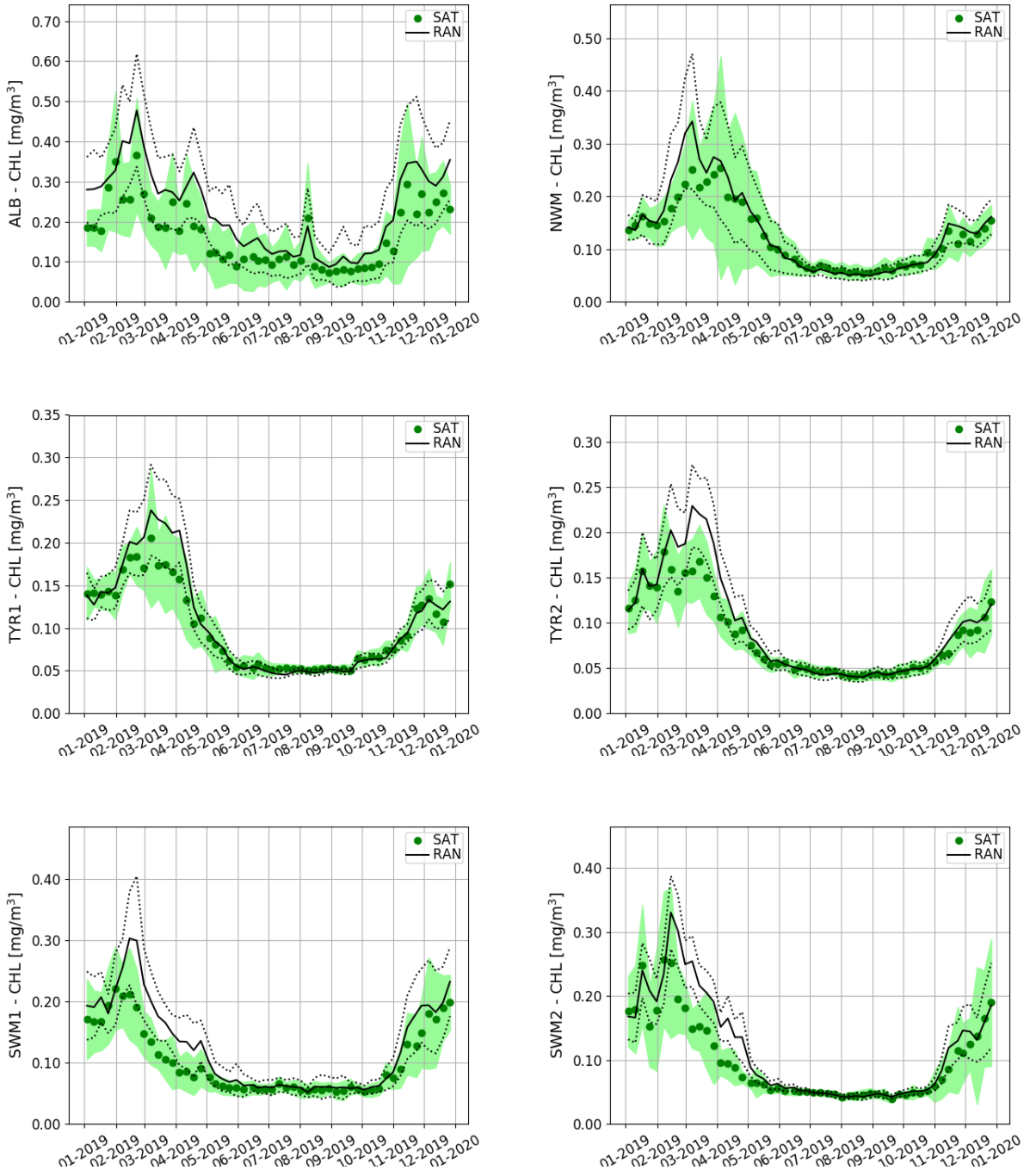

Figure IV.1.2. Time series of the weekly qualification run mean surface chlorophyll concentration of open sea (black solid line, RAN) with the spatial standard deviation (STD, dotted black line) and the NRT multi-sensor satellite data (green dots, SAT) with its STD (shaded green area) for 14 of the 16 sub-basins of Fig. III.1. Model data (sub-surface 0-1 0 m layer) and satellite data are reported only for open sea areas (continues overleaf).

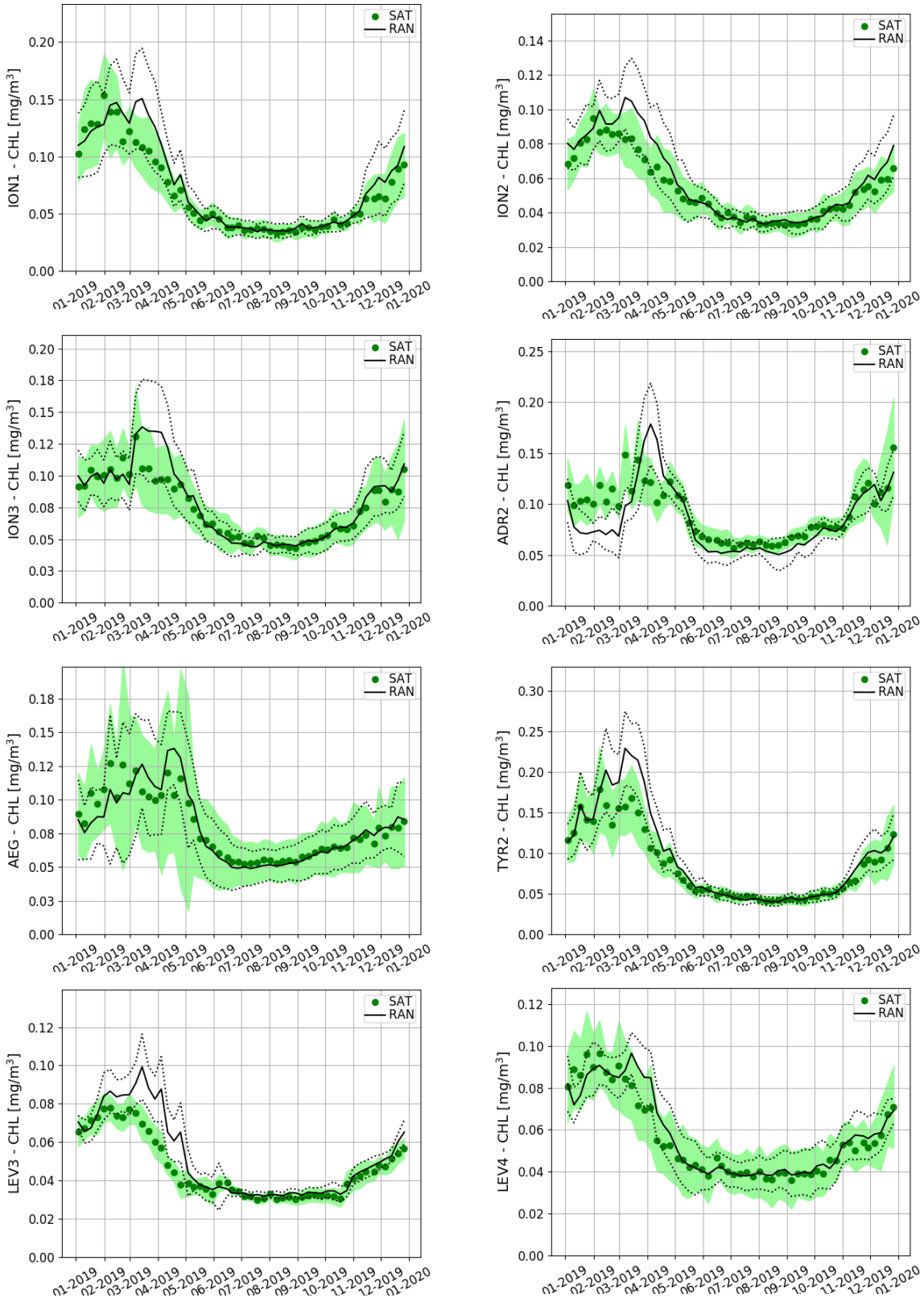

Figure IV.1.2. Same as above.

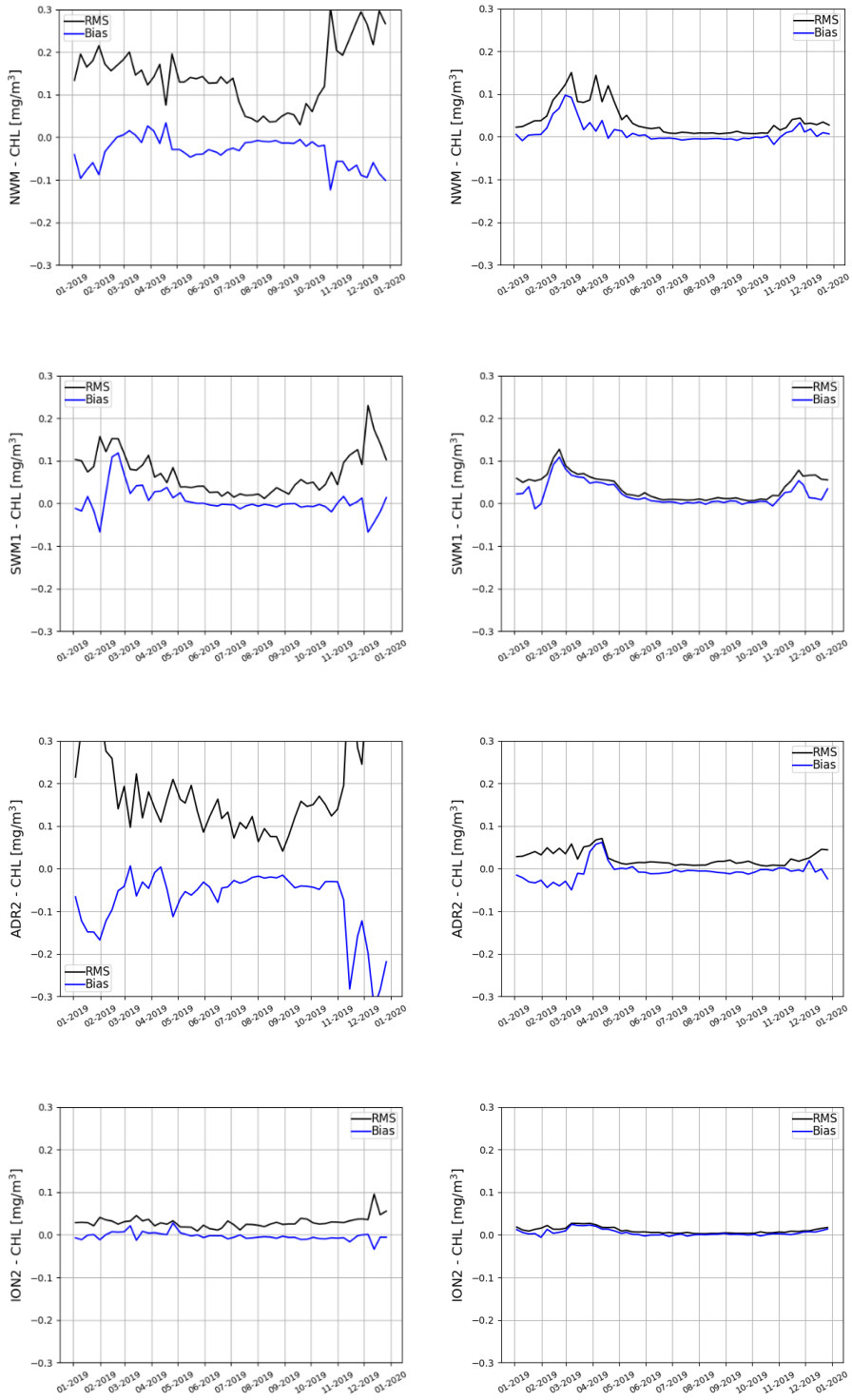

Figure IV.1.3. Weekly time series of BIAS (mod-ref; blue) and RMSD (black) metrics computed for 5 of the 16 Mediterranean sub-basins reported in Fig. III.1. Computation of BIAS (left) and RMSD (right) is based on weekly mean surface chlorophyll concentration referred to the coastal (left) and the open sea (deeper than 200 m, right) areas as shown by the Fig. III.1.

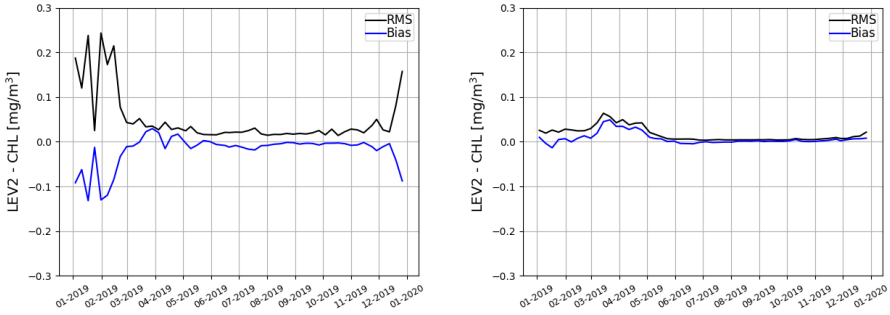

Figure IV.1.3. (continue) Same as above.

OPEN SEA	Surface (0-10 m) chlorophyll Mod-Sat [mg/m^3]				Surface (0-10 m) chlorophyll log_{10}(Mod)-log_{10}(Sat)			
	RMSD		BIAS		RMSD		BIAS	
	win	sum	win	sum	win	sum	win	sum
alb	0.14	0.06	0.09	0.03	0.21	0.17	0.15	0.10
swm1	0.07	0.01	0.05	<0.005	0.18	0.06	0.14	0.02
swm2	0.09	0.01	0.05	<0.005	0.19	0.05	0.13	0.01
nwm	0.08	0.01	0.03	<0.005	0.15	0.06	0.07	-0.03
tyr1	0.05	0.01	0.02	<0.005	0.12	0.05	0.05	-0.02
tyr2	0.05	0.01	0.03	<0.005	0.12	0.05	0.08	-0.01
adr1	0.03	0.01	0.01	-0.01	0.09	0.06	0.02	-0.05
adr2	0.04	0.01	-0.01	-0.01	0.17	0.12	-0.07	-0.07
aeg	0.03	0.01	<0.005	<0.005	0.11	0.05	0.00	-0.02
ion1	0.03	<0.005	0.01	<0.005	0.10	0.04	0.05	0.01
ion2	0.02	<0.005	0.01	<0.005	0.09	0.05	0.06	<0.005
ion3	0.03	0.01	0.01	<0.005	0.10	0.05	0.04	-0.01
lev1	0.03	0.00	0.02	<0.005	0.14	0.05	0.10	<0.005
lev2	0.04	0.01	0.02	<0.005	0.14	0.05	0.08	<0.005
lev3	0.02	<0.005	0.01	<0.005	0.11	0.05	0.08	0.01
lev4	0.02	0.01	<0.005	<0.005	0.09	0.07	0.02	0.01
Med ave	**0.05**	**0.01**	**0.02**	**<0.005**	**0.13**	**0.06**	**0.06**	**<0.005**

Table IV.1.1. Mean RMSD [mg/m^3] and BIAS [mg/m^3] between surface chlorophyll model maps and satellite maps referred to open sea areas (deeper than 200 m) for the period January – December 2019. On the right side, the skill indexes are computed on the log-transformed model and satellite chlorophyll. Winter (win) corresponds to January to April, summer (sum) corresponds to June to September.

COAST	Surface (0-1 0 m) chlorophyll Mod-Sat [mg/m^3]				Surface (0-1 0 m) chlorophyll log_{10}(Mod)-log_{10}(Sat)			
	RMSD		BIAS		RMSD		BIAS	
	win	sum	win	sum	Win	sum	Win	sum
alb	0.21	0.07	0.06	0.01	0.22	0.15	0.11	0.05
swm1	0.10	0.03	0.03	-0.01	0.18	0.10	0.10	-0.01
swm2	0.25	0.04	-0.01	0.00	0.22	0.11	0.06	-0.01
nwm	0.16	0.08	-0.02	-0.02	0.18	0.12	0.02	-0.04
tyr1	0.20	0.09	-0.05	-0.02	0.20	0.16	-0.03	-0.07
tyr2	0.19	0.07	-0.01	-0.01	0.20	0.13	0.03	-0.02
adr1	0.35	0.50	-0.09	-0.16	0.15	0.20	-0.03	-0.13
adr2	0.22	0.11	-0.08	-0.03	0.17	0.14	-0.05	-0.08
aeg	0.19	0.07	-0.03	-0.01	0.15	0.09	-0.01	-0.04
ion1	0.32	0.79	-0.06	-0.18	0.17	0.23	0.00	-0.08
ion2	0.03	0.02	0.00	-0.01	0.11	0.13	0.02	-0.04
ion3	0.08	0.03	-0.02	-0.01	0.15	0.11	-0.04	-0.05
lev1	0.02	0.01	0.02	0.00	0.13	0.11	0.10	0.02
lev2	0.10	0.02	-0.04	-0.01	0.21	0.13	-0.06	-0.04
lev3	0.62	0.58	-0.29	-0.23	0.24	0.29	-0.07	-0.15
lev4	0.40	0.35	-0.15	-0.13	0.27	0.29	-0.11	-0.16
Med ave	**0.21**	**0.18**	**-0.05**	**-0.05**	**0.18**	**0.16**	**<0.005**	**-0.05**

Table IV.1.2. Mean RMSD [mg/m^3] and BIAS [mg/m^3] between surface chlorophyll model maps and satellite maps referred to coastal areas (shallower than 200 m, Fig. III.1) for the period January – December 2019. On the right side, the skill indexes are computed on the log-transformed model and satellite chlorophyll. Winter (win) corresponds to January to April, summer (sum) corresponds to June to September.

The comparison of modelled chlorophyll with the BGC-Argo floats data evaluates the skill of the MedBFM model in reproducing the temporal evolution of the vertical dynamics of the phytoplankton in the Mediterranean Sea. Thus, we provide not just the *accuracy* of the CMEMS chlorophyll product (i.e., BIAS and RMSD for selected layers and sub-basins in Figure IV.1.5 and Table IV.1.3), but also the *consistency* of the MedBFM to simulate key coupled physical-biogeochemical processes is corroborated (Figures IV.1.4 and 6 and Table IV.1.4) at the mesoscale and weekly scale. This validation framework (details in Salon et al., 2019) is based on the concept of matching a BGC-Argo float profile with the corresponding (in time and space; i.e. GODAE class 4 metric) modelled profile (Figure IV.1.4). Based on the model-float vertical match-up, specifically developed metrics are:

- surface concentration and 0-200 m vertically averaged values (4th and 5th panels of Fig. IV.1.4);
- correlation between model and BGC-Argo float profiles (6th panel of Fig. IV.1.4);
- thickness of the vertically mixed winter bloom layer (WBL, estimated between surface and the depth at which chlorophyll concentration is 10% of surface concentration during winter period, 7th panel of Fig. IV.1.4) and depth of the deep chlorophyll maximum (DCM, 7th panel of Fig. IV.1.4).

The chlorophyll BIAS and RMSD metrics are reported as time series for selected layers and aggregated sub-basins in Figure IV.1.5, then averaged over year 2019 in Table IV.1.3. These metrics comparing model and BGC-Argo floats are reported operationally every week in the thematic regional validation webpage medeaf.inogs.it/nrt-validation, and show that the model has stable performance as long as the number of available BGC-Argo floats remains constant.
Table IV.1.3 shows that the RMSD is of the order of 0.03-0.09 mg/m^3 at the surface and 0.05-0.07 mg/m^3 in the layer 60-100 m. It is worth to note that, in general, the modelled surface chlorophyll slightly

overestimates the satellite data, especially in the western basins (BIAS in Table IV.1 and Fig IV.1.1) and underestimates the BGC-Argo float data at surface (0-10 m BIAS in Tab. IV.1.3). While this might point out an issue of consistency between the estimates of chlorophyll from satellite and BGC-Argo, it reinforces the very good performance of the MedBFM model, which lies in between the two observing systems.

As an example of the novel metrics development, the Hovmoller diagrams of chlorophyll (2nd and 3rd panels of Fig. VI.1.4) show the very good qualitative agreement of the MedBFM model with the BGC-Argo floats in reproducing the temporal succession of the winter vertically mixed blooms, the onset and temporal dynamics of the deep chlorophyll maximum, and the depth of the deep chlorophyll maximum. The 4th-7th panels of Fig. IV.1.4 show the time series of the quantitative metrics computed on the vertical profiles comparison. The agreement between model (lines) and float (dots) at the surface, at the DCM and the 0-200 m vertical averaged chlorophyll values is pretty good (4th and 5th panels of Fig. IV.1.4). The depth of the DCM (blue line and dots in the lower panel of Fig. IV1..4) is very well reproduced both in terms of vertical displacement and temporal evolution. The thickness of the winter bloom layer (WBL, red lines and dots in the lower panel of Fig. IV.1.4) is fairly good reproduced, although it is not always computable from BGC-Argo float data or model results.

Figure IV.1.6 summarises the new metrics in monthly time series for the aggregated sub-basins, while Table IV.1.4 reports the average of the time series. Statistics for the ALB sub-basin are not available for lack of floats in that area while for SWM sub-basin they are not reliable considering the very low number of BGC-Argo float profiles. The number of available BGC-Argo floats measuring chlorophyll was 23 in the year 2019, and even if the use of BGC-Argo discloses new perspectives of the model validation, some cautions should be considered before generalizing the conclusions, since the relatively poor spatial coverage, the highly variable presence of BGC-Argo floats in the sub-basins and the on-going improvement of product quality procedures of the BGC-Argo data.

Nevertheless, as a conclusion, the MedBFM model has a very high skill in reproducing the vertical dynamics of the phytoplankton chlorophyll, both considering the very high spatial heterogeneity of the Mediterranean Sea and the seasonal cycle of the coupled physical-biogeochemical processes. In particular, the correlation between vertical profiles of model and observation is above of 0.8 in all sub-basins (Fig. IV.1.6 and Tab. IV.1.4). The DCM depth and the WBL thickness are characterized by a mean uncertainty of 13 m and 24 m, respectively. The RMSD of the 0-200 m vertical averages is always less than 0.04 mg/m^3 in all the aggregated sub-basins.

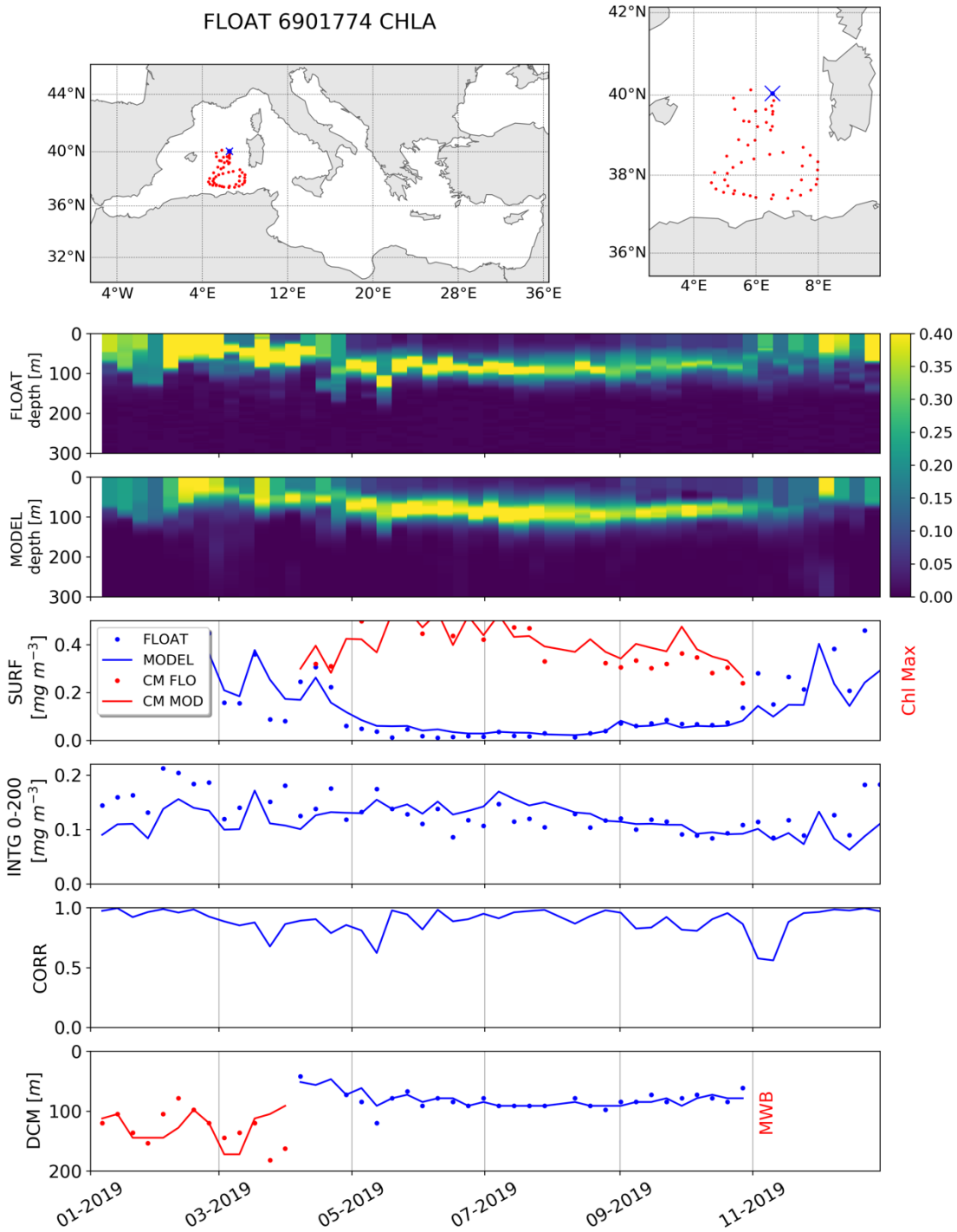

Figure IV.1.4. Hovmoller diagrams of chlorophyll for three selected floats (2nd panel) and the matched-up model output (3rd panel) for the year 2019, and computation of selected skill indexes for model (lines) and float data (dots). The skill indexes are: chlorophyll at surface and at DCM (SURF and Chl Max, 4th panel), 0-20 0 m vertically averaged chlorophyll (INTG, 5th panel), correlation (CORR, 6th panel), depth of the deep chlorophyll maximum (DCM, blue) and thickness of the winter layer bloom (WBL, red, 7th panel). Trajectories of the BGC-Argo floats are reported in the upper panel, with deployment position (blue cross) (continues overleaf).

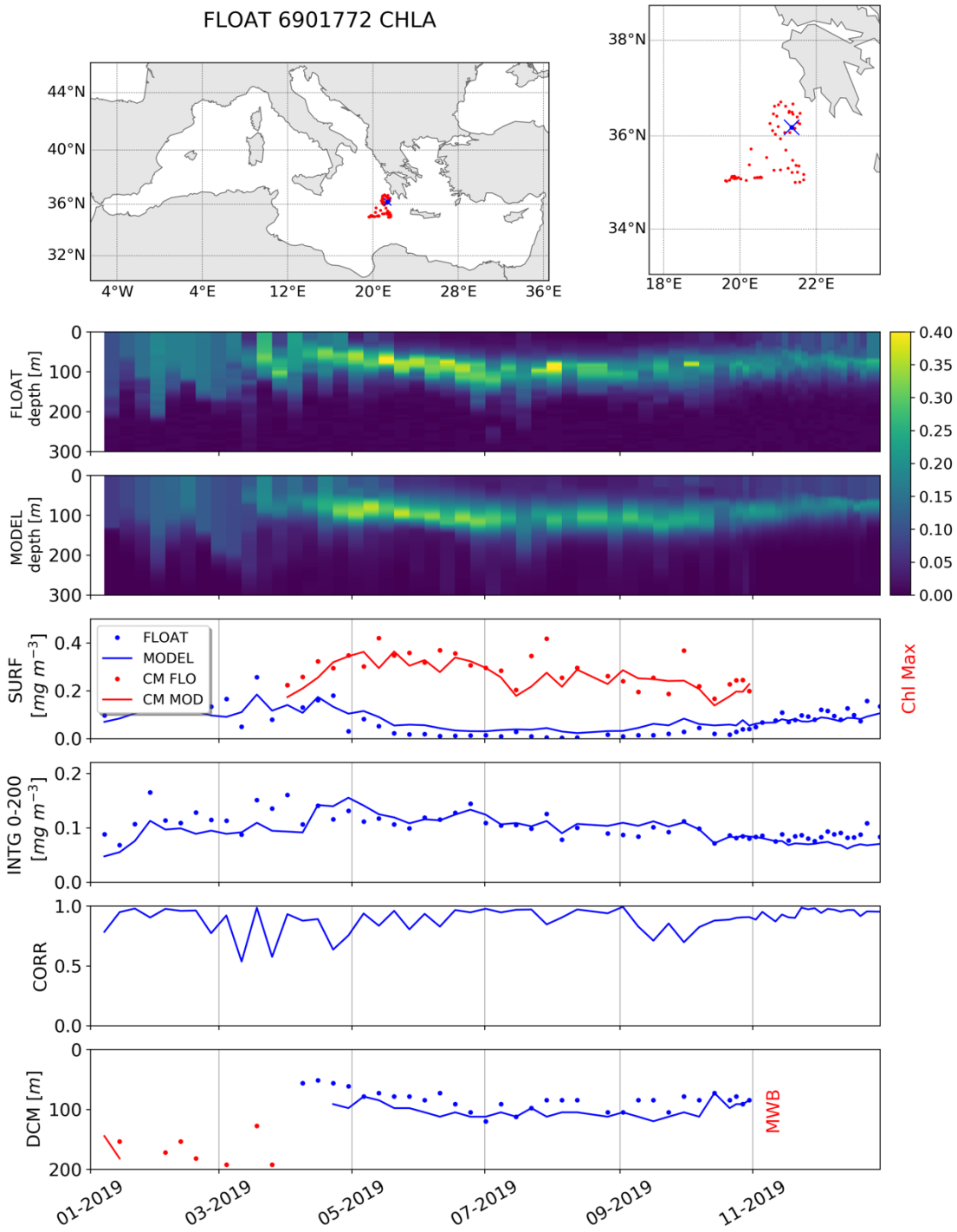

Figure IV.1.4. Same as above, continues overleaf.

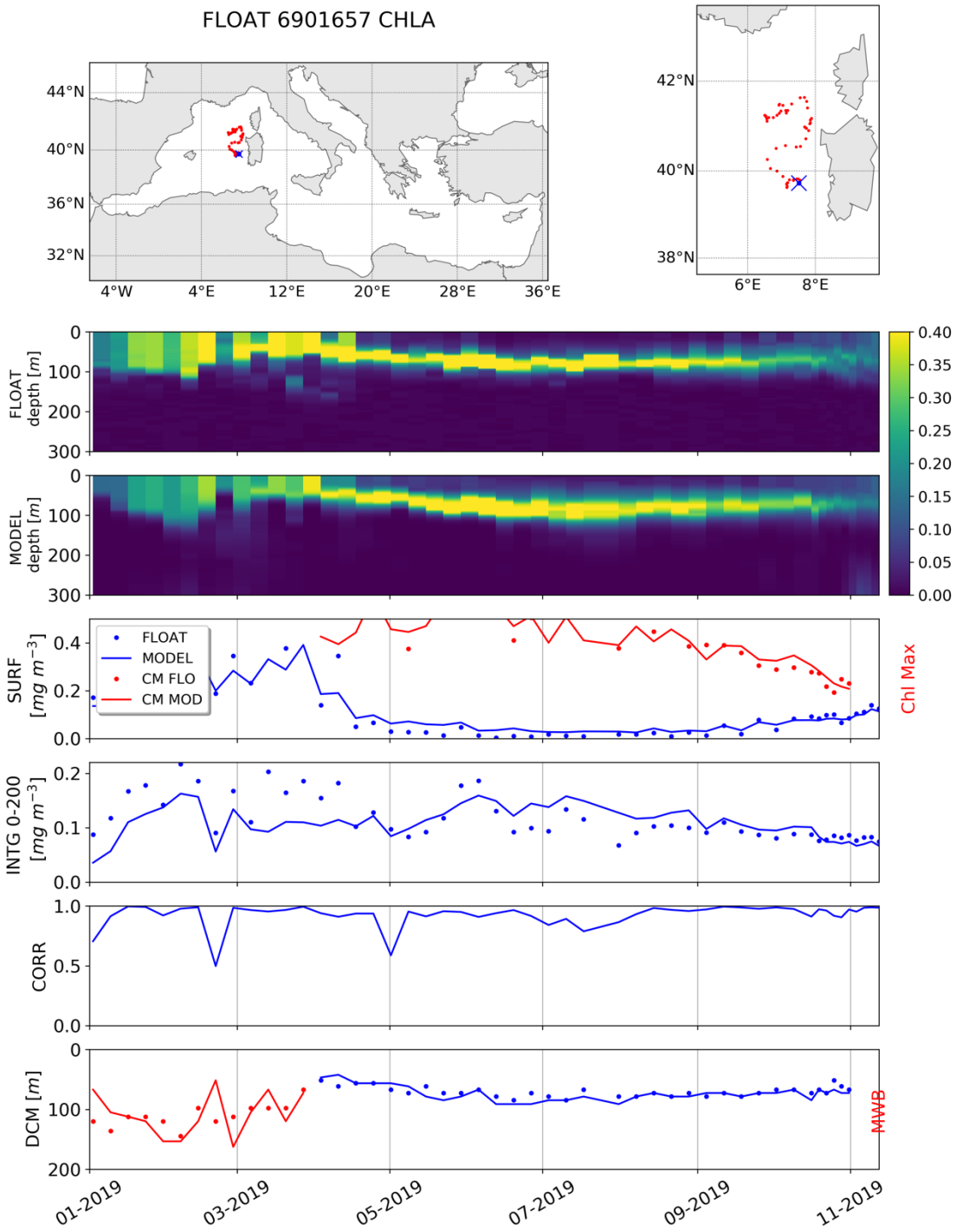

Figure IV.1.4. Same as above.

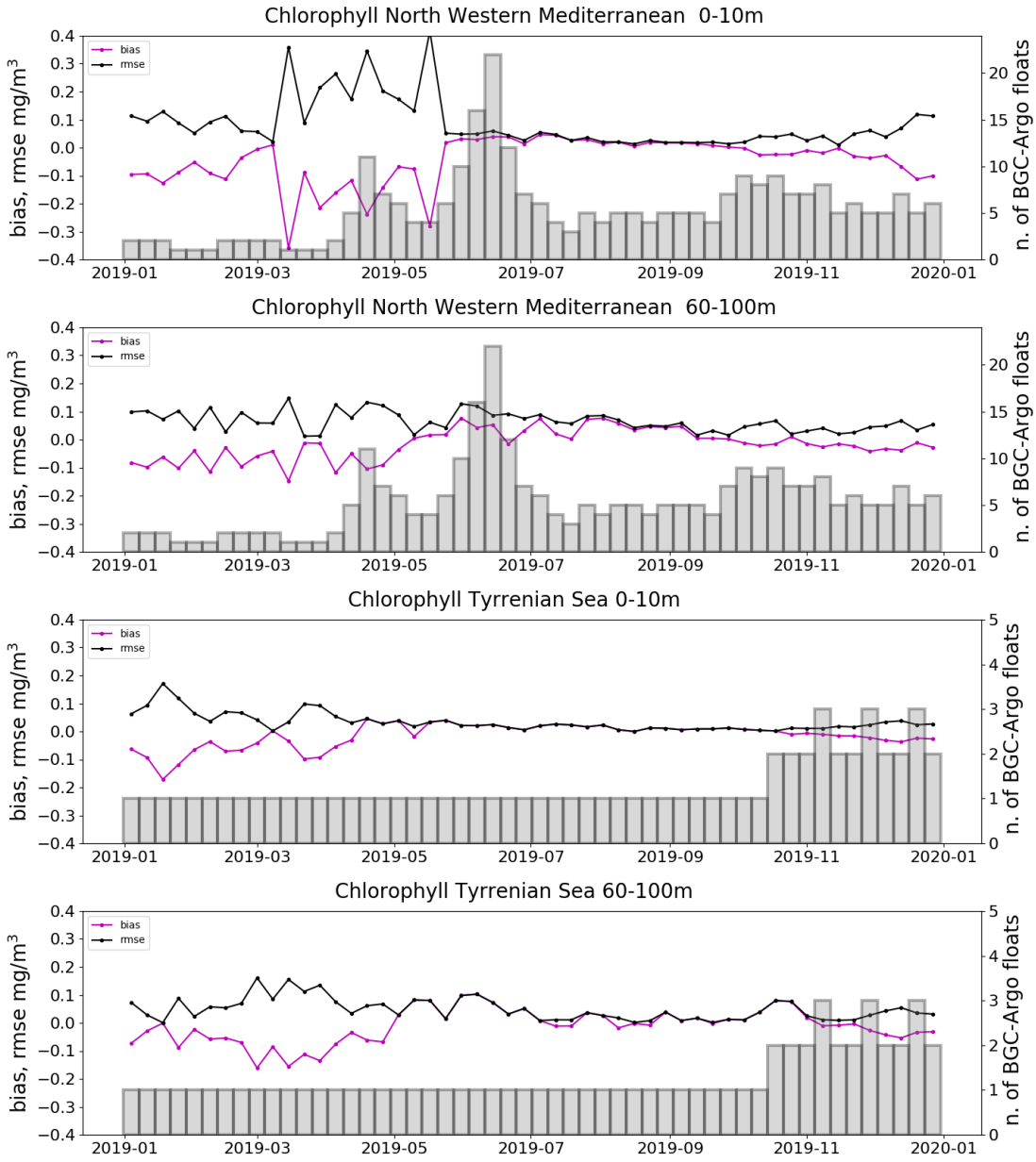

Figure IV.1.5. Time series of BIAS (purple) and RMSD (black) of the comparison between BGC-Argo float data and model for 0-10 m and 60-100 m layers and aggregated sub-basins (nwm, tyr = tyr1+tyr2, swm = swm1+swm2, ion = ion1+ion2+ion3, lev = lev1+lev2+lev3+lev4 of Fig. III.1). The number of data profiles used is shown with the grey vertical bars. These statistics are weekly updated in Near Real Time mode for the ANALYSISFORECAST product in the operational regional thematic validation website medeaf.inogs.it/nrt-validation (continues overleaf).

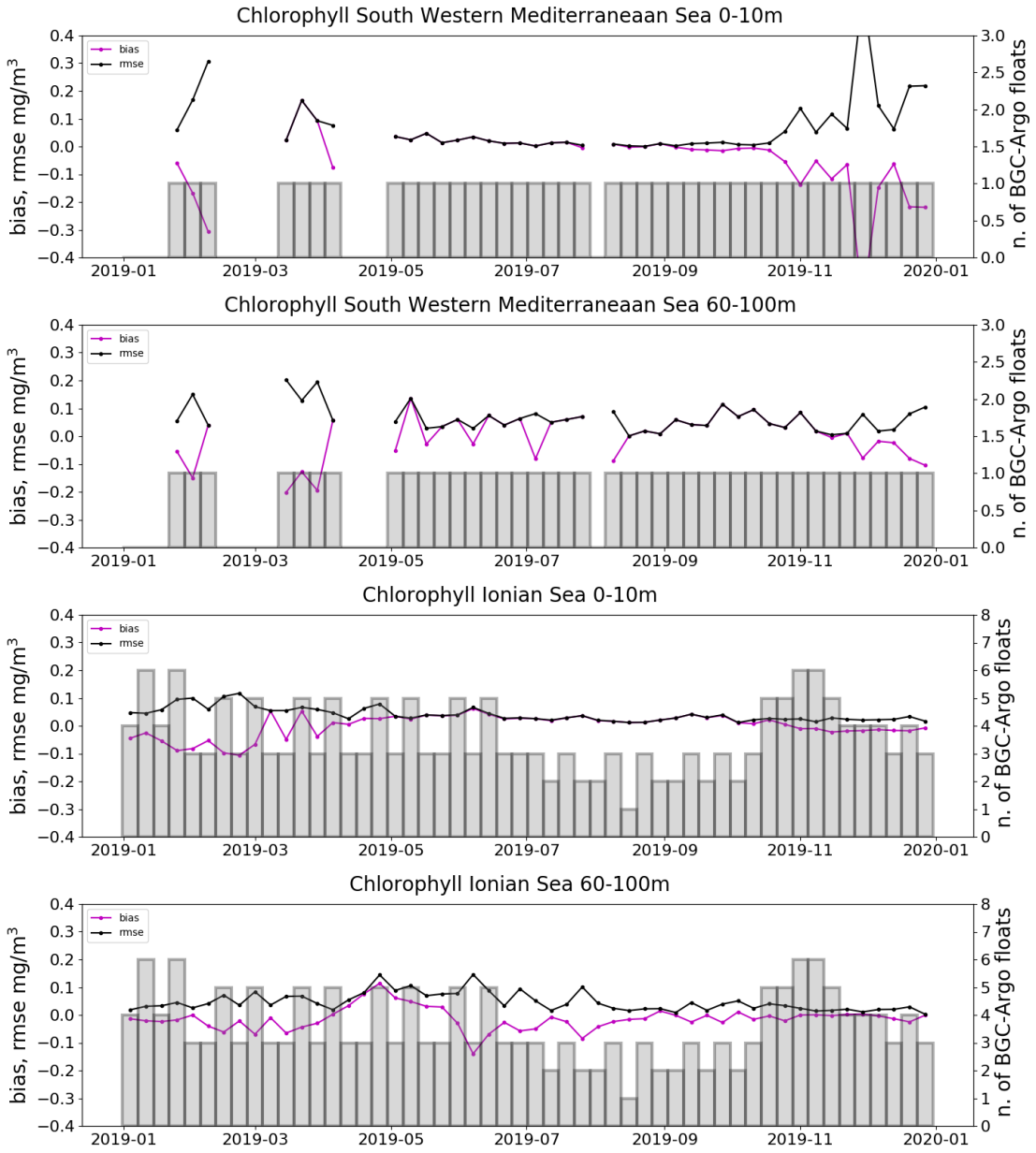

Figure IV.1.5. Same as above.

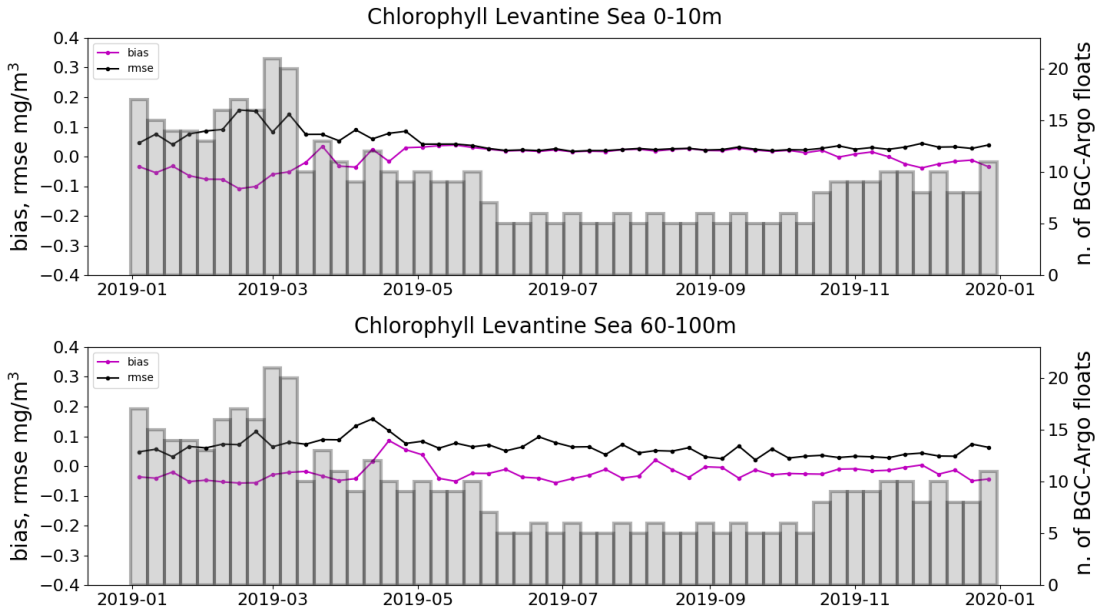

Figure IV.1.5. Same as above

	BIAS					RMSD				
	# 0-10 m	10-30 m	30-60 m	60-100 m	100-150 m	# 0-10 m	10-30 m	30-60 m	60-100 m	100-150 m
alb	-	-	-	-	-	-	-	-	-	-
swm	-0.04	-0.05	-0.05	0.00	<0.005	0.07	0.07	0.09	0.06	0.04
Nwm	-0.05	-0.05	-0.09	-0.02	<0.005	0.09	0.08	0.14	0.07	0.03
Tyr	-0.02	-0.01	-0.01	-0.01	0.02	0.03	0.04	0.04	0.05	0.04
Adr	-0.04	-0.03	-0.04	-0.04	-0.01	0.05	0.05	0.06	0.06	0.02
Ion	0.00	0.00	-0.02	-0.01	0.02	0.04	0.04	0.04	0.05	0.05
Lev	0.00	-0.01	-0.02	-0.02	0.02	0.05	0.05	0.06	0.06	0.05

Table IV.1.3. Time averaged BIAS and RMSD of chlorophyll (mg/m^3) for selected layers and aggregated sub-basins for the period January – December 2019. Statistics are computed using the match-ups of model with BGC-Argo float data.

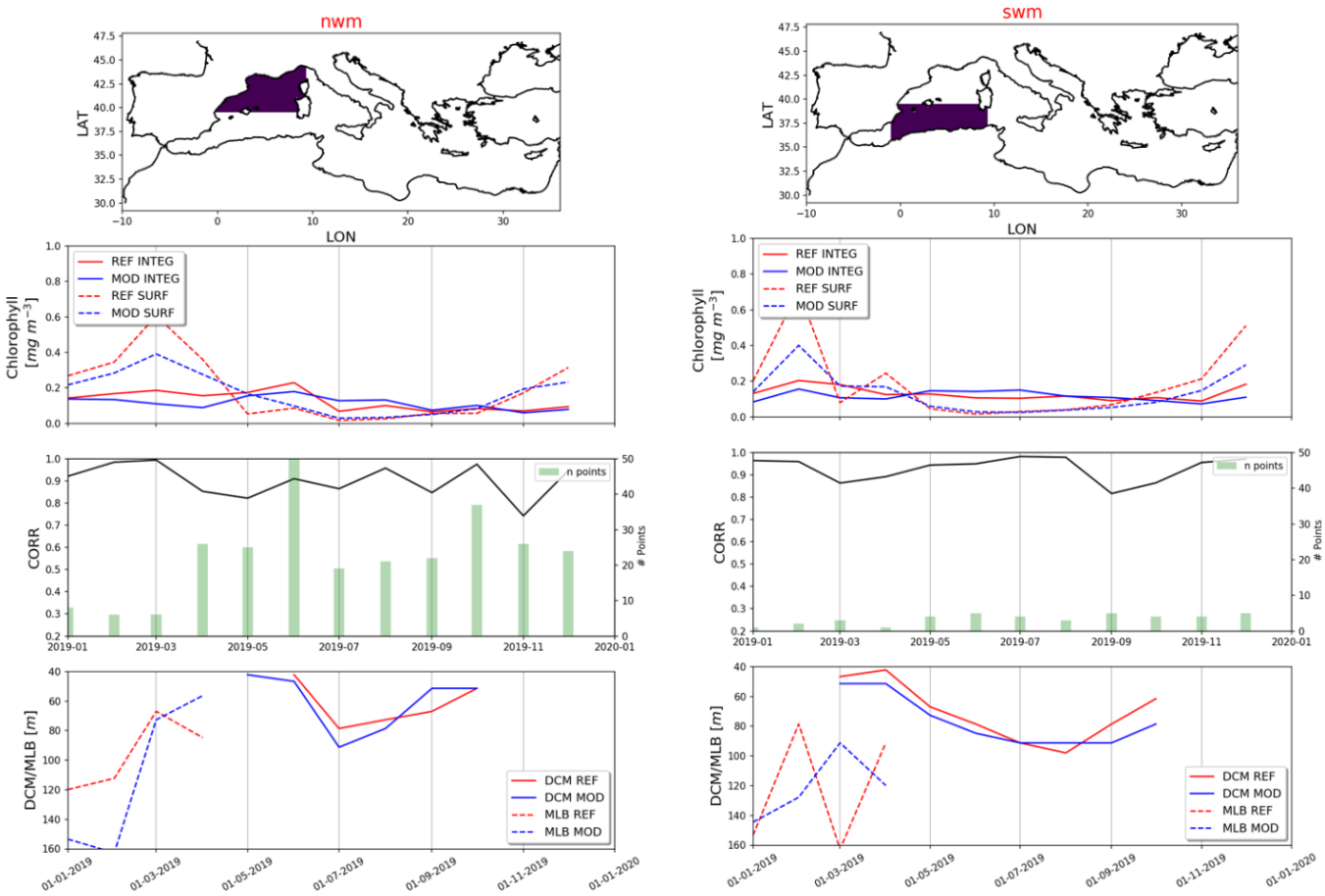

Figure IV.1.6. Monthly time series of chlorophyll ecosystem indicators based on the comparison between BGC-Argo float data (red lines) and model (blue lines) for aggregated sub-basins for the period January 2019 – December 2019. Map: location of sub-region; panel #1: Chl concetration; panel #2: number of grid points with float profiles per month (green bars) & correlation; panel #3: DCM/WBL. The ecosystem indicators are those reported in Fig. IV.4: vertical averaged chlorophyll (solid lines) and surface chlorophyll (dashed lines) in panel #1; correlation (black line) panel #2; depth of the DCM (solid lines) and thickness of the WBL (dashed lines) in panel #3 (continues overleaf).

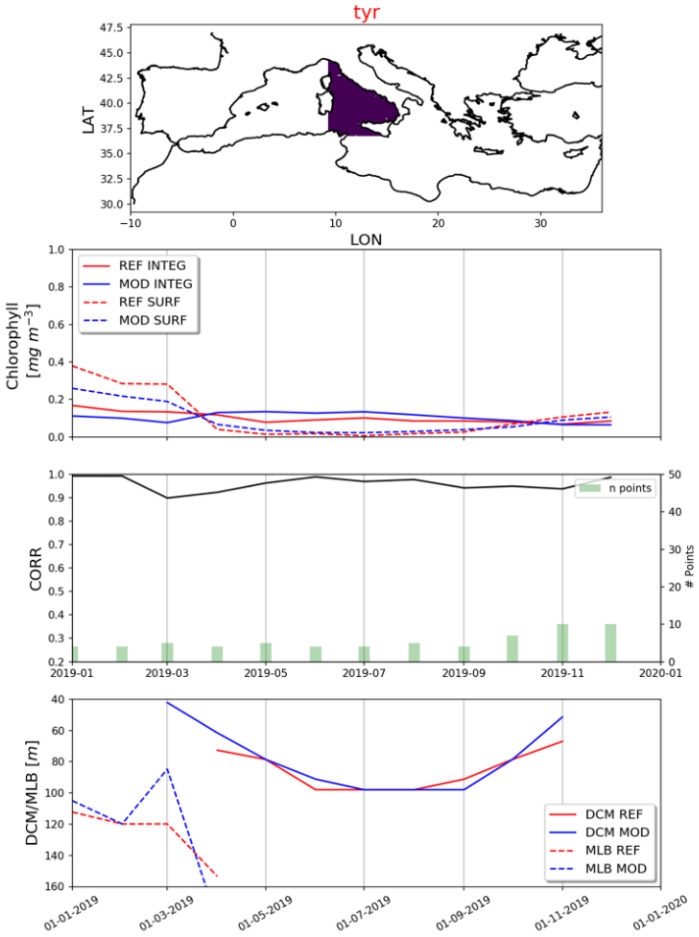

Figure IV.1.6. Same as above.

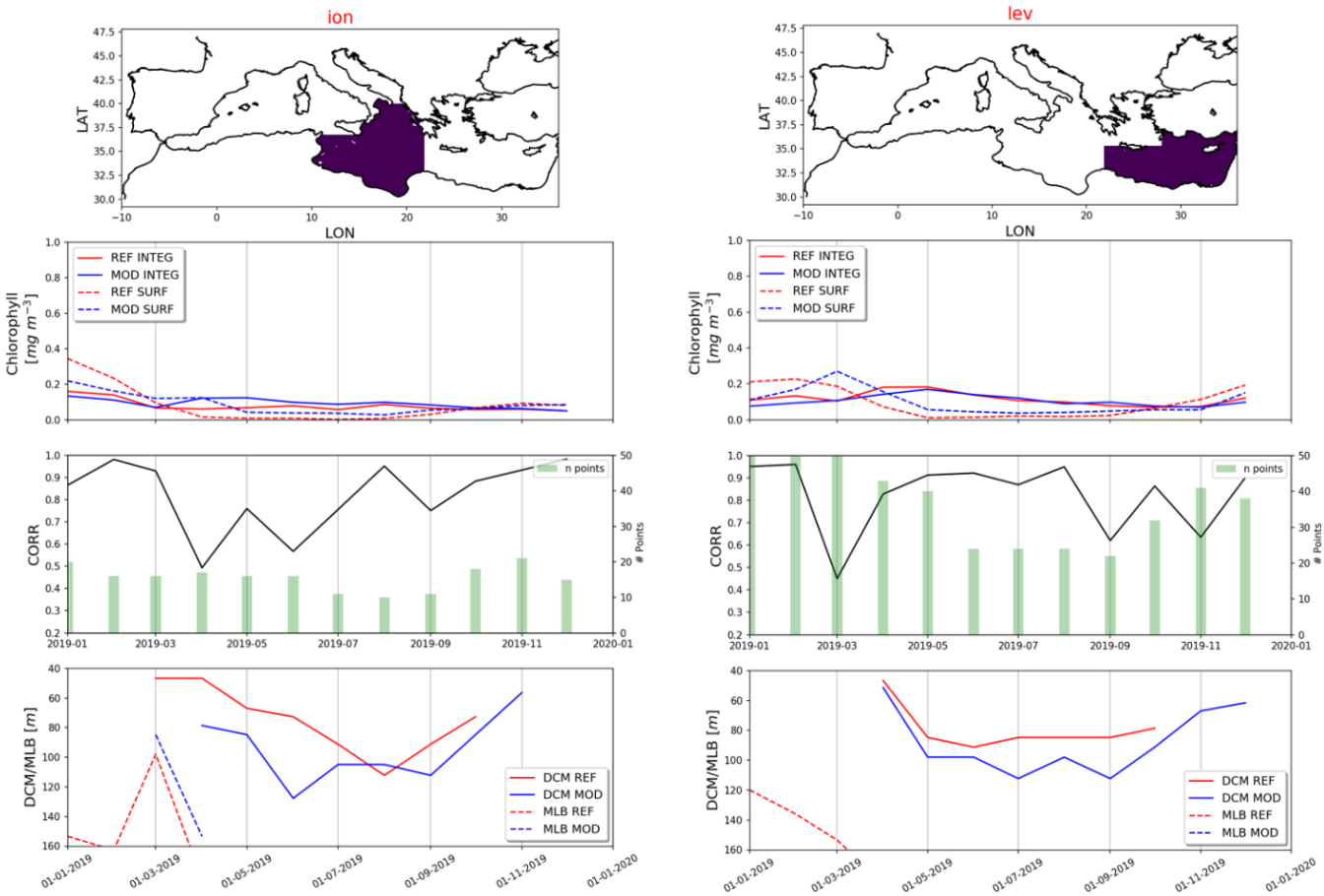

Figure IV.1.6. Same as above.

	CORR	Average 0-200 m [mg/m^3]		Depth of the deep chlorophyll maximum [m]		Depth of the vertically mixed bloom in winter [m]		average number of available profiles per month
		BIAS	RMSD	BIAS	RMSD	BIAS	RMSD	
alb	-	-	-	-	-	-	-	0
swm	0.93	-0.02	0.04	6	9	2	42	3
nwm	0.9	-0.01	0.04	2	10	12	30	23
tyr	0.96	0	0.04	-3	8	-3	21	6
adr	0.89	-0.03	0.03	0	6	-10	14	6
ion	0.82	0.01	0.03	21	27	-6	18	16
lev	0.82	-0.01	0.02	15	17	-13	17	40

Table IV.1.4. Time averages of the chlorophyll ecosystem indicators based on the BGC-Argo floats and model comparison for the period January – December 2019.

IV.2 Net primary production

Net primary production (NPP) is the measure of the net uptake of carbon by phytoplankton groups (gross primary production minus fast release processes – e.g. respiration). The lack of any extensive dataset of measures of primary production prevents the application of quantitative metrics for the assessment of the quality of this product. Thus, the product quality consists in a qualitative assessment of the consistency of the modelled NPP with previous estimates published in scientific literature (Fig. IV.2.1 and Tab. IV.2.1). Averaged NPP in the different sub-basins are consistent with basin-wide estimates (maps from Lazzari et al., 2012 and Bosc et al., 2004) and with sub-basin estimations (Tab. IV.2.1)

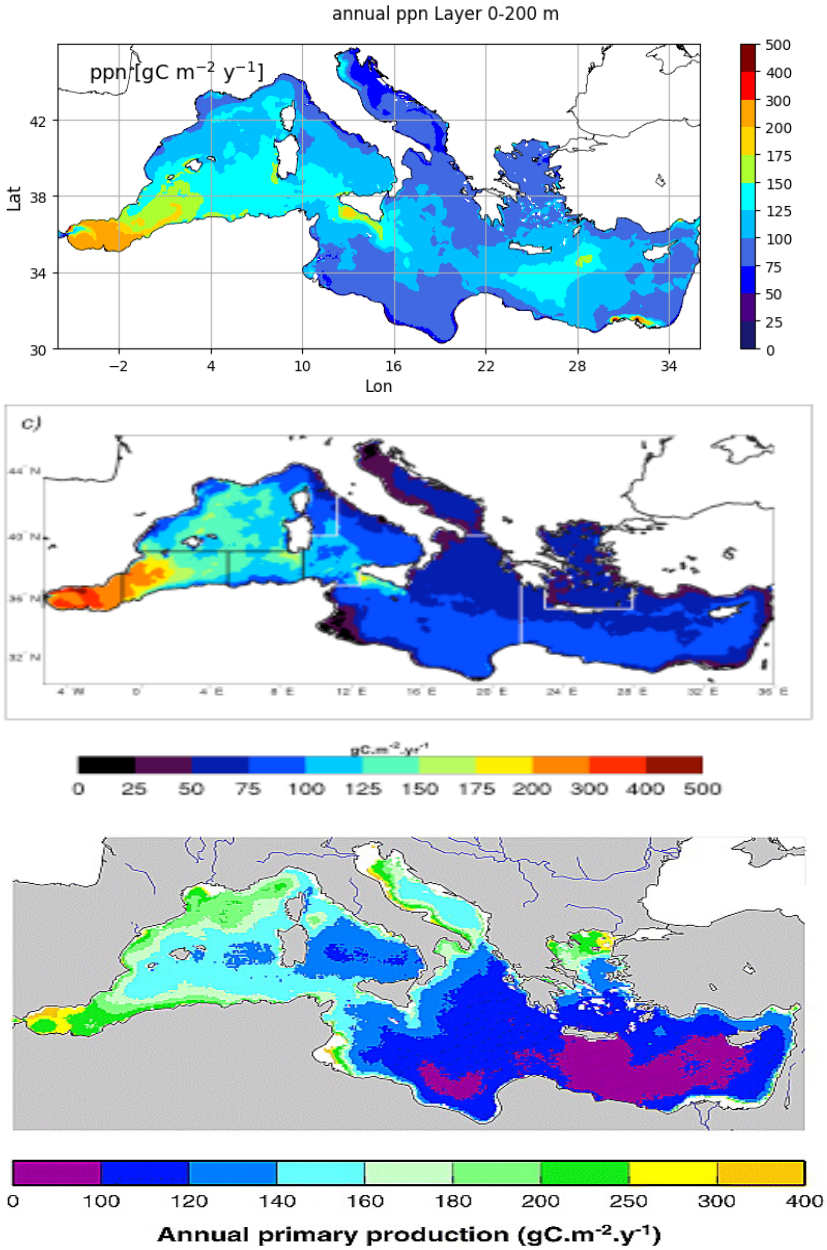

Figure IV.2.1. Annual averaged vertically integrated primary production (gC m^{-2} yr^{-1}) from the qualification run (average of the period January– December 2019; top panel), reference multi-annual simulation (from Lazzari et al., 2012; middle) and from climatological satellite estimation based on the period September 1997 – December 2001 (Bosc et al., 2004; bottom panel with different colorbar limits).

	MODEL Lazzari et al. (2012)	SATELLITE Colella (2006)	IN-SITU ESTIMATES Siokou-Frangou et al., 2010 (Reported in Table 1, only in-situ estimates)		CMEMS qualification for year 2019
	Annual mean [gC/m²/y]	Annual mean [gC/m²/y]	Annual mean [gC/m²/y]	Short term estimates [mgC/m³/d]	Annual mean [gC/m²/y]
Mediterranean Sea (MED)	98±82	90±48			109
Alboran Sea (ALB)	274±155	179±116		353–996; May-Jun1996 142; Nov2003	198
South West Med – West (SWM1)	160±89	113±43		186–636 (avg. 440) Oct1996	148
South West Med –East (SWM2)	118±70	102±38			132
North West Med (NWM)	116±79	115±67	105.8-119.6 86-232 (only DYFAMED station) 140-170 (South Gulf of Lion)	353–996; May–Jun1996 401; Mar-Apr1998 (G. Lion) 166; Jan-Feb1999 (G. Lion) 160–760; May-Jul (Cat-Bal) 150–900; Apr1991 (Cat-Bal) 450, 700; Jun1993 (Cat-Bal) 210, 250; Oct1992 (Cat-Bal) 1000±71 Mar1999 (Cat-Bal) 404±248 Jan-Feb00 (Cat-Bal)	115
Levantine (LEV1+LEV2+LEV3+LEV4)	76±61	72±21	59 (Cretan Sea)		108
Ionian Sea (ION1+ION2+ION3)	77±58	79±23	61.8	119–419; May-June 1996 208–324; April-May 1999 186±65; August 1997-98	96
Tyrrhenian Sea (TYR1 + TYR2)	92±5	90±35		398; May–Jun1996 273; Jul2005 429; Dec2005	111

Table IV.2.1. Annual averages and short period estimates of the vertically integrated primary production for some selected sub-regions. Estimates are from multi-annual simulation (Lazzari et al., 2012), from satellite model (Colella, 2006), from in-situ estimates (Siokou-Frangou et al., 2010) and from CMEMS system reanalysis.

IV.3 Phytoplankton biomass

The phytoplankton biomass is the content of carbon (mgC/m^3) in phytoplankton cells. The BFM model, featured by the MedBFM model system, simulated 4 phytoplankton functional groups and variable chlorophyll to carbon ratio, which depends on photoacclimatation and balance between synthesis and loss terms (Lazzari et al., 2012). Thus, phytoplankton biomass along with chlorophyll should be accounted for studying the evolution and variability of the primary producer biomass.

The accuracy of the phytoplankton biomass is assessed by class4 metrics using BGC-Argo optical data. Observations for biomass of phytoplankton (PhytoC) are retrieved from particulate backscattering coefficient at 700nm (bbp700) data using Bellacicco et al. (2019) relationship. Statistics computed for the comparison of vertical profiles (Table IV.3.1) show that the shape of profiles is reproduced with a correlation always higher than 0.6 except for ADR and that the 0-20 0 m averaged values are reproduced with an accuracy of around 0.8 mgC/m^3 over a mean value of 2.7 mgC/m^3 for the modelled vertical averaged phytoplankton biomass on the float locations. The uneven distribution of BGC-Argo floats (i.e., only in open sea areas and some sub-basins) limits the effectiveness of this comparison.

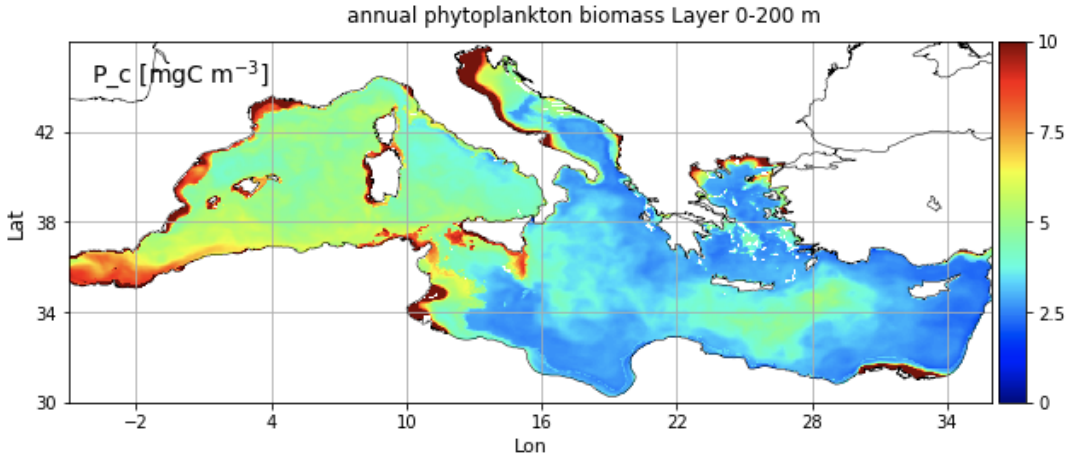

Fig. IV.3.1. Averaged mean annual map of phytoplankton carbon biomass (mg/m^3) for the 0-20 0 m layers.

	Model mean average 0-20 0 m [mgC/m3] *	Model mean average 0-20 0 m [mgC/m3] for the BGC-Argo locations **	Skill metrics for average 0-200 m [mgC/m^3]		Correlation	Average number of available profiles per month
			BIAS	RMSD		
alb	8.51±3.84	-	-	-	-	0
swm	5.77±1.21	3.24	1.04	1.7	0.87	7
nwm	5.46±2.08	3.26	0.88	1.07	0.78	29
tyr	4.86±1.58	1.97	0.55	0.56	0.87	6
adr	6.75±7.33	1.8	-0.31	0.79	0.37	6
ion	3.73± 2.10	2.62	0.24	0.52	0.64	16
lev	3.68±3.59	3.32	0.08	0.43	0.85	41

Table IV.3.1. 2019 time averages of the phytoplankton carbon biomass and skill performance metrics based on the BGC-Argo floats data for the aggregated sub-basins. *mean of the model vertical profile 0-20 0 m over the whole subbasin areas. **mean of model vertical profile 0-20 0 m for the locations of the BGC-Argo floats, which are located on open sea area only.

IV.4 Zooplankton biomass

Zooplankton biomass expressed as carbon represents the sum of the carbon content of the four zooplankton functional groups of the BFM model (i.e., heterotrophic nanoflagellates (HNF), microzooplankton and 2 groups of mesozooplankton). The lack of any extensive dataset of measurements of zooplankton biomass prevents the application of quantitative metrics for the assessment of the quality of this product. Thus, the product validation consists in a qualitative assessment of the consistency of the modelled zooplankton biomass with measurements published in scientific literature (Tab. IV.4.1). Measurements of zooplankton are often reported as biomass (or abundancy) over square meter of a portion of the water column (often considering the layer 0-200 m) given the usual sampling methodologies for this ecosystem component. Scientific studies generally address one of the three components (i.e., HNF, micro and mesozooplankton), seldom all three zooplankton components are simultaneously sampled, and studies refer to a few very sparse locations for non-synoptic and non-repeated temporal samplings (e.g., a single month in a single year). Thus, only literature reporting at least data from large samplings (i.e., extended in some of the Mediterranean sub-basins at least) or addressing all zooplankton components are considered. The scarcity and inhomogeneity of the data prevents the direct comparison between the total carbon biomass of zooplankton simulated by the model and the sum of the measurements for the different zooplankton compartments from different sources.
Notwithstanding these limitations, the qualitative comparison between the map of Fig IV.4.1 and the values of Table IV.4.1 shows that the model satisfactory simulated the order of magnitude of the variable (i.e., in the range of 0.5-2 gC/m^2 for the layer 0-20 0 m) and the basin-wide gradient with higher values in the western sub-basins and lower values in the eastern ones.

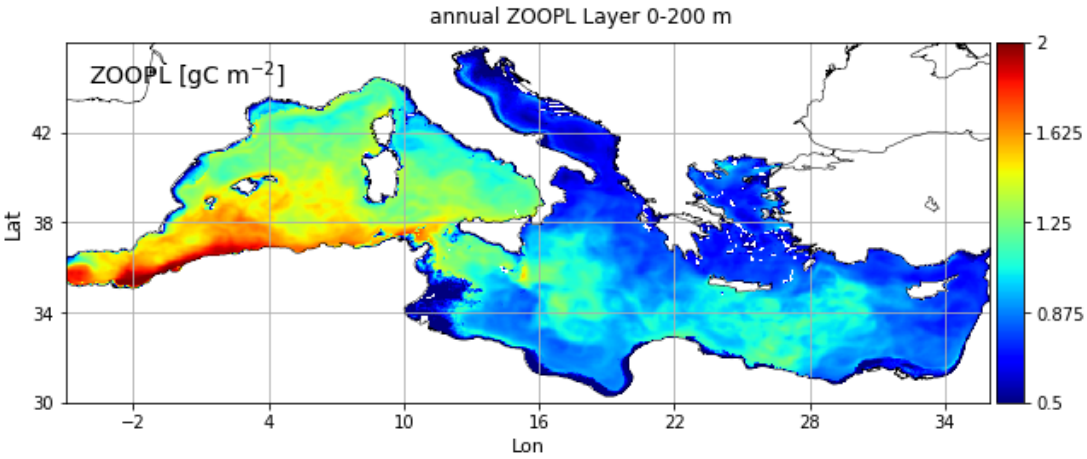

Fig. IV.4.1. Averaged annual maps of the vertical integrated biomass of total zooplankton [gC/m^2]. The average is computed considering the year 2019. The vertical integral considers the 0-20 0 m layer. The total zooplankton biomass is the sum of the carbon content of the four zooplankton function groups of the BFM model (i.e., heterotrophic nano flagellates, microzooplankton and 2 groups of mesozooplankton).

Model subbasin	Heterotrophic Nanoflagelates [gC/m²] in layer 0-20 0 m		Microzooplankton [gC/m²] in layer 0-20 0 m		Mesozooplankton [gC/m²] in layer 0-20 0 m		Model Total carbon biomass of Zooplankton [gC/m²] in layer 0-20 0 m
ALB					0.26	Apr [e]	1.56 ± 0.29
					0.72;0.5****	Winter/spring [c]	
SWM1					1.45***	Jun [f]	1.54 ± 0.23
SWM2	0.5	Jun/Jul [a]					1.44 ± 0.17
NWM	0.88	Jun/Jul [a]	0.1-0.2*	May/Jun [d]	0.82±0.15	Apr [e]	1.22 ± 0.19
	0.46-1.3** (NW Med current) 0.17-1.7** (NW offshore transect)	May/Jun [c]			0.9***	Jun [f]	
					0.58; 1.16; 1.6	different studies [c]	
					0.3;0.4;0.45***	Mar/Spring[c]	
TYR							1.17 ± 0.23
ADR					0.30±00.05 0.15±00.02	Feb/Oct [e]	0.64 ± 0.15
AEG	0.2* 0.8*	Mar/Sep [b]	0.16±0.04* 0.12±0.05*	Mar/Sep [b]	0.19±0.04* 0.16±0.04*	Mar/Sep [b]	0.75 ± 0.13
					0.2 – 0.4****	Mar/Spring[c]	
ION	0.25 (western) 0.45 (southern) 0.40 (northern)	Jun/Jul [a]	0.02-0.28*	May/Jun [d]	Sicily channel 0.24±0.04 0.19±0.02	Mar/Sep [e]	0.90 ± 0.22
					0.4****	Mar [c]	
					0.24±0.03 0.22±0.02	Mar/Aug [e]	
					0.95*** (eastern) 1.05*** (central) 0.85*** (central)	Jun [f]	
					0.4	Spring [c]	
LEV	0.25 (western) 0.26 (southern) 0.30 (Cyprus) 0.31 (Rhode gyre)	Jun/Jul [a]	0.08-0.12*	May/Jun [d]	0.44±0.26 (Rhode gyre) 0.20±0.02	Mar/Sep/Oct [e]	0.91 ± 0.17
	0.23-0.52**	Sep [c]			0.7*** (rhode gyre) 0.4*** (south Cyprus) 0.65*** (MersaMatruh gyre)	Jun [f]	

Table IV.4.1. Measurements of the vertically integrated zooplankton biomass for the three components for some selected sub-regions. Model total carbon biomass of zooplankton [gC/m²] in the 0-200 m layer (last column). [a] Data from Christaki et al. (2001); [b] Southern Aegeran for layer 0-100 m, data from Siokou-Frangou et al. (2002); [c] data for from Siokou-Frangou et al. (2010); [d] Data for from Dolan et al., (1999); [e] data from Mazzocchi et al., (2014); [f] data from Siokou et al., 2019. *data for 0-100 m; **data converted from abundance to biomass using 2.9 pg/ind (estimation retrieved using data from Cristaki et al., 2001); ***data converted from 0-100 0 m to 0-20 0 m using the conversion factor of 0.75; ****dry weigh converted to biomass using the factor 4 grDW: 1grC.

IV.5 Phosphate

The quality of CMEMS Med-MFC phosphate product is assessed by Class 1 metrics: the quantitative comparison between model average vertical profiles and the reference climatological profiles (Figures IV.15.1; appendix A) and of the skill performance statistics computed using the 16 sub-basins climatological values and the corresponding model annual means (Table IV.5.1).
The CMEMS Med-MFC phosphate product has a good accuracy in reproducing the average values and shape of the profiles along the Mediterranean sub-basins. In particular, the modelled profiles are within the range of variability of the EMODnet2018_int climatological profiles (Fig. IV.15.1, appendix A), and the along-profile correlation values are generally higher than 0.9 (calculated but not shown here). On average, phosphate RMSD is 0.03 mmol/m^3 in the upper layers and ranges between 0.02 and 0.05 mmol/m^3 in the layers below 60 m (Table IV.5.1). The results enforce the good performance of the MedBFM model in reproducing the decreasing nutrient concentration values in the deep layers from the western to the eastern sub-basins (correlation values higher than 0.7 below 3 0 m). Low phosphate values in the surface layer affect the model capability to clearly reproduce the west-to-east gradient, thus the correlation value is low.

	Phospate		
Layer depth	**BIAS**	**RMSD**	**CORR**
0-10 m	-0.01	0.03	0.31
10-30 m	-0.01	0.03	0.25
30-60 m	-0.01	0.03	0.70
60-100 m	0.00	0.02	0.92
100-150 m	0.03	0.05	0.89
150-300 m	0.02	0.03	0.96
300-600 m	-0.04	0.05	0.98
600-1000 m	-0.03	0.04	0.97

Table IV.5.1 Skill metrics (BIAS, RMSD and correlation) for the comparison of phosphate (model outputs averaged over the sub-basins and the period January – December 2019) with respect to climatology in open sea (EMODnet2018_int dataset). The metric is calculated for the selected layers of Table III.1.

IV.6 Nitrate

The quality of CMEMS Med-MFC nitrate product is assessed in two phases:

(i) the quantitative comparison with EMODnet2018_int vertical climatological profiles shows the skill in reproducing the vertical characteristics along the 16 Mediterranean sub-basins (Fig. IV.15.1, appendix A) and Table. IV.6.1;

(ii) the quantitative comparison with BGC-Argo floats data illustrates the quality of the model in reproducing the nitrate dynamics at the mesoscale and at weekly temporal scale (Figs. IV.6.1,2 and 3 and Tabs. IV.6.2 and 3).

The CMEMS Med-MFC nitrate product has a good accuracy in reproducing the average values and shape of the profiles along the Mediterranean sub-basins. In particular, the modelled profiles are within the range of variability of the EMODnet2018_int climatological profiles (Fig. IV.15.1, appendix A), and the along-profile correlation values are generally larger than 0.95 (calculated but not shown here). On average, the RMSD of nitrate is 0.5 mmol/m^3 in the upper layers and around 0.9 mmol/m^3 in the layers below 60 m; absolute BIAS never exceeds 0.2 mmol/m^3 in the upper layers. Both nitrate and phosphate

results corroborates the good performance of the MedBFM model in reproducing the deepening of the nutricline and the decreasing concentration values in the deep layers from the western to the eastern sub-basins. Low nitrate values in the surface layer affect the model capability to clearly reproduce the west-to-east gradient, thus the correlation value is low.

	Nitrate		
Layer depth	**BIAS**	**RMSD**	**CORR**
0-10 m	-0.04	0.42	0.33
10-30 m	0.08	0.44	0.19
30-60 m	-0.03	0.58	0.44
60-100 m	-0.15	0.77	0.80
100-150 m	0.16	0.80	0.87
150-300 m	-0.14	0.72	0.94
300-600 m	-0.81	1.11	0.93
600-1000 m	-0.60	0.84	0.94

Table IV.6.1 Skill metrics for the comparison of nitrate with respect to climatology in open sea.

Validation of nitrate can benefit from the availability of BGC-Argo floats data. Even if the number of BGC-Argo floats mounting a nitrate sensor is smaller than that for chlorophyll (i.e., 6 BGC-Argo floats during year 2019) and the product quality control activity for BGC-Argo nitrate is still under development, the float data undoubtedly represent a fundamental source of information to validate the MedBFM model results at the mesoscale and weekly scale.

The comparison of modelled nitrate with the BGC-Argo float data evaluates not just the *accuracy* of the CMEMS nitrate product (i.e., BIAS and RMSD for selected layers and sub-basins in Fig. IV.6.3 and Tab. IV.6-3), but also the *consistency* of the MedBFM to simulate key coupled physical-biogeochemical processes (i.e., water column nutrient content, nitracline and effect of winter mixing and summer stratification on the shape of nitrate profile; Figs. IV.6.1 and 2 and Table IV.6.2). This validation framework is based on matching a BGC-Argo float profile with the corresponding (in time and space) modelled profile (left column of Fig. IV.6.1). Based on the model-float vertical match-up, specifically developed metrics are:

- surface concentration and 0-200 m vertically averaged values (4th and 5th panels of Fig. IV.6.1);
- correlation between model and BGC-Argo float profiles (6th panel of Fig. IV.16.1);
- depth of the nitracline (NITRACL1 defined as the depth at which the nitrate concentration is 2 mmol/m^3; and NITRACL2 defined as the depth at which the depth derivative of the nitrate profile is maximum; 7th panel of Fig. IV.6.1).

The two Hovmoller plots of Fig. IV.6.1 exemplify the high level of potentiality of the BGC-Argo float data for validating the model results. From a qualitative point of view the nitrate signatures of the two floats are pretty well reproduced by the MedBFM model simulation (2nd and 3rd panel of Fig. IV.6.1). From a quantitative point of view we observe a good model performance in reproducing the temporal evolution of the 0-200 m averaged values, the shape of the profile (i.e. correlation values) and of the nitracline depth (4th – 7th panel of Fig. IV.6.1).

The nitrate metrics of the 6 floats are averaged over the aggregated sub-basins in monthly time series (Fig. IV.6.2) and in overall means (Table IV.6.2). Even if the scarcity of the available floats possibly limits the generalization of the results, our validation framework highlights that the MedBFM model system shows a good performance in simulating the shape of profiles and the seasonal evolution of the mesoscale dynamics. In particular, the mean value of nitrate on the 0-200 m layer is simulated, with an accuracy of about 0.3 mmol/m^3 (Tab. IV.6.2), the correlation is always higher than 0.89 and the depth of the nitracline (NITRACL1) is simulated with a mean uncertainty of 20 m in all aggregated sub-basins (but

36m in LEV, Tab. IV.6.2). Further, accordingly with BGC-Argo float observations (Fig. IV.6.2), the MedBFM is reproducing significantly well the Mediterranean basin scale heterogeneity with a nitracline at around 80-120 m in the western sub-basins and below 120-140 m in the eastern sub-basins.

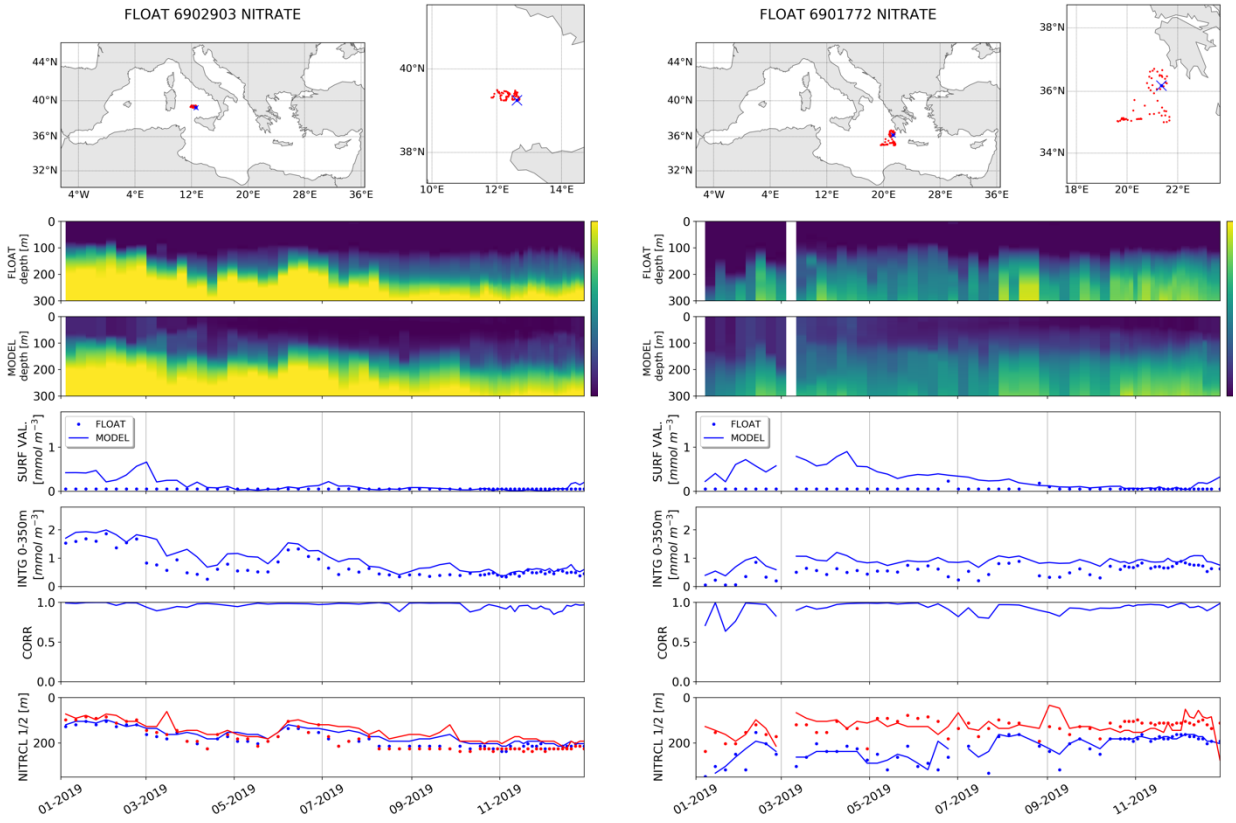

Figure IV.6.1. Hovmoller diagrams of nitrate of BGC-Argo floats (2nd panel) and model outputs (3rd panel) matched-up with float position (top) for year 2019. Time series of nitrate indicators based on model (MOD) and BGC-Argo floats (REF) comparison: nitrate concentration at surface (SURF, 4th panel) and 0-35 0 m vertically averaged concentration (INTG, 5th panel), correlation between profiles (CORR, 6th panel), depth of the nitracline (NITRACL1 defined as the depth at which the nitrate concentration is 2 mmol/m^3; and NITRACL2 defined as the depth at which the depth derivative of the nitrate profile is maximum). Trajectories of the BGC-Argo floats are reported in the upper panels, with deployment position (blue cross).

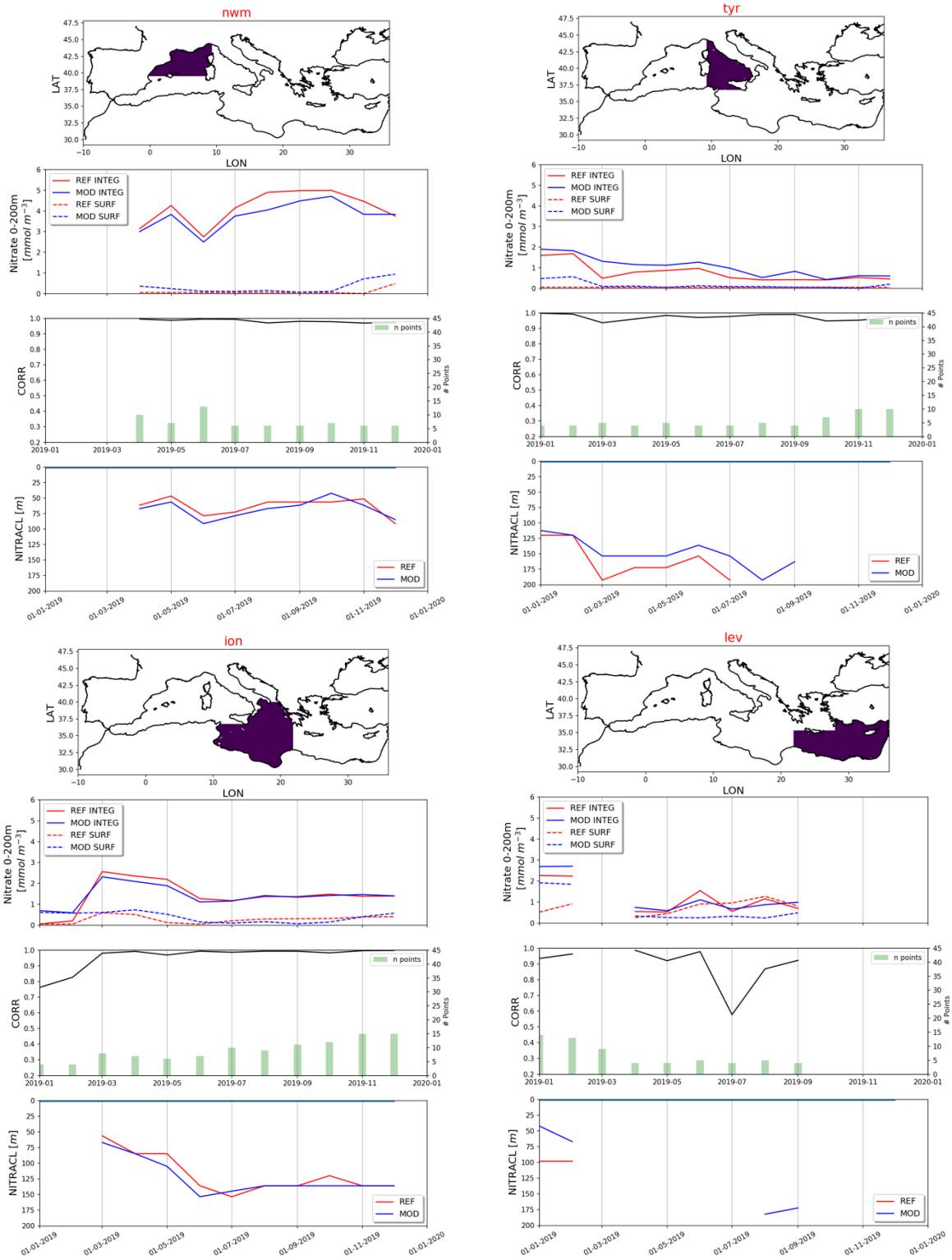

Figure IV.6.2. Monthly time series of nitrate indicators based on model (MOD) and BGC-Argo floats (REF) comparison for four selected aggregated sub-basins: nitrate concentration at surface (SURF) and 0-200 m vertically averaged concentration (INTG), correlation between profiles (CORR), depth of the nitracline (NITRCL1). Number of float profiles is reported by the green bars in the middle panel (# of floats per month).

Finally, BIAS and RMS of nitrate concentration between model and BGC-Argo floats are computed for selected layers (listed in Table III.1) and aggregated sub-basins and they are reported as time series in Fig. IV.6.3 and averaged in Tab. IV.6.3. These metrics, which are reported and operationally updated weekly in the thematic regional validation webpage medeaf.inogs.it/nrt-validation, show that the model has stable performance as long as the number of available BGC-Argo floats remains constant (Fig. IV.6.3). The availability of a sufficient number of floats equipped with the nitrate sensor might pose some issue on the reliability and sustainability of these metrics. In fact, as an example, there are no floats available in Adriatic, Alboran and South West Mediterranean sub-basins in 2019 and statistics in Ionian and North Western Mediterranean sub-basins might be biased by the sparse and uneven distribution of the floats (Fig. III.4). In spite of these limitations, the metrics show that the mean RMSD is less than 0.3 mmol/m^3 in the upper 60 m and less than 0.4 mmol/m^3 in layers between 60 and 600 m (with a few exceptions).

		mean nitrate concentration 0-20 0 m [mmol/m^3]		Depth of the nitracline [m]		Average number of profiles per month
	CORR	BIAS	RMSD	BIAS	RMSD	
alb	-	-	-	-	-	0
swm	-	-	-	-	-	0
nwm	0.98	-0.38	0.46	4	9	6
tyr	0.97	0.28	0.35	-20	24	6
adr	-	-	-	-	-	0
ion	0.96	0.01	0.26	6	11	9
lev	0.89	0.1	0.32	-10	36	5

Table IV.6.2. Averages of the monthly nitrate indicators plotted in Figure IV.6.2 during the period January – December 2019. The indicators are the correlation between model and BGC-Argo float data, the BIAS and RMSD of the vertically 0-200 m averaged nitrate concentration, the BIAS and RMSD of the depth of the nitracline (depth of nitrate concentration reaching 2 mmol/m^3). Statistics are computed for selected aggregated sub-basins.

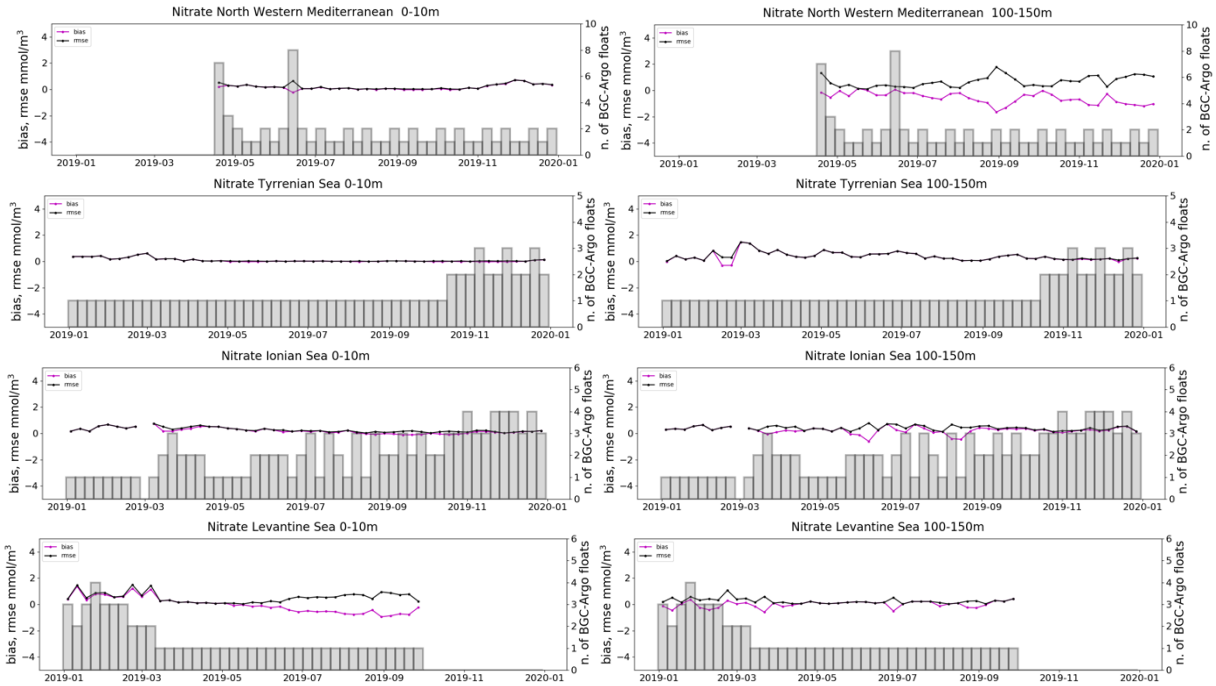

Figure VI.6.3. Time series of BIAS (purple) and RMSD (black) of nitrate concentration [mmol/m^3] of the comparison between BGC-Argo float data and model for the 0-1 0 m (left) and 100-15 0 m (right) layers and 4 aggregated sub-basins (nwm, tyr = tyr1+tyr2, ion = ion1+ion2+ion3, lev = lev1+lev2+lev3+lev4 of Fig. III.1). Number of data profiles used is shown by the grey vertical bars. These statistics are updated every week in the operational regional thematic validation website: medeaf.inogs.it/nrt-validation.

Layer Depth (m)	BIAS								RMSD							
	0-10	10-30	30-60	60-100	100-150	150-300	300-600	600-1000	0-10	10-30	30-60	60-100	100-150	150-300	300-600	600-1000
alb	-	-	-	-	-	-	-	-	-	-	-	-	-	-	-	-
swm	-	-	-	-	-	-	-	-	-	-	-	-	-	-	-	-
nwm	0.16	0.15	0.16	-0.72	-0.58	-0.36	-0.28	-1.29	0.20	0.20	0.41	0.92	0.66	0.41	0.31	1.29
tyr	0.08	0.06	0.09	0.31	0.37	0.23	-0.02	-0.10	0.10	0.10	0.13	0.31	0.40	0.30	0.10	0.17
adr	-	-	-	-	-	-	-	-	-	-	-	-	-	-	-	-
ion	0.19	0.18	0.22	0.29	0.23	0.02	-0.25	-1.06	0.26	0.26	0.29	0.43	0.40	0.23	0.32	1.06
lev	-0.03	0.07	0.17	0.14	0.01	-0.07	-0.34	-1.23	0.52	0.39	0.26	0.21	0.25	0.47	0.41	1.23

Table IV.6.3. Averaged BIAS and RMSD of nitrate w.r.t. BGC-Argo floats for the layers of Tab. III.1, aggregated sub-basins (nwm, tyr = tyr1+tyr2, ion = ion1+ion2+ion3, lev = lev1+lev2+lev3+lev4) for the period January – December 2019.

IV.7 Dissolved Oxygen

The quality of CMEMS Med-MFC dissolved oxygen is assessed in two phases:

(i) the quantitative comparison with EMODnet2018_int vertical climatological profiles shows the skill in reproducing the vertical characteristics along the 16 Mediterranean sub-basins (Fig. IV.15.1, appendix A, and Table IV.7.1);

(ii) the quantitative comparison with BGC-Argo float illustrates the quality of the model in reproducing the oxygen dynamics at the mesoscale spatial and weekly temporal scales (Figs. IV.7.1, 2 and 3 and Tabs. IV.7.2 and 3).

Modelled oxygen profiles are well simulated within the range of variability of the climatology (Fig. IV.15.1, appendix A), with absolute BIAS and RMSD lower than 6 mmol/m^3 in all selected layers, with an exception of layer 300-60 0 m (Tab. IV.7.1).

	Oxygen		
Layer depth	**BIAS**	**RMSD**	**CORR**
0-1 0 m	1.5	4.8	0.77
10-3 0 m	-1.4	4.7	0.84
30-6 0 m	-5.1	6.8	0.79
60-10 0 m	1.8	5.4	0.76
100-15 0 m	4.4	7.1	0.72
150-30 0 m	4.6	6.7	0.88
300-60 0 m	11.94	12.71	0.94
600-100 0 m	5.91	8.51	0.81

Table IV.7.1 Skill metrics for the comparison of oxygen with respect to climatology in open sea.

The validation of dissolved oxygen can benefit from the availability of BGC-Argo floats data, however the product quality activity of dissolved oxygen is under development: an increasing number of floats include the intercalibration in air (Bittig et al., 2019) but data are released in delay mode with non-regular delay. The present assessment, which uses only delay mode oxygen data, might not represent the NRT validation capability when no or few delay mode oxygen data are available. Figure IV.7.1 shows the Hovmoller diagram of one selected BGC-Argo float and the corresponding model profiles along the trajectory covered by the floats. The MedBFM simulates, consistently with the BGC-Argo float data, the seasonal evolution of the oxygen, reproducing the mixed water column in winter and the formation of a maximum oxygen layer in correspondence of the DCM during summer and the depletion of the oxygen content at surface during summer.

Figure IV.7.2 reports the time series of the BIAS and RMSD metrics computed in the layers and aggregated sub-basins, and Table IV.7.2 reports their averages showing an absolute BIAS between 0 and 2 mmol/m^3 and an RMSD lower than 7 mmol/m^3 in the surface layer. Higher uncertainty is computed for the layers below 10 0 m with RMSD values between 10 and 20 mmol/m^3. The time series of Fig. IV.7.2 displaying BIAS and RMSD are reported and operationally updated weekly in the thematic regional validation webpage medeaf.inogs.it/nrt-validation.

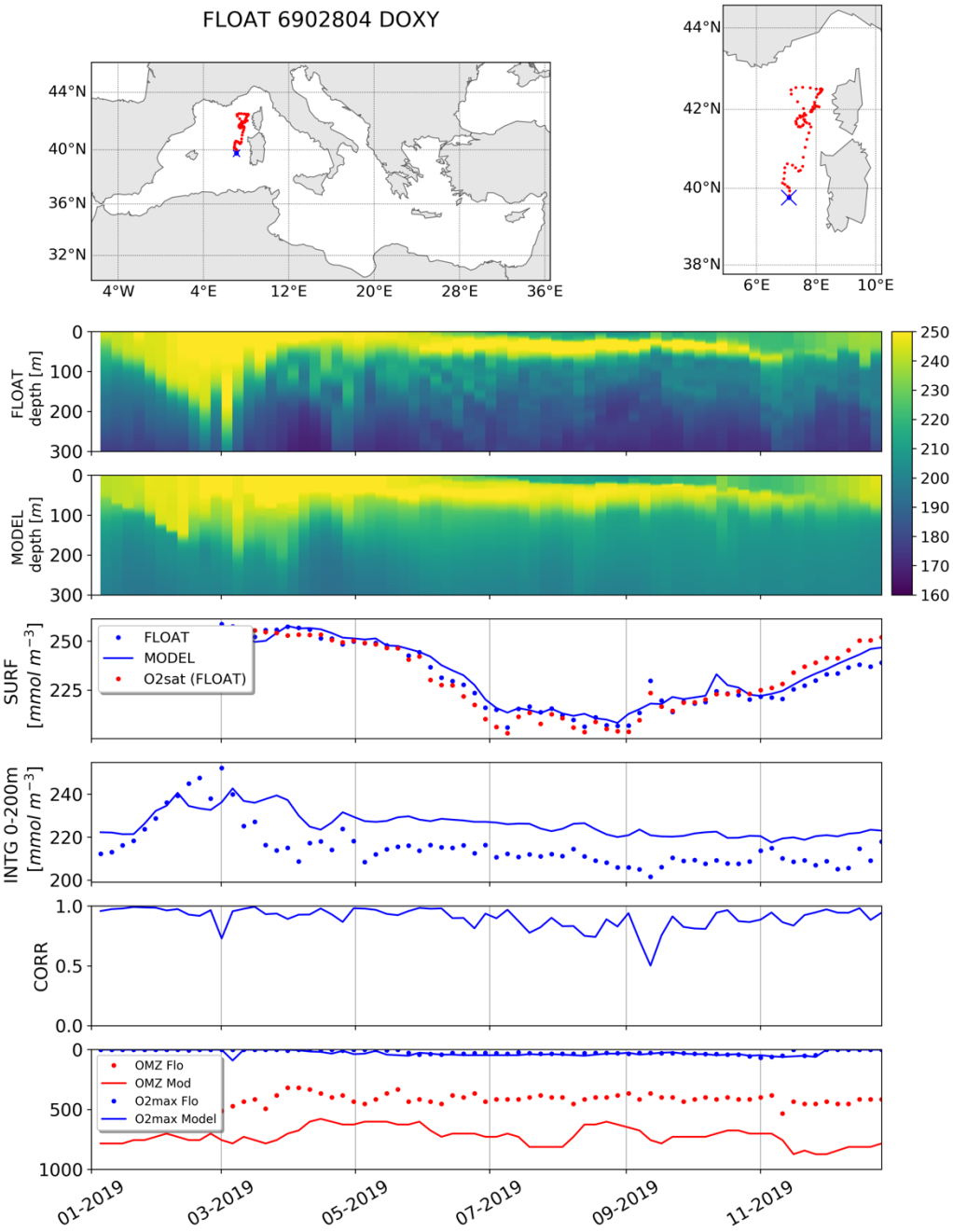

Figure IV.7.1 Hovmoller diagrams of dissolved oxygen of a BGC-Argo float (2nd panel) and model outputs (3rd panel) matched-up with the float data position for the year 2019. Time series of oxygen indicators based on model (MOD) and BGC-Argo floats (FLOAT) comparison: oxygen concentration at surface (SURF, 4th panel) and 0-20 0 m vertically averaged concentration (INTG, 5th panel), correlation between profiles (CORR, 6th panel). The trajectory of the BGC-Argo float is reported in the upper panels, with deployment position (blue cross).

Figure VI.7.2. Time series of dissolved oxygen BIAS and RMSD [mmol/m^3] of the comparison between BGC-Argo float data and model for 0-1 0 m (left) and 60-10 0 m (right) layers and the aggregated sub-basins (nwm, swm, ion = ion1+ion2+ion3, lev = lev1+lev2+lev3+lev4, tyr = tyr1+tyr2, of Fig. III.1). Number of data profiles used is shown by the grey vertical bars. These statistics are weekly updated in Near Real Time mode for the analysis and forecast product in the operational regional thematic validation website: medeaf.inogs.it/nrt-validation.

Layer Depth (m)	BIAS								RMSD							
	0-10	10-30	30-60	60-100	100-150	150-300	300-600	600-1000	0-10	10-30	30-60	60-100	100-150	150-300	300-600	600-1000
alb	-	-	-	-	-	-	-	-	-	-	-	-	-	-	-	-
swm	1.5	-3.0	-4.5	5.4	7.7	13.3	21.1	13.6	3.2	5.8	7.8	9.5	12.0	13.9	21.5	13.6
nwm	1.0	0.0	3.1	10.1	10.8	16.5	20.6	13.9	5.5	5.8	11.4	15.2	16.0	19.2	21.3	14.4
tyr	-0.7	-5.4	-10.4	-2.4	-2.0	2.5	11.1	8.4	3.3	6.8	13.1	9.4	10.0	9.2	11.7	8.9
adr	-	-	-	-	-	-	-	-	-	-	-	-	-	-	-	-
ion	-0.4	-2.6	-7.3	0.1	6.1	8.5	11.8	10.5	3.9	4.9	10.1	6.2	8.2	10.0	12.9	10.9
lev	-1.1	-4.0	-5.8	0.2	5.8	7.2	15.5	14.8	6.9	9.1	10.0	8.3	9.7	10.3	16.3	15.2

Table IV.7.3. Averaged dissolved oxygen BIAS and RMSD of the comparison between BGC-Argo float and model values for the layers of Tab. III.1 and aggregated sub-basins of Fig. III.1.

IV.8 Ammonium

Ammonium accuracy is assessed with Class 1 metrics: it consists of the comparison between model average vertical profiles and the EMODnet2018_int reference climatological profiles (Figures IV.15.1; appendix A) and the statistics computed using the 16 sub-basins climatological values and the corresponding model annual means (Table IV.8.1). As reported in Table IV.7.1, ammonium concentrations are simulated by the MedBFM model with an error of less than 0.4 mmol/m^3 in the upper layers and of 0.3-0.6 mmol/m^3 in the deeper layers (i.e., below 10 0 m). The low and negative correlation values indicate that the model has some deficiencies in reproducing typical vertical profiles and spatial gradient of ammonium, however the low data availability (only 7 sub-basins covered) might have affected the accuracy evaluation.

	Nitrate		
Layer depth	BIAS	RMSD	CORR
0-1 0 m	-0.35	0.40	-0.30
10-3 0 m	-0.16	0.21	-0.47
30-6 0 m	-0.09	0.15	-0.10
60-10 0 m	-0.02	0.24	-0.51
100-15 0 m	-0.04	0.31	-0.44
150-30 0 m	-0.21	0.32	-0.34
300-60 0 m	-0.38	0.44	0.72
600-100 0 m	-0.41	0.55	0.47

Table IV.8.1 Skill metrics for the comparison of ammonium with respect to climatology in open sea.

IV.9 Silicate

Silicate validation is peformed with Class 1 metrics assessment: it consists in the comparison between model average vertical profiles and the EMODnet2018_int reference climatological profiles (Figures IV.15.1; appendix A) and the statistics computed using the 16 sub-basins climatological values and the corresponding model annual means (Table IV.9.1). As shown in figures IV.15.1 (appendix A), the profiles are well simulated within the range of variability of the climatology except in the western basins where the model overestimates concentration at the surface. As reported in Table IV.9.1, silicate concentrations are simulated by the MedBFM model with an uncertainty of 0.9 mmol/m^3 in the upper layers and of about 0.5-0.7 mmol/m^3 in the deeper layers (i.e., below 6 0 m). Low correlation value in the surface layer indicates that the model has some deficiencies in reproducing the typical surface spatial gradient of silicate concentration, that occurs especially in the western basin. The correlation values of

the deep layers are pretty high (around 0.8) highlighting that subsurface modelled gradients are consistent with observations.

	Silicate		
Layer depth	**BIAS**	**RMSD**	**CORR**
0-1 0 m	0.80	0.93	0.22
10-3 0 m	0.83	0.96	0.20
30-6 0 m	0.68	0.78	0.40
60-10 0 m	0.44	0.55	0.80
100-15 0 m	0.53	0.70	0.77
150-30 0 m	0.48	0.73	0.80
300-60 0 m	-0.39	0.73	0.87
600-100 0 m	-0.14	0.85	0.75

Table IV.9.1 Skill metrics for the comparison of silicate with respect to climatology in open sea.

IV.10 pH

pH validation is performed with Class 1 metrics assessment: it consists in the comparison between model average vertical profiles and the EMODnet2018_int reference climatological profiles (Figure IV.15.2 appendix A). The comparison between model vertical profiles and the reference climatological profiles (Class1 metric validation of Figures IV.15.2 in appendix A) shows the good skill of the model in representing the basin-wide gradient and sub-basin vertical pH profiles. The statistics computed using the 16 sub-basins climatological values and the corresponding model annual means (Table IV.10.1) highlights that uncertainty, which never exceeds 0.033, is lower at deeper layers than at surface.

	pH in total scale		
Layer depth	**BIAS**	**RMSD**	**CORR**
0-1 0 m	-0.017	0.033	0.81
10-3 0 m	-0.018	0.027	0.69
30-6 0 m	-0.024	0.033	0.48
60-10 0 m	-0.004	0.026	0.62
100-15 0 m	0.009	0.018	0.78
150-30 0 m	0.009	0.017	0.91
300-60 0 m	0.015	0.017	0.96
600-100 0 m	0.006	0.009	0.96

Table IV.10.1 Skill metrics for the comparison of pH with respect to sub-basin profiles climatology in open sea.

IV.11 Alkalinity

The validation of the Alkalinity (ALK) is performed with Class 1 metrics assessment: it consists in the comparison between model average vertical profiles and the EMODnet2018_int reference climatological profiles (Figure IV.15.2 appendix A). It is worth to note that alkalinity is typically reported as μmol/kg whereas the CMEMS product is reported as mol/m^3. The density of seawater is needed for the conversion. As shown in figures IV.15.2 (appendix A), the profiles are well simulated within the range of variability of the climatology except in the western basins where the model overestimates concentration of alkalinity at the surface. As reported in Table IV.10.1, alkalinity concentrations are

simulated by the MedBFM model with an error of around 40 μmol/kg in the upper layers and of about 10-20 μmol/kg in the deeper layers (i.e., below 6 0 m). High correlation values in all layers indicate that the model reproduces the typical spatial gradient of alkalinity.

	Alkalinity		
Layer depth	**BIAS** [μmol kg^{-1}]	**RMSD** [μmol kg^{-1}]	**CORR**
0-1 0 m	28.86	44.34	0.94
10-3 0 m	27.97	38.69	0.95
30-6 0 m	21.39	30.63	0.96
60-10 0 m	9.32	21.35	0.93
100-15 0 m	11.00	14.76	0.97
150-30 0 m	3.09	13.22	0.92
300-60 0 m	0.89	10.79	0.88
600-100 0 m	-0.51	9.54	0.90

Table IV.11.1 Skill metrics for the comparison of alkalinity with respect to sub-basin profiles climatology in open sea.

IV.12 Dissolved Inorganic Carbon (DIC)

The validation of dissolved inorganic carbon (DIC) is performed with Class 1 metrics assessment: it consists in the comparison between model average vertical profiles and the EMODnet2018_int reference climatological profiles (Figure IV.15.2, appendix A). It is worth to note that DIC is typically reported as μmol/kg whereas the CMEMS product is reported as mol/m^3. The density of seawater is needed for the conversion. As shown in figures IV.15.2 (appendix A), the profiles are well simulated within the range of variability of the climatology except in the western and ION1 sub-basins where the model slightly overestimates concentration of DIC at the surface. As reported in Table IV.11.1, DIC concentrations are simulated by the MedBFM model with an error of around 40 μmol/kg in the upper layers and of about 5-20 μmol/kg in the deeper layers (i.e., below 6 0 m). High correlation values in all layers indicate that the model reproduces the typical spatial gradient of DIC.

It is worth to note that higher uncertainty of DIC and alkalinity is associated with high variability of the two variables. In fact, DIC and alkalinity profiles are characterized by high variability in the upper layers (down to 6 0 m) whereas deeper values remain almost constant during the year. This high variability at the surface of DIC and also ALK dynamics is determined by three major factors: the input in the eastern marginal seas (the terrestrial input from the Po and other Italian rivers and the input from the Dardanelles), the effect of evaporation in the eastern basin (which has a seasonal component), and the influx of the low-ALK and low-DIC Atlantic waters in the western basin. The thermohaline basin-wide circulation modulates the intensity and the patterns of the spatial gradients. Intermediate and deep layers show weaker dynamics and less variability (see figures IV.15.2, appendix A).

	Dissolved inorganic carbon		
Layer depth	**BIAS** [µmol kg^{-1}]	**RMSD** [µmol kg^{-1}]	**CORR**
0-1 0 m	30.07	43.82	0.96
10-3 0 m	31.43	39.73	0.96
30-6 0 m	22.61	30.83	0.92
60-10 0 m	7.39	19.41	0.83
100-15 0 m	1.23	16.52	0.82
150-30 0 m	-3.84	9.37	0.72
300-60 0 m	-8.85	12.93	0.61
600-100 0 m	-3.08	5.54	0.91

Table IV.12.1 Skill metrics for the comparison of dissolved inorganic carbon with respect to sub-basin profiles climatology in open sea.

IV.13 Surface partial pressure of CO2 (spCO2)

Variable pCO2 (partial pressure of carbon dioxide in sea water) has been validated using a climatology derived from the CarbSys datasets of Table III.3 and Fig. III.3. Mean vertical profiles are computed over the sub-basin of Fig. III.1. Model results (January 2019 – December 2019) are aggregated to the corresponding vertical and horizontal discretization and skill performance metrics are computed.
Two reference datasets are used for the validation of surface pCO2: one of in situ or recalculated pCO2 values derived from the EMODnet 2018 dataset and the dedicated global dataset SOCAT v2 of pCO2 measurements. Climatological reference values at sub-basin scale are derived from the two datasets and the modelled 2019 average is compared.
Given the much higher data availability of the SOCAT v2 dataset, skill performance metrics of SOCAT v2 are ultimately used for the validation of surface pCO2. Then, skill statistics of pCO2 together with those of DIC, alkalinity and pH, provide a comprehensive outlook of the carbonate system functioning.
Class 1 comparison between surface pCO2 model and the reference climatological surface values from from Emodnet2018 (Class1 metric validation) are shown in Figure IV.15.2 in appendix A. The mean monthly evolutions of SOCAT and model for selected subbasins (class 1 comparison) are shown in Figure IV.13.1
As shown in the comparison between model and the two reference climatologies the spatial gradients and seasonal cycle are well reproduced (high correlation values in Tab. IV.13.1 and values in Fig IV.15.2 and IV.13.1). The model overestimation, mostly in summer months (Fig. IV.13.1), and the consequent error are partly due to the fact that the two climatologies refer to a past condition (observations from the 2000-2015 period). Thus, the current trend of surface pCO2 is not fully accounted in the reference datasets but simulated by the model. The lack of NRT observations represents a limit for an accurate validation of this variable.

Dataset	**Surface pCO2 [µatm]**		
	BIAS	**RMSD**	**CORR**
EMODnet2018; pCO2 at 0-1 0 m	23.29	40.15	0.73
SOCAT v2; surface pCO2	43.32	49.95	0.95

Table IV.13.1 Skill metrics for the comparison of surface pCO2 with respect to sub-basin climatology in open sea.

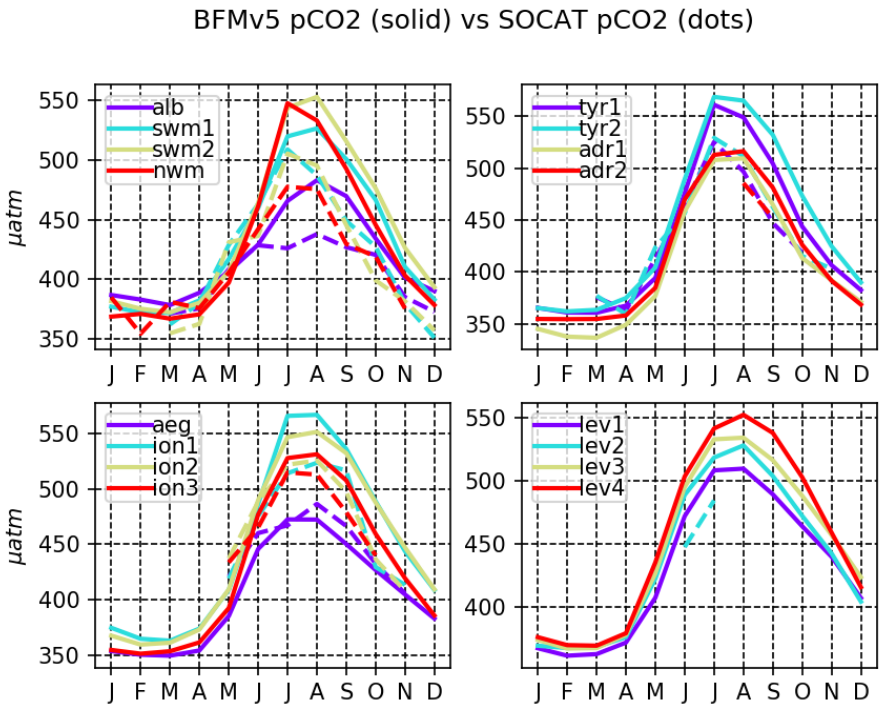

Figure IV.13.1 Monthly evolution of surface pCO2 [µatm] of model (solid lines) and climatology derived from SOCAT dataset (dashed lines when present) for the Mediterranean sub-basins.

IV.14 Surface flux of CO2

The modelled mean annual surface flux of CO2 (Fig. IV.14.1) can be qualitatively compared with previous published estimations (section 1.7 of the Ocean State Report in von Schuckmann et al., 2018; d'Ortenzio et al., 2008; Melaku Canu et al., 2015). The mean annual patterns, i.e. western-to-eastern and the northern-to-southern decreasing gradients and the almost neutral condition are consistently in agreement with the previous estimations. The west to east gradient of the surface flux of CO2 simulated by the operational product is consistent with the reanalysis product presented in the Ocean State Report, even if values tend to be mostly positive in this specific year (sink flux from the atmosphere to the sea), however reasonable.

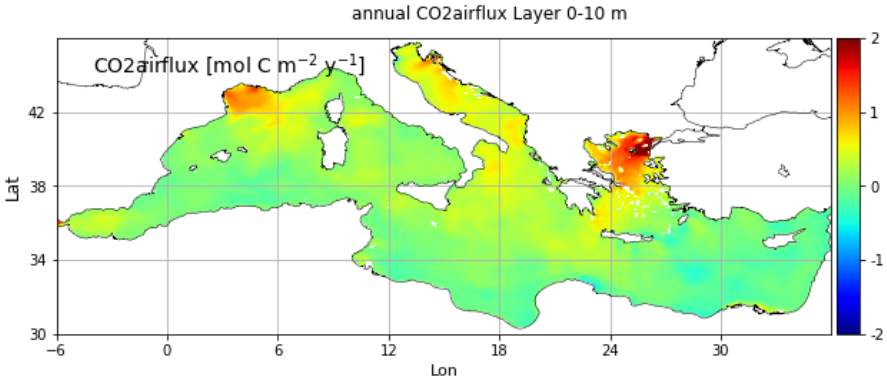

Figure IV.14.1. Mean annual map of surface flux of CO2.

IV. 15 Appendix A: class 1 climatological comparison

This section reports the class 1 visual comparison for all the model variables. Weekly (grey lines) and overall average (black lines) profiles for the model run 2019 are compared with climatological vertical profiles (red dots for means and dashed lines for standard deviations) for the 16 sub-basins of Fig. III.1. Two sets of figures are presents: one for oxygen and nutrient variables (Figure IV.15.1), and one for carbonate system variables (Figures IV.15.2).

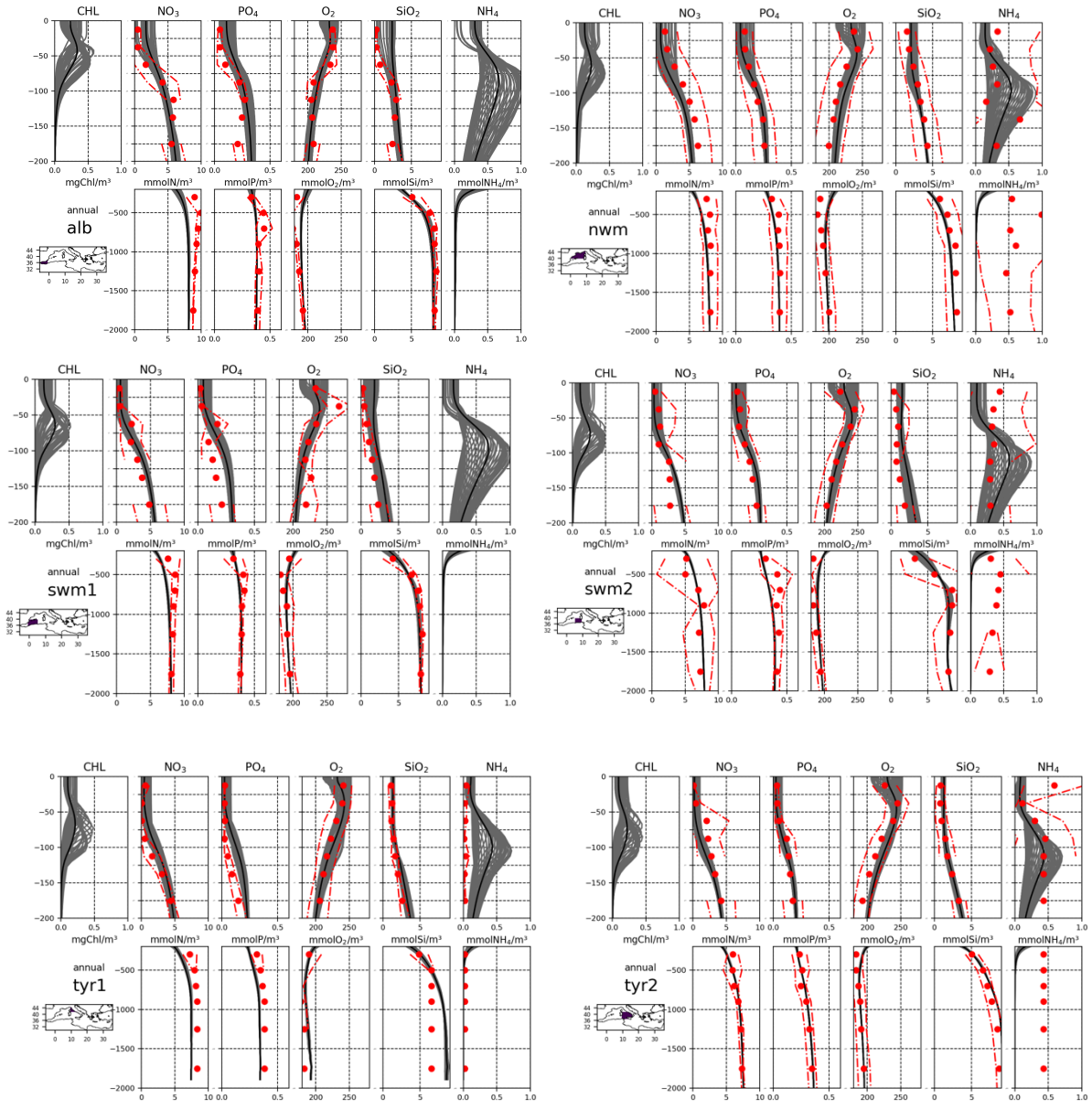

Fig. IV.15.1 Continues overleaf

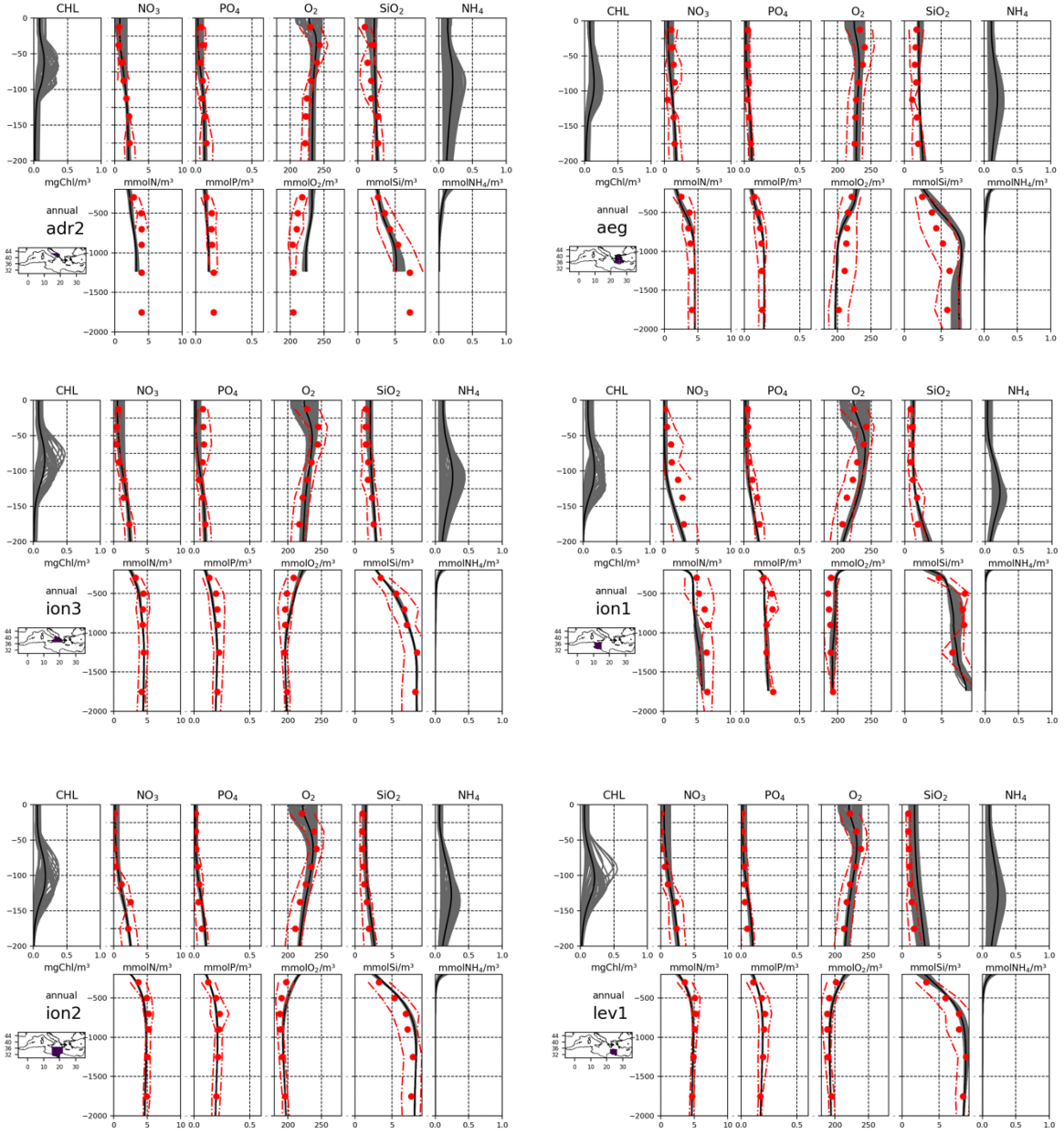

Fig. IV.15.1 Continues overleaf

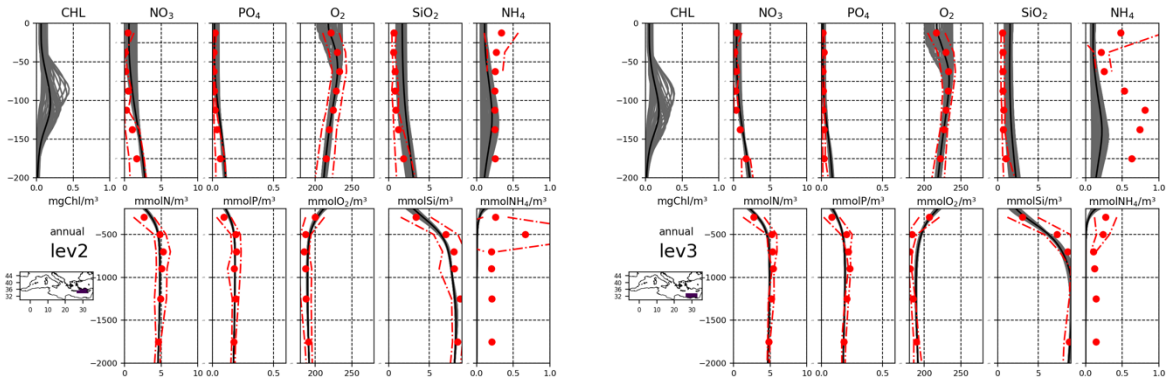

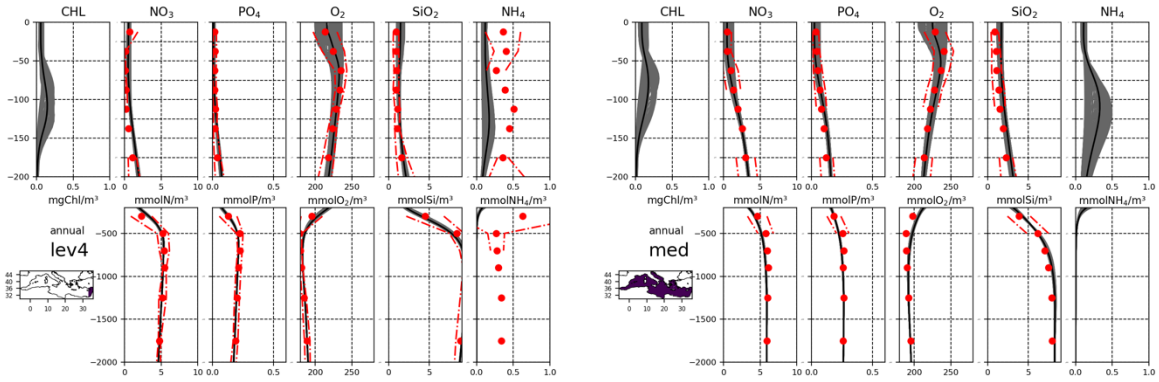

Fig. IV.15.1 Comparison between weekly (grey lines) and annual (black lines) vertical profiles from the CMEMS model run for the Mediterranean sub-basins (except ADR1 due to lack of reference data) and climatological profiles of nitrate, phosphate and dissolved oxygen, Silicate and Ammonium retrieved from EmodeNET dataset (red dots).

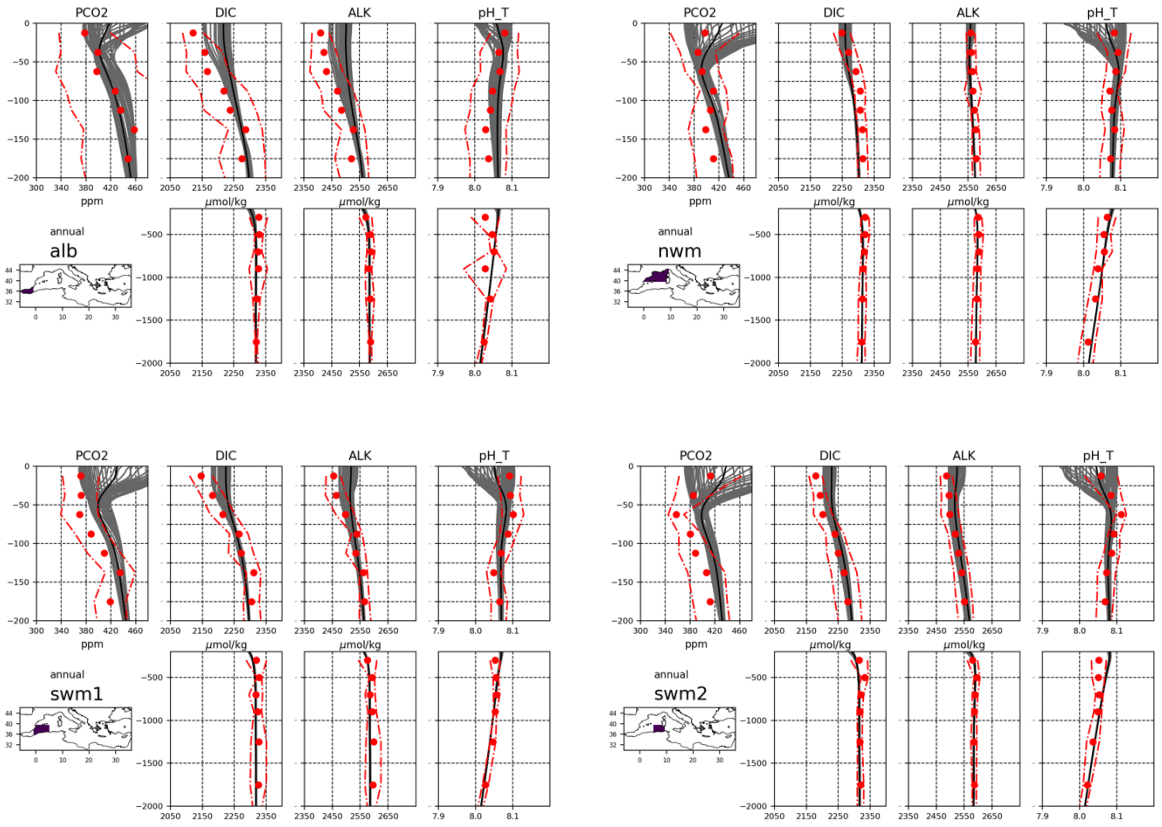

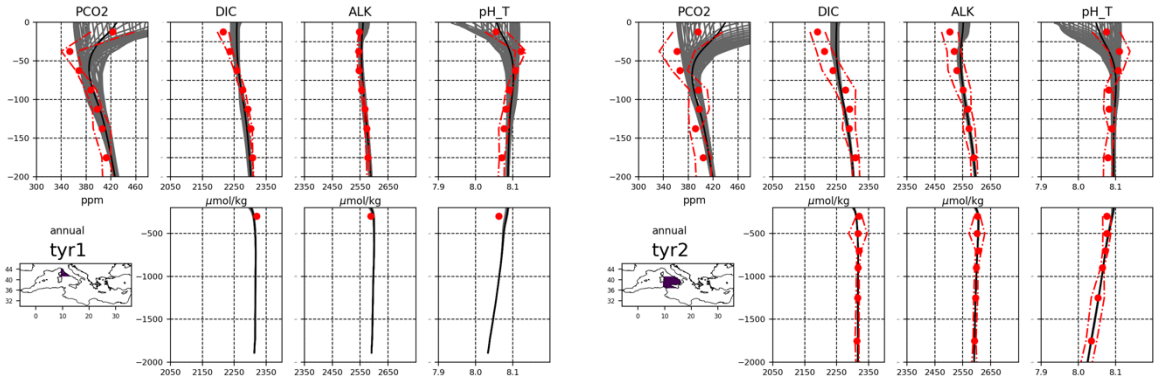

Fig. IV.15.2 Continues overleaf

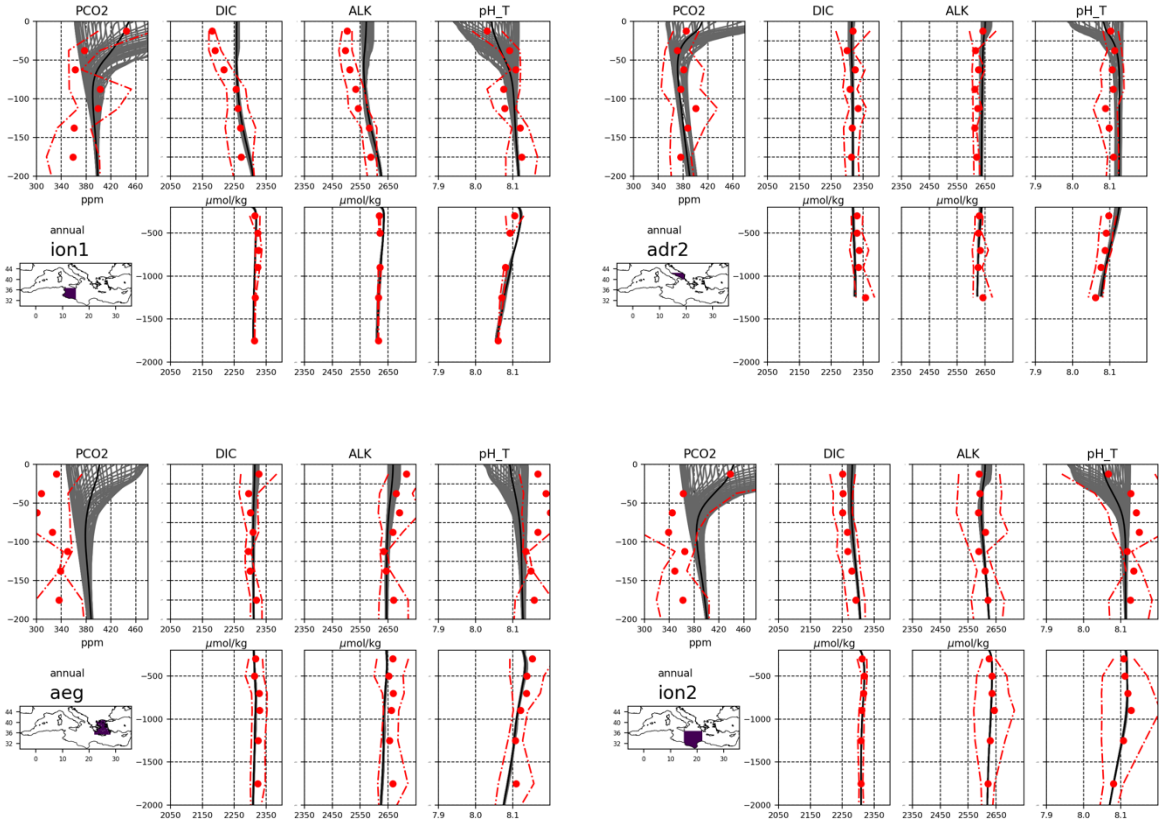

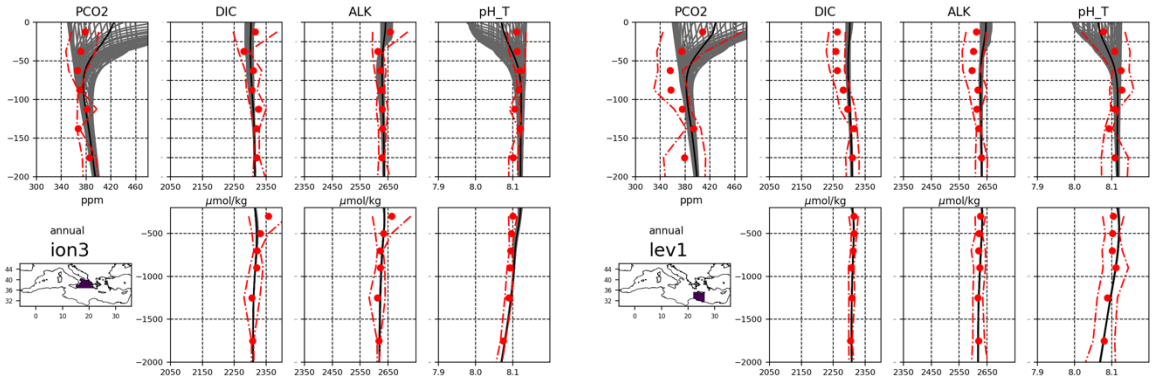

Fig. IV.15.2 Continues overleaf

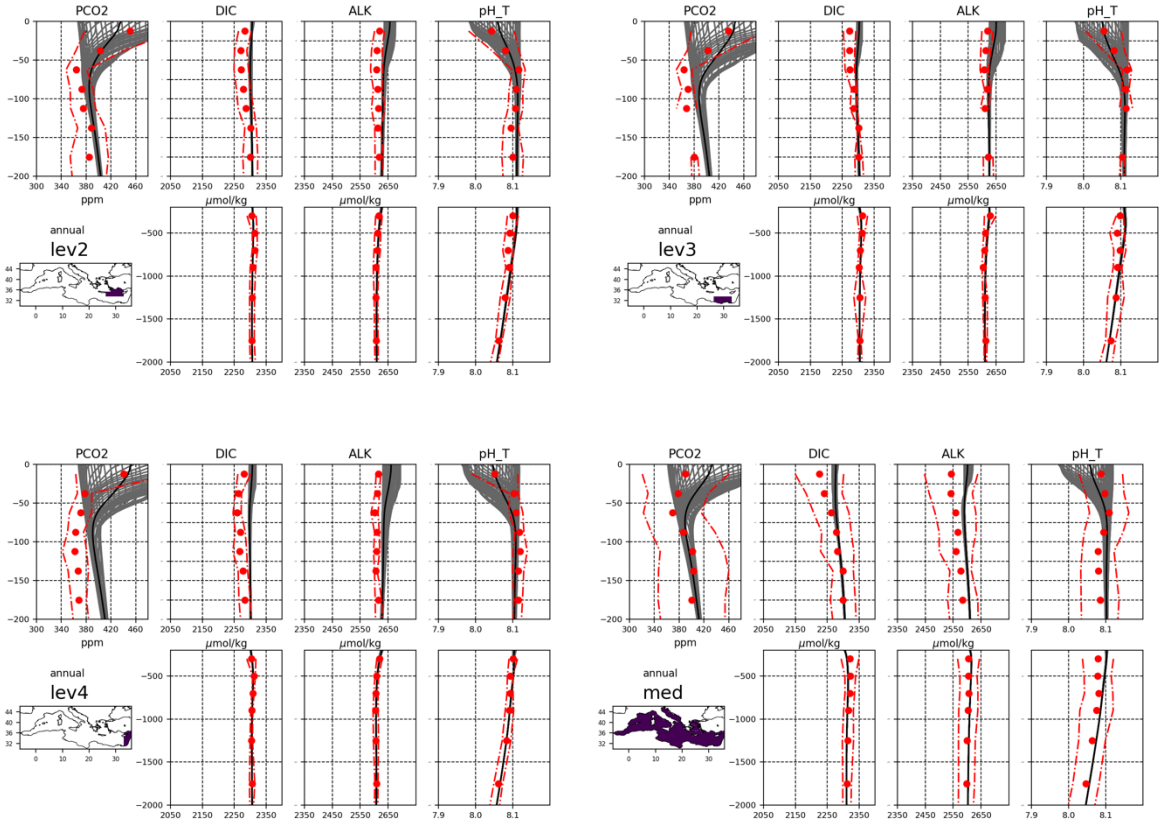

Figure IV.15.2 Profiles of pCO2, DIC, ALK and pH in total scale: mean weekly model profiles (grey color lines; from January to December 2019), mean annual model profiles (black lines) and CarbSys derived climatological (±standard deviation) profiles (red dots and dashed lines) for the sub-basins of Fig. III.1.

V SYSTEM'S NOTICEABLE EVENTS, OUTAGES OR CHANGES

Date	Change/Event description	System version	other
25/09/2017	First release of Mediterranean Sea biogeochemical analysis and forecast at 1/24° including assimilation of satellite chlorophyll over the entire domain	MedBFM2	V3.2 version
30/04/2018	Changes in the physical model (see CMEMS-MED-QUID-006-013 v1.1) and recalibration of boundary condition at the Atlantic buffer.	MedBFM2.1	V4.1 version
28/01/2018	Upgrade of the BFM model to the official version 5. Open boundary condition at the Dardanelles Strait consistently with the Med-PHY configuration.	MedBFM3.0	Q2/2019
06/12/2019	Upgrade of the 3DVarBio data assimilation scheme with assimilation of BGC-Argo floats data and daily forecast production cycle	MedBFM3.1	Q1/2020
15/01/2021	Upgrade of boundary condition in the Atlantic Ocean. Addition of new products (ammonium, silicate and zooplankton carbon biomass). Update of the off-line coupling with the physical system by considering tide and new physical data assimilation.	MedBFM3.2	Q2/2021
03/09/2021	Release of version Q4/2021 of the Med-biogeochemistry with the addition of the daily discharges of nutrients and carbonate system variables for the Po River (Adriatic Sea). No substantial changes in the quality of the NRT product.	MedBFM3.2	Q4/2021

VI QUALITY CHANGES SINCE PREVIOUS VERSION

The present version differs from the previous one for the following points.

- the quality evaluation of the Mediterranean Sea Analysis and Forecast BIO product considers skill performance metrics for 14 variables. Three new variables have been added to the product (ammonium, silicate and zooplankton carbon biomass).
- New internal QC procedures for BGC-Argo float data have greatly improved the NRT validation framework. Phytoplankton Carbon Biomass is validated against estimations from bbp700 optical data. Oxygen delay mode increases the number of available profiles. Implementation of a neural network procedure increases the quality of nitrate profiles.
- Update of the reference dataset for class 1 metrics validation. Quality of variables assessed with class1 metrics has not changed.
- A dependency of the Med-biogeochemistry model system is changed: addition of the daily observed Po River discharges for nutrients and carbonate system variables. Quality of the Med-BIO NRT product in the Adriatic Sea (assessment done using satellite chlorophyll) has not changed.

VII REFERENCES

Álvarez, M.; Sanleón-Bartolomé, H.; Tanhua, T.; Mintrop, L.; Luchetta, A.; Cantoni, C.; Schroeder, K.; Civitarese, G. (2014) The CO2 system in the Mediterranean Sea: a basin wide perspective, Ocean Science, 10(1), pp.69-92

Bakker, D. C. E., Pfeil, B. Landa, C. S., Metzl, N., O'Brien, K. M., Olsen, A., Smith, K., Cosca, C., Harasawa, S., Jones, S. D., Nakaoka, S., Nojiri, Y., Schuster, U., Steinhoff, T., Sweeney, C., Takahashi, T., Tilbrook, B., Wada, C., Wanninkhof, R., Alin, S. R., Balestrini, C. F., Barbero, L., Bates, N. R., Bianchi, A. A., Bonou, F., Boutin, J., Bozec, Y., Burger, E. F., Cai, W.-J., Castle, R. D., Chen, L., Chierici, M., Currie, K., Evans, W., Featherstone, C., Feely, R. A., Fransson, A., Goyet, C., Greenwood, N., Gregor, L., Hankin, S., Hardman-Mountford, N. J., Harlay, J., Hauck, J., Hoppema, M., Humphreys, M. P., Hunt, C. W., Huss, B., Ibánhez, J. S. P., Johannessen, T., Keeling, R., Kitidis, V., Körtzinger, A., Kozyr, A., Krasakopoulou, E., Kuwata, A., Landschützer, 3 P., Lauvset, S. K., Lefèvre, N., Lo Monaco, C., Manke, A., Mathis, J. T., Merlivat, L., Millero, F. J., Monteiro, P. M. S., Munro, D. R., Murata, A., Newberger, T., Omar, A. M., Ono, T., Paterson, K., Pearce, D., Pierrot, D., Robbins, L. L., Saito, S., Salisbury, J., Schlitzer, R., Schneider, B., Schweitzer, R., Sieger, R., Skjelvan, I., Sullivan, K. F., Sutherland, S. C., Sutton, A. J., Tadokoro, K., Telszewski, M., Tuma, M., Van Heuven, S. M. A. C., Vandemark, D., Ward, B., Watson, A. J., Xu, S. (2016) A multi-decade record of high quality fCO2 data in version 3 of the Surface Ocean CO2 Atlas (SOCAT). Earth System Science Data 8: 383-413. doi:10.5194/essd8-383-2016.

Berner, R. A., & Morse, J. W.,1974. Dissolution kinetics of calcium carbonate in sea water; IV, Theory of calcite dissolution. American Journal of Science, 274(2), 108-134.

Bergametti, G., Remoudaki, E., Losno, R., Steiner, E., Chatenet, B., 1992. Source, transport and deposition of atmospheric Phosphorus over the northwestern Mediterranean, J. Atmos. Chem., 14, 501–513.

Bethoux, J. P., Morin, P., Chaumery, C., Connan, O., Gentili, B., and Ruiz-Pino, D., 1998. Nutrients in the Mediterranean Sea, mass balance and statistical analysis of concentrations with respect to environmental change, Mar. Chem., 63, 155–169.

Bittig, H. C., Steinhoff, T., Claustre, H., Fiedler, B., Williams, N. L., Sauzède, R., Körtzinger, A., Gattuso, J. P., 2018: An Alternative to Static Climatologies: Robust Estimation of Open Ocean CO2 Variables and Nutrient Concentrations From T, S, and O2 Data Using Bayesian Neural Networks. Frontiers in Marine Science. DOI: 10.3389/fmars.2018.00328

Bellacicco, M., Vellucci, V., Scardi, M., Barbieux, M., Marullo, S., D'Ortenzio, F., 2019. Quantifying the Impact of Linear Regression Model in Deriving Bio-Optical Relationships: The Implications on Ocean Carbon Estimations. Sensors 19, 3032. https://doi.org/10.3390/s19133032

Bosc, E., Bricaud, A., & Antoine, D. (2004). Seasonal and interannual variability in algal biomass and primary production in the Mediterranean Sea, as derived from 4 years of SeaWiFS observations. Global Biogeochemical Cycles, 18(1).

Buga L., G. Sarbu, L. Fryberg, W. Magnus, K. Wesslander, J. Gatti, D. Leroy, S. Iona, M. Larsen, J. Koefoed Rømer, A.K. Østrem, M. Lipizer, A. Giorgetti 2018 EMODnet Thematic Lot n° 4/SI2.749773 EMODnet Chemistry Eutrophication and Acidity aggregated datasets v2018 doi: 10.6092/EC8207EF-ED81-4EE5-BF48-E26FF16BF02E

Christaki, U., Giannakourou, A., Van Wambeke, F., & Grégori, G. (2001). Nanoflagellate predation on auto-and heterotrophic picoplankton in the oligotrophic Mediterranean Sea. *Journal of Plankton Research*, *23*(11), 1297-1310.

Copin-Montegut C., 1993. Alkalinity and carbon budgets in the Mediterranean Sea. Global Biogeochemical Cycles, 7(4), pp. 915-925.

Cornell, S., Rendell, A., Jickells, T., 1995. Atmospheric inputs of dissolved organic Nitrogen to the oceans, Nature, 376, 243–246.

Cossarini, G., Lazzari, P., Solidoro, C., 2015. Spatiotemporal variability of alkalinity in the Mediterranean Sea. Biogeosciences, 12(6), 1647-1658.

Crise, A., Solidoro, C., and Tomini, I.: Preparation of initial conditions for the coupled model OGCM and initial parameters setting, MFSTEP report WP11, subtask 11310, 2003.

de la Paz, M., Huertas, E.M., Padín, X.-A., Gónzalez-Dávila, M., Santana-Casiano, M., Forja, J.M., Orbi, A., Pérez, F.F., Ríos, A.F., Reconstruction of the seasonal cycle of air–sea CO2 fluxes in the Strait of Gibraltar, In Marine Chemistry, Volume 126, Issues 1–4, 2011, Pages 155-162.

Dobricic, S., Pinardi, N., 2008. An oceanographic three-dimensional variational data assimilation scheme. Ocean Modelling, 22, 3-4, 89-105.

Dolan JR., Vidussi F. , Claustre H., 1999. Planktonic ciliates in the Mediterranean Sea: longitudinal trends Deep-Sea Research I 46 (1999) 2025}2039

D'Ortenzio, Fabrizio, David Antoine, and Salvatore Marullo. "Satellite-driven modeling of the upper ocean mixed layer and air–sea CO2 flux in the Mediterranean Sea." *Deep Sea Research Part I: Oceanographic Research Papers* 55.4 (2008): 405-434.

Foujols, M.-A., Lévy, M., Aumont, O., Madec, G., 2000. OPA 8.1 Tracer Model Reference Manual. Institut Pierre Simon Laplace, pp. 39.

Garcia, H. E., K. Weathers, C. R. Paver, I. Smolyar, T. P. Boyer, R. A. Locarnini, M. M. Zweng, A. V. Mishonov, O. K. Baranova, D. Seidov, and J. R. Reagan, 2018. World Ocean Atlas 2018, Volume 4: Dissolved Inorganic Nutrients (phosphate, nitrate and nitrate+nitrite, silicate). A. Mishonov Technical Ed.; NOAA Atlas NESDIS 84, 35 pp.

Guerzoni, S., Chester, R., Dulac, F., Herut, B., Loÿe-Pilot, M.-D., Measures, C., Migon, C., Molinaroli, E., Moulin, C., Rossini, P., Saydam, C., Soudine, A., Ziveri, P., 1999. The role of atmospheric deposition in the biogeochemistry of the Mediterranean Sea. Prog. Oceanogr., 44 (1-3): 147-190.

Herut, B. and Krom, M.: Atmospheric input of nutrients and dust to the SE Mediterranean, in: The Impact of Desert Dust Across the Mediterranean, edited by: Guerzoni, S. and Chester, R., Kluwer Acad., Norwell, Mass., 349–358, 1996.

Huertas, I. E., Ríos, A. F., García-Lafuente, J., Makaoui, A., Rodríguez-Gálvez, S., Sánchez-Román, A., Orbi, A., Ruíz, J., and Pérez, F. F.: Anthropogenic and natural CO2 exchange through the Strait of Gibraltar, Biogeosciences, 6, 647-662, 2009.

Kempe, S., Pettine M., Cauwet, G., 1991. Biogeochemistry of european rivers. In Degensempe & Richey eds, biogeochemistry of Major World Rivers, SCOPE 42 John Wiley 169-211

Kourafalou, V. H., & Barbopoulos, K. (2003). High resolution simulations on the North Aegean Sea seasonal circulation. In Annales Geophysicae (Vol. 21, No. 1, pp. 251-265).

Krasakopoulou E., Souvermezoglou E., Giannoudi L., Goyet C., 2017. Carbonate system parameters ad anthropogenic CO2 in the North Aegean Sea during October 2013. Continental Shelf Research, 149, 69-81.

Krom, M.D., Kress, N., Brenner, S., Gordon, L.I., 1991. Phosphorus limitation of primary productivity in the eastern Mediterranean Sea. Limnology and Oceanography, 36(3) 424-432.

Lazzari, P., Teruzzi, A., Salon, S., Campagna, S., Calonaci, C., Colella, S., Tonani, M., Crise, A. 2010. Pre-operational short-term forecasts for the Mediterranean Sea biogeochemistry. Ocean Science, 6, 25-39.

Lazzari, P., Solidoro, C., Ibello, V., Salon, S., Teruzzi, A., Béranger, K., Colella, S., and Crise, A., 2012. Seasonal and inter-annual variability of plankton chlorophyll and primary production in the Mediterranean Sea: a modelling approach. Biogeosciences, 9, 217-233.

Lazzari, P., Solidoro, C., Salon, S., Bolzon, G., 2016. Spatial variability of phosphate and nitrate in the Mediterranean Sea: a modelling approach. Deep Sea Research I, 108, 39-52.

Lueker, T. J., Dickson, A. G., and Keeling, C. D.: Ocean pCO2 calculated from dissolved inorganic carbon, alkalinity, and equations for K1 and K2: validation based on laboratory measurements of CO2 in gas and seawater at equilibrium, Mar. Chem., 70, 105–119, 2000.

Mazzocchi M. G., Siokou I., Tirelli V., Bandelj V., de Puelles M. F., Örek Y. A., de Olazabal A., Gubanova A., Kress N., Protopapa M., Solidoro C., Taglialatela S., Terbiyik Kurt T., 2014. Regional and seasonal characteristics of epipelagic mesozooplankton in the Mediterranean Sea based on an artificial neural network analysis. *Journal of Marine Systems*, *135*, 64-80

Mehrbach, C., Culberson, C. H., Hawley, J. E., and Pytkowitcz, R. M.: Measurements of the apparent dissociation constants of carbonic acid in seawater at atmospheric pressure, Limnol. Oceanogr., 18, 897–907, 1973.

Meybeck M., Ragu A., 1995 River Discarges to the Oceans: An Assessment of suspended solids, major ions and nutrients UNEP STUDY

Mignot A., F. D'Ortenzio, V. Taillandier, G. Cossarini, S. Salon, L. Mariotti, 2017. Estimation of BGC-Argo chlorophyll fluorescence and nitrate observational errors using the triple collocation method. 6th Euro-Argo Users Meeting July 4-5, 2017 in Paris, France.

Loÿe-Pilot, M. D., J. M. Martin, and J. Morelli, 1990. Atmospheric input of inorganic nitrogen to the western Mediterranean. Biogeochem., 9: 117-134.

Deliverable D4.6: SES land-based runoff and nutrient load data (1980 -2000), edited by Bouwman L. and van Apeldoorn D., 2012 PERSEUS H2020 grant agreement n. 287600.

Olsen, A., R. M. Key, S. van Heuven, S. K. Lauvset, A. Velo, X. Lin, C. Schirnick, A. Kozyr, T. Tanhua, M. Hoppema, S. Jutterström, R. Steinfeldt, E. Jeansson, M. Ishii, F. F. Pérez and T. Suzuki. The Global Ocean Data Analysis Project version 2 (GLODAPv2) – an internally consistent data product for the world ocean, Earth Syst. Sci. Data, 8, 297–323, 2016, doi:10.5194/essd-8-297-2016

Olsen, A., Lange, N., Key, R. M., Tanhua, T., Álvarez, M., Becker, S., Bittig, H. C., Carter, B. R., da Cunha, L., Feely, R. A., van Heuven, S., Hoppema, M., Ishii, M., Jeansson, E., Jones, S. D., Jutterström, S., Karlsen, M. K., Kozyr, A., Lauvset, S. K., Lo Monaco, C., Murata, A., Pérez, F. F., Pfeil, B., Schirnick, C., Steinfeldt, R., Suzuki, T., Telszewski, M., Tilbrook, B., Velo, A. and Wanninkhof, R.: GLODAPv2.2019 -- an update of GLODAPv2, Earth Syst. Sci. Data, 11(3), 1437–1461, doi:10.5194/essd-11-1437-2019, 2019.

Orr and Epitaloni, 2015: "Improved routines to model the ocean carbonate system: mocsy 2.0." GMD 8.3 : 485-499.

Orr, J. C., Najjar, R. G., Aumont, O., Bopp, L., Bullister, J. L., Danabasoglu, G., ... & Griffies, S. M., 2017. Biogeochemical protocols and diagnostics for the CMIP6 Ocean Model Intercomparison Project (OMIP), Geosci. Model Dev., 10, 2169–2199.Petihakis, G., Tsiara, K., Triantafyllou, G., Kalaroni, S., & Pollani, A. (2014). Sensitivity of the N. AEGEAN SEA ecosystem to Black Sea Water inputs. Mediterranean Marine Science, 15(4), 790-804. doi:http://dx.doi.org/10.12681/mms.955

Ribera d'Alcalà M., Civitarese G., Conversano F., Lavezza R., 2003. Nutrient ratios and fluxes hint at overlooked processes in the Mediterranean Sea. Journal of Geophysical Research, 108(C9), 8106, doi:10.1029/2002JC001650.

Salon, S., Cossarini, G., Bolzon, G., Feudale, L., Lazzari, P., Teruzzi, A., Solidoro, C., Crise, A., 2019. Marine Ecosystem forecasts: skill performance of the CMEMS Mediterranean Sea model system. Ocean Sci. Discuss. 1–35. https://doi.org/10.5194/os-2018-145

Schmechtig, C., Poteau, A., Claustre, H., D'Ortenzio, F., Dall'Olmo, G., Boss, E., 2018. Processing Bio-Argo particle backscattering at the DAC level. https://doi.org/10.13155/39468

Schneider, A., Wallace, D. W. R., and Kortzinger, A.: Alkalinity of the Mediterranean Sea, Geophys. Res. Lett., 34, L15608, doi:10.1029/2006GL028842, 2007.

Siokou-Frangou, I., Bianchi, M., Christaki, U., Christou, E. D., Giannakourou, A., Gotsis, O., Souvermezoglou, E., 2002. Carbon flow in the planktonic food web along a gradient of oligotrophy in the Aegean Sea (Mediterranean Sea). Journal of Marine Systems 33– 34 (2002) 335–353

Siokou-Frangou, I., Christaki, U., Mazzocchi, M. G., Montresor, M., Ribera d'Alcalà, M., Vaqué, D., & Zingone, A. (2010). Plankton in the open Mediterranean Sea: a review.

Siokou, I., Zervoudaki, S., Velaoras, D., Theocharis, A., Christou, E. D., Protopapa, M., & Pantazi, M. (2019). Mesozooplankton vertical patterns along an east-west transect in the oligotrophic Mediterranean sea during early summer. *Deep Sea Research Part II: Topical Studies in Oceanography*, *164*, 170-189.

Somot, S., Sevault, F., Déqué, M., Crépon, M., 2008. 21st century climate change scenario for the Mediterranean using a coupled atmosphere–ocean regional climate model, Global and Planetary Change, 63, 2–3: 112–126.

Souvermezoglou, E., Krasakopoulou, E., Pavlidou, A., 2014. Temporal and spatial variability of nutrients and oxygen in the North Aegean Sea during the last thirty years. Mediterranean Marine Science, 15/4, 805-822.

Teruzzi, A., Dobricic, S., Solidoro, C., Cossarini, G. 2014. A 3D variational assimilation scheme in coupled transport biogeochemical models: Forecast of Mediterranean biogeochemical properties, Journal of Geophysical Research, doi:10.1002/2013JC009277.

Teruzzi, A., Bolzon, G., Salon, S., Lazzari, P., Solidoro, C., Cossarini, G., 2018. Assimilation of coastal and open sea biogeochemical data to improve phytoplankton simulation in the Mediterranean Sea. Ocean Modelling, 132, 46-60

Teruzzi, A., Di Cerbo, P., Cossarini, G., Pascolo, E., Salon, S., 2019. Parallel implementation of a data assimilation scheme for operational oceanography: the case of the MedBFM model system. Computers & Geosciences 124, 103-114.

Teruzzi, A., Bolzon, G., Salon, S., Lazzari, P., Solidoro, C., and Cossarini, G. (2018). Assimilation of coastal and open sea biogeochemical data to improve phytoplankton simulation in the Mediterranean sea. Ocean Modelling, 132:46–60.

Thingstad, T.F., Rassoulzadegan, F., 1995. Nutrient limitations, microbial food webs, and 'biological C-pumps': suggested interactions in a P-limited Mediterranean. Marine Ecology Progress Series, 117: 299-306.

Tugrul, S., Besiktep,e T., Salihoglu, I., 2002. Nutrient exchange fluxes between the Aegean ad tBlack Seas through the Marmara Sea. Mediterranean Marine Science, 3/1, 33-42.

von Schuckmann, K., Le Traon, P.Y., Smith, N., Pascual, A., Brasseur, P., Fennel, K. and Djavidnia, S., et al., 2018. Copernicus marine service ocean state report. Journal of Operational Oceanography, 11(sup1), pp.S1-S142.

World Ocean Atlas 2013 database, https://www.nodc.noaa.gov/OC5/woa13/

Yalcin B., Artuz M.L., Pavlidou A., Cubuk S., Dassenakis M., 2017. Nutrient dynamics and eutrophication in the Sea of Marmara: data from recent oceanographic research. Science of the Total Environment, 601-602, 405-424.

Zeebe, R.E. and Wolf Gladrow, D., 2001. CO2 in seawater: equilibrium, kinetics, isotopes, Elsevier oceanography series. Elsevier.

Wanninkhof 2014, OCMIP2 design document & OCMIP2 Abiotic HOWTO. Limnol. Oceanograph. Methods, 12, 351-362.